UNIVERSITY OF OKLAHOMA

GRADUATE COLLEGE

A BINDING ISOTHERM BETWEEN FERROCENE MEDIATORS AND GLUCOSE OXIDASE FOR USE IN BIOANODE DEVELOPMENT AND INITIAL STUDIES OF AN ELECTROCATALYTIC DEOXYDEHYDRATION REACTION

A DISSERTATION

SUBMITTED TO THE GRADUATE FACULTY

in partial fulfillment of the requirements for the

Degree of

DOCTOR OF PHILOSOPHY

By

Daniel A Bamper
Norman, Oklahoma
2019

A BINDING ISOTHERM BETWEEN FERROCENE MEDIATORS AND GLUCOSE OXIDASE FOR USE IN BIOANODE DEVELOPMENT AND INITIAL STUDIES OF AN ELECTROCATALYTIC DEOXYDEHYDRATION REACTION

A DISSERTATION APPROVED FOR THE
DEPARTMENT OF CHEMISTRY AND BIOCHEMISTRY

BY

Dr. Daniel Glatzhofer

Dr. Kenneth Nicholas

Dr. Steven Crossley

Dr. Wai Tak Yip

Dr. Ronald Halterman

© Copyright by Daniel A Bamper 2019
All rights reserved

Acknowledgements

There are so many people that have helped me along my journey towards finishing my PhD. In fact, there are entirely too many to thank individually, but I will do my best. I would first and foremost like to thank my parents, Terri, Brian, Daniel, and Wendy, for their support in starting and finishing my degree. I could not have done this without your love and support. I would also like to thank Kevin and Bridgette for their support in handling the IntegriTeam while I have been away the last few months. Your leadership and support remind me of what being a true friend is. Finally, a big thank you to Michael for reminding me of how much I have done, and how close I was to finishing. I would not have done this without you pushing me to be the best I can be.

I would like to thank my committee for their guidance and patience over the last few years. Dr Glatzhofer and Dr Nicholas have been very gracious advisors over the last years and your guidance has invaluable chemically, professionally, and personally. I would also like to thank Dr. Crossley, Dr. Halterman, and Dr. Yip for the opportunities you have afforded me over my graduate career. I cannot thank you all enough. I would also like to thank Mrs. Heather Skeldon, my high school chemistry teacher. You sparked a life-long interest in the chemistry of breakfast that has led me places I never knew I could go.

A final important acknowledgement is to my graduate student family that has helped me over my years in Norman. Logan and Tara Nickels kept me grounded and focused in a very difficult period of time. Nick Godman, Matt Houck, Rachel Roccanova, Abby Ntreh, David Hickey, and Justin Garrett kept the lab a great place to work and provided years of memories and comradery. Thank you all to everyone I wasn't able to mention in this document, as your impact has been too numerous to list. I hope I've made you proud.

Table of Contents

Table Of Figures

Abstract

Enzymatic bioelectrodes are powered by renewable biomass sources. Glucose-powered bioelectrodes are prepared from ferrocene-functionalized linear poly(ethylenimine) (Fc-LPEI) cross-linked with ethylene glycol diglycidyl ether (EGDGE). Glucose bioanodes are normally only powered by the oxidation of glucose, however it can be envisioned that the bioanode could be used to power an electrochemical reduction. In considering a disproportionation-like system, a reaction that reduces glucose could be powered by an anodic oxidation of glucose. A potential candidate for the electrochemical reduction is deoxydehydration (DODH), as glucose contains vicinal hydroxyl groups.

In this work, a Langmuir binding isotherm was detected electrochemically using cyclic voltammetry when Glucose Oxidase is treated as an inhibitor for (ferrocenylmethyl)trimethylammonium chloride (FcTAMCl) oxidation/reduction. A binding constant, K_a, was calculated from cyclic voltammetric data. This binding isotherm was observed in other ferrocene molecules, including ferrocencarboxylic acid, (((methoxy)ethoxy)ethoxy)methylferrocene, and bis(trimethylammoniummethyl)ferrocene, and were on the magnitude of 2.0×10^6 through 6.4×10^7. The magnitude of the binding isotherm varies between each derivative, with the glycol ether derivative exhibiting the strongest isotherm. Based on this K_a, a new glycol ether containing ferrocene-functionalized LPEI (FcG2LPEI) was prepared. The amperometric performance of this new material in the presence of 100 mM glucose is compared against similarly substituted ferrocenymethyl-functionalized LPEI (FcC1LPEI) that was developed by the Glatzhofer group. The amperometric performance of the FcG2LPEI is better than the amperometric performance of the FcC1LPEI, suggesting that this

binding isotherm may be indicative of potential mediator performance in the polymer-supported state.

Rhenium-based deoxydehydration catalysts were prepared and are demonstrated to be effective DODH catalysts for vicinal diols, using a variety of molecular and elemental reductants. The electrochemical behavior of $(Me_3TACN)ReO_3PF_6$ wa investigated in aprotic media in the absence and presence of a variety of acids. The strength of the acid appears to affect the reduction potential of the complex. Attempts to prepare the Re(V) glycolate made from $ReOCCl_3(PPh_3)_2$, Me_3TACN, and styrene glycol were successful in deuterated dichloromethane, but not successful in deuterated acetonitrile. Attempts to prepare the Re(V) glycolate using bulk electrolysis were not successful.

Chapter 1: Introduction

1.1 - Current Energy Needs and Introduction to Conventional Batteries

The United States and the world largely rely on oil and other fossil fuels as their primary power sources. These oil sources, however, are limited in supply. Looking at annual energy consumption, approximately 90% of the world's energy supply comes from fossil fuels, such as coal, petroleum, and natural gas[1]. It is predicted that even over the upcoming decades, there will still be a significant dependence of about 75%. Regarding fossil fuel consumption, it is estimated that about three-fourths of fossil fuels consumed are used in the transportation sector, while one-tenth is used in petroleum chemical production. These fossil fuel sources, however, are limited and are not easily renewed. It can take millions of years for dead material from plants and animals to be converted into fossil fuels. Herein lies an inherent demand for the world's energy sources to change to more renewable sources. Such an effort has been made in nuclear, wind, hydroelectric, and solar power advancements[2]. However, the development of these fields is still underway[2].

To replace the dependence on fossil fuels, multiple forms of energy will be necessary to power our society's needs. Aforementioned sources, such as wind, hydroelectric, solar, and nuclear energy, are not the focus of this work. This work will focus primarily on the possibilities of biomass. Biomass, as a general term, is a broad scope term that can include an array of plant materials that require further processing before use as a fuel resource. Biomass serves as an attractive renewable energy source from multiple perspectives, especially if it can act as a feedstock to more than one energy field. In 2011, it was estimated that biomass sources could

satisfy up to 30% of the current petroleum use in the United States alone, in both fuel and electricity needs[3].

The needs for immediate, short-term energy for small devices such as cellular telephones, wireless devices, and other small electronic devices are currently fulfilled by batteries. Battery technology is based on a two-electrode component redox system. Commercial alkaline batteries are designed around a manganese dioxide-zinc redox couple where potassium hydroxide is the electrolyte-bridge in between the two electrodes[4]. These systems are one-time-use materials and cannot be recharged. However, rechargeable lithium ion batteries are currently the main power-storage device used in most small electronics. These batteries are functionally dependent on the transport of lithium ions across a polymer electrolyte membrane[5]. One of the major drawbacks of this technology is that lithium can be toxic to humans, as it is known to induce schizophrenia and renal failure in non-schizophrenic patients[6]. In addition, these commercial batteries can contain other heavy metals that are toxic to the environment and can host very acidic or very alkaline media. These limitations provide a need for a technology that uses renewable, less toxic materials.

Figure 1.1 demonstrates the core components of a common battery source, showing an inner carbon rod for electrical conduction to the needed circuit, a manganese (IV) oxide layer to act as a cathode, an ammonium chloride layer to act as an ionic bridge, and an outer layer of zinc to act as the anode.

Since this initial design of a battery was developed, there have been advances in the components of a battery. The main changes have been in the components of the cathode and conducting electrolyte[7]. Lithium-lithium oxide cathodes have led to the advent of rechargeable batteries, but presented the issue of "battery memory." Battery memory is caused by the

irreversible formation of Li_2O on the anode instead of the cathode. This memory diminishes the maximum charge capacity on a rechargeable battery and limits its versatility as a rechargeable source. Since then, other developments include the use of polymers capable of shuttling lithium ions across a membrane[8-9]. While these advances have led to improved battery performance, lithium is still known to be an environmental and health hazard to humans, which leaves the disposal or recycling of these batteries to be a difficult task.

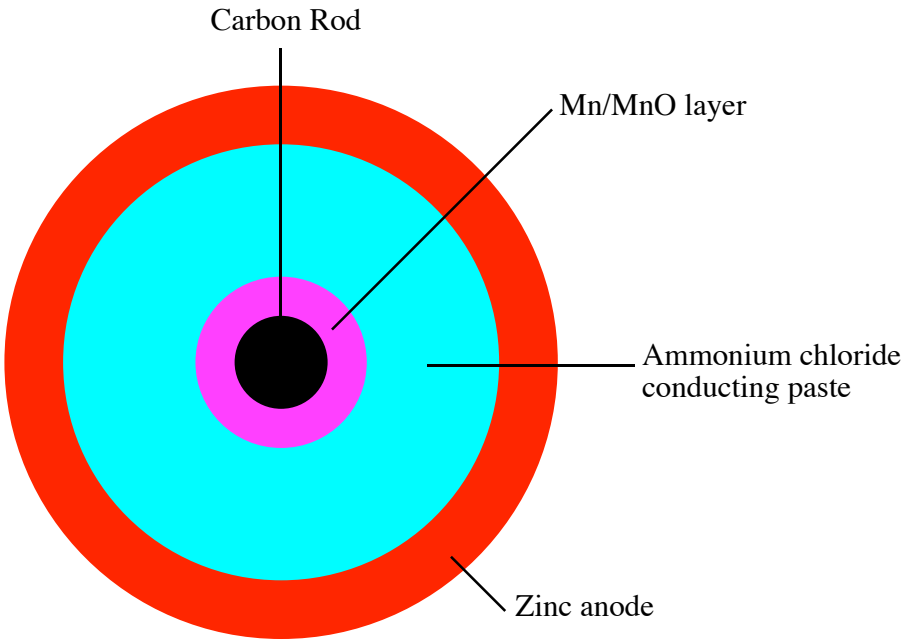

Figure 1.1 – A cross-sectional view of a conventional battery

1.2 - Biofuel Cells

Biofuel Cells (BFC) are an attractive alternative to conventional batteries, as they eliminate many of the concerns of disposal. In the most general sense, a biofuel cell is an electrochemical device that utilizes biological molecules to convert a chemical signal into an electrical signal. This transduction from a chemical signal to an electrical signal was first shown by Porter in 1911 in an experiment, where Baker's Yeast was deposited onto platinum electrodes. Glucose was fed to the yeast to generate 3.5 V of potential[10]. However, the idea of using biological molecules for transducing between chemical and electrical signals/currents was

not explored thoroughly until the 1950's. The original electrochemical biofuel cell systems were used to generate an amperometric current from waste produced during space flights[11-12]. Since then, BFCs have gained momentum as alternatives to traditional fuel cells[13-17]. Both microbial and enzymatic biofuel cells have been developed since then, but the work presented herein will focus on enzymatic biofuel cells.

While most batteries operate under highly acidic or highly alkaline conditions, enzymatic biofuel cells operate at physiological pH, between room and physiological temperature, and do not require metal ions to operate. In addition to their environmental compatibility, BFCs can demonstrate high selectivity for a narrow array of substrates, depending on the enzyme or cells used to catalyze the reaction. In most BFCs, enzymes are used to catalyze the signal transduction from the chemical reaction to the electrical signal. In these instances, the high substrate selectivity of the enzyme eliminates the need for substrate isolation from the opposing counter electrode, and thus the need for a barrier between the anode and the cathode. These simplified operating conditions have even been demonstrated to allow for physiologically-compatible operating conditions to the point of implantation[18]. These benefits also allow for facile fabrication of fuel cells and allows for a simple design to be incorporated. One additional feature regarding the oxidoreductase class of enzymes is their use of a co-oxidant or co-reductant to remove the electrons from their active site. In the case of Glucose Oxidase (GOx), Flavin Adenine Dinucleotide (FAD) is the redox component of the active site. In nature, oxygen acts as the co-oxidant for the FAD unit in the active site. When glucose comes into contact with FAD in the active site, it is oxidized to gluconolactone, while the FAD unit is reduced to $FADH_2$. The gluconolactone diffuses from the active site and molecular oxygen then enters the active site to react with the $FADH_2$ unit to make water and regenerate the active FAD. **Figure 1.2** summarizes

this process. It has also been demonstrated with multiple oxidoreductases that more than one molecule can act as the co-oxidant or co-reductant. In the case of GOx, it has been demonstrated that ferrocenes, quinones, hexacyanoferrate ions, and others are all capable of acting as co-oxidants for GOx in the absence of molecular oxygen[19]. When these molecules are used as co-oxidants to shuttle electrons to an electrode surface, they are referred to as "mediators."

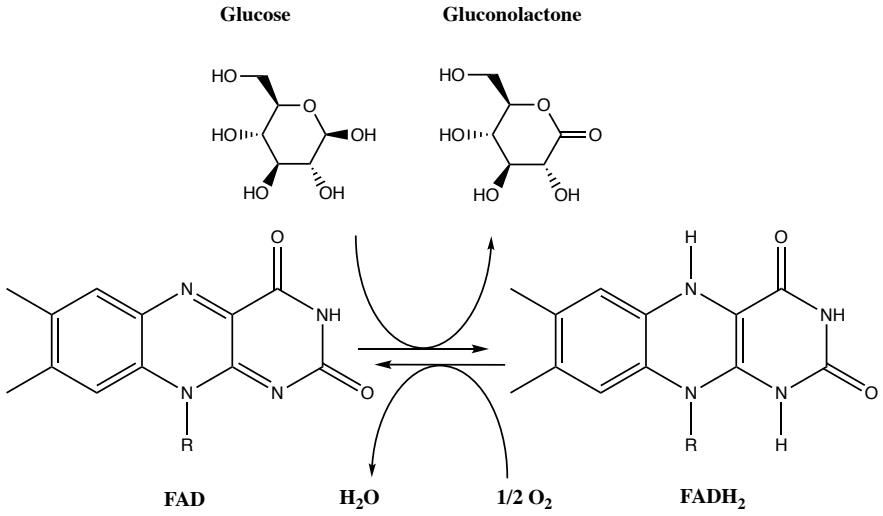

Figure 1.2 The oxidation of glucose by the adenine portion of FAD in the active site of GOx to form gluconolactone and $FADH_2$. The reaction of $FADH_2$ with oxygen as a co-oxidant is also shown to show how the FAD is regenerated to restore the enzyme to its active form. It should be noted that the enzyme immobilizes glucose into a beneficial conformation for oxidation to occur.

A general biofuel anode paired with a platinum cathode for simplicity is shown in **Figure 1.3**. Substrate A is selectively oxidized by the FAD in the active site of Enzyme A, further referred to simply as "Enzyme A" to make product A and the reduced $FADH_2$ in the active site of Reduced Enzyme A, further referred to simply as "Reduced Enzyme A." To regenerate enzyme A, oxidized Mediator A is reduced by the Reduced Enzyme A shown in blue to generate Mediator A and Enzyme A. The electrode then takes the electron from Mediator A to make Oxidized Mediator A and shuttles the electron to the Pt electrode where molecular oxygen and

protons are reduced to water. A similar enzyme schematic could be envisioned for the second electrode, where an enzymatic cascade accepts electrons from the electrode to power a corresponding reduction reaction. In **Figure 1.4**, such a schematic is demonstrated, where working electrode 1 mimics the oxidative process that moves the electrons to working electrode 2 where Mediator B is reduced by the electrode to make Reduced Mediator B, represented by Med B- in Figure 1.4. Reduced Mediator B (Med B-) reacts with oxidized Enzyme B to regenerate Mediator B and Enzyme B. Enzyme B then reacts with substrate B to make product B and oxidized Enzyme B. By pairing two enzymatic processes together, a general schematic for a completely enzymatic biofuel cell is envisioned.

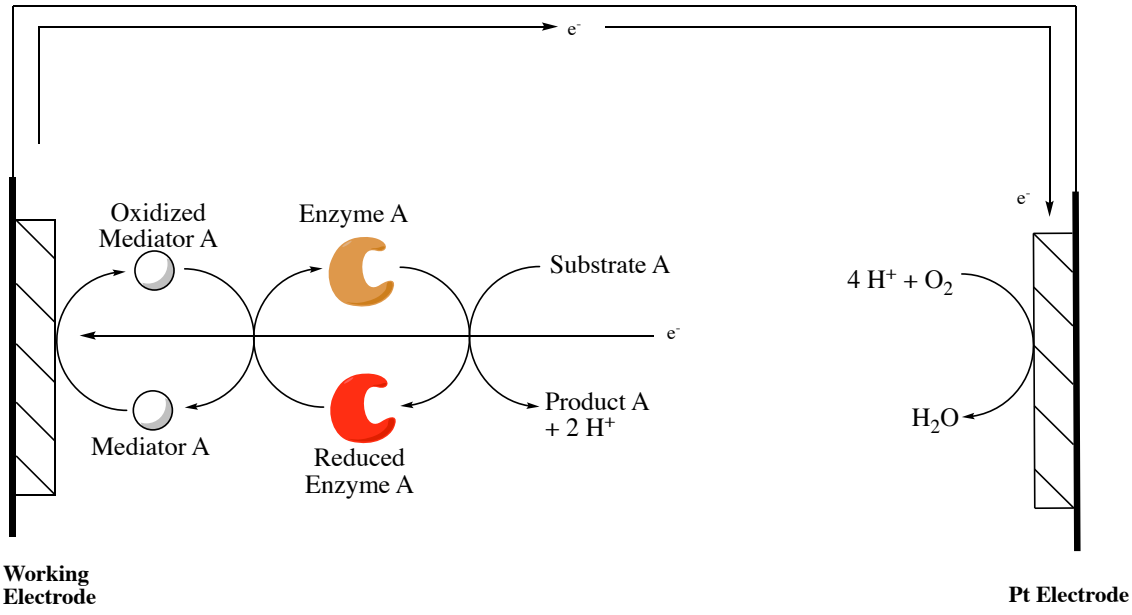

Figure 1.3 The generic mechanism for an enzymatic Biofuel Cell. The direction of the electron flow (e^-) is indicated to show how the electrons harvested from the substrate are transferred to the other electrode.

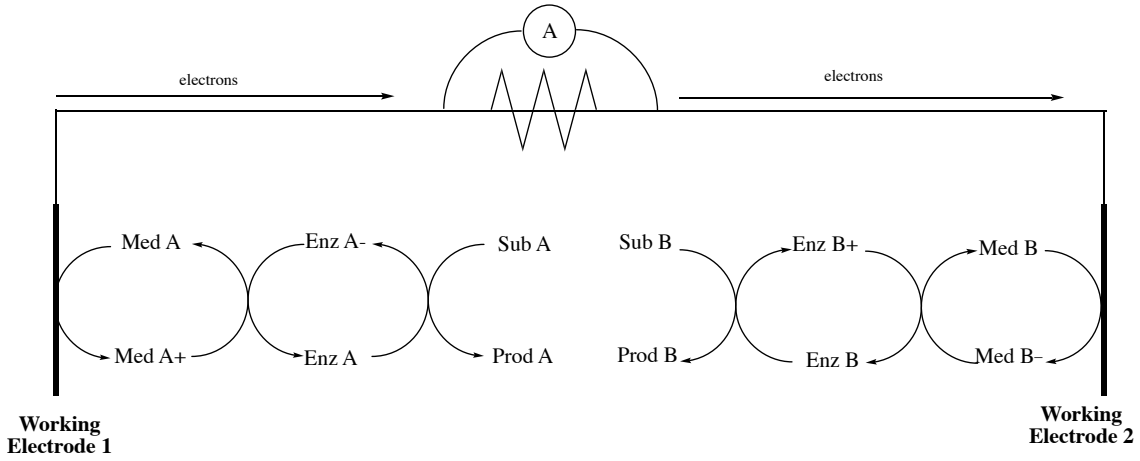

Figure 1.4 The pairing of an oxidizing and reducing set of enzymatic reactions where an electron mediator is shown in lieu of a co-oxidant or co-reductant to demonstrate how the system behaves in the absence of these biologically necessary molecules.

1.2.1 – Bioelectrode Fabrication Strategies

Each electrode in a BFC normally needs three components to operate: an oxidoreductase, an appropriate substrate, and a method of transferring electrons from an active site to the electrode. The methods used to carry out the electron transfer, however, have developed through three "generations." This term was originally used to describe the development of biosensors. However contemporaries use this term to describe the methods used in moving the electrons from the active site of an enzyme to the electrode surface. **Figure 1.5** briefly summarizes the three main methods of electron transfer between an enzyme's active site and the electrode surface. For the sake of simplicity, this section detailing the generations of biosensors and biofuel cells will only focus on the fabrication methods of one bioelectrode component of a biofuel cell.

Some of the earliest biofuel cells were used to detect the electrochemically active product of an enzymatic reaction, as shown in example A of Figure 1.5. One of the most common examples was the detection of hydrogen peroxide. Hydrogen peroxide was one of the most commonly detected molecules in first generation biosensors, as oxygen is reduced at biocathodes

to produce hydrogen peroxide. Since hydrogen peroxide is electrochemically active, the current produced is directly proportional to the concentration of hydrogen peroxide, and, indirectly, the concentration of substrate. Some drawbacks regarding this methodology are that a complex matrix may interfere with the detection of the product. In the case of hydrogen peroxide it was demonstrated that other biological compounds, such as ascorbic acid and dopamine, can interfere with the detection of hydrogen peroxide, as their redox potentials are similar[20-21]. In addition, since the product must diffuse from the active site of the enzyme to the surface of the electrode, these enzymes are often covalently linked to the electrode surface to minimize the diffusion of hydrogen peroxide away from the electrode surface and/or reduce further complications from the matrix.

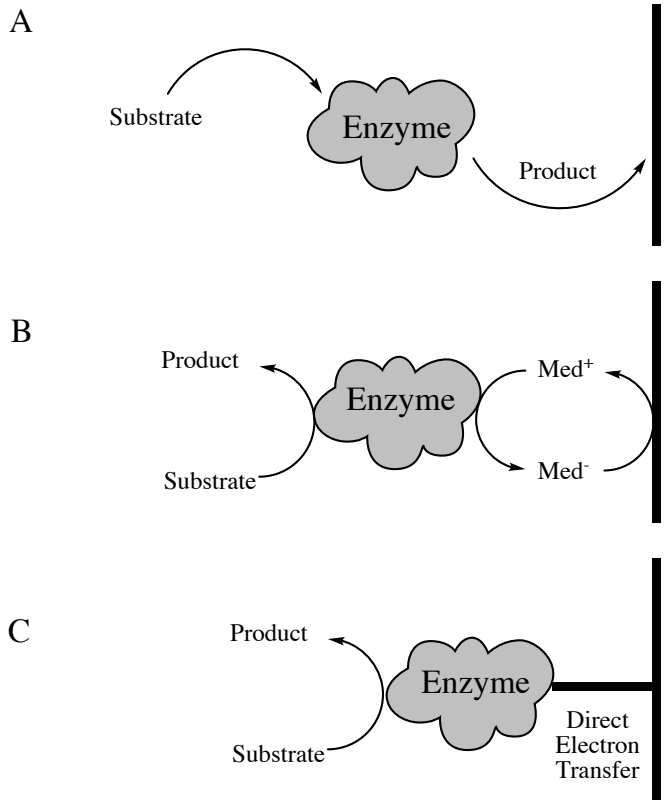

Figure 1.5 shows the idea of electron transfer between the enzyme's active site and the electrode surface for: A) a first generation bioelectrode B) a second generation bioelectrode, and C) a third generation bioelectrode.

A second-generation bioelectrode uses an electron-transfer mediator (ETM) to move electrons between the active site and the electrode surface, as shown in diagram B of Figure 5.1. The electron-transfer mediator, further referred to as simply "mediator," is a small electroactive molecule that diffuses between the enzyme's active site and the electrode surface. The mediator must demonstrate a fully reversible electrochemical reaction, and be compatible with the enzyme to act as a mediator for a second-generation bioelectrode material. Among second generation bioelectrodes, two approaches have been used in fabrication. The earliest systems allowed the mediator, enzyme, and substrate diffuse freely through solution. The second approach uses a solid-state support functionalized with the mediator to immobilize the enzyme. This immobilization keeps the mediator in close proximity to the enzyme, allowing for a theoretically more efficient method of electron exchange between the mediator and the enzyme. Sol gels and polymer materials have both been demonstrated to act as a means of support. For the purpose of this work, the focus will be geared toward the use of polymers as a means of immobilization for both the mediator and the enzyme.

Third generation bioelectrodes use the approach of direct electron transfer between the enzyme's active site and the electrode surface. Some oxidoreductases have the electroactive component of the active site on the outside of the enzyme, where electron transfer is unhindered. Other oxidoreductases, such as GOx, have their electroactive components buried approximately 15 Å deep within the enzyme. In these instances, direct electron transfer is very difficult to achieve[22]. Carbon nanotubes are often used to increase the electronic conductivity of a film[23]. Even when these carbon nanotubes are used, it is very difficult for the nanotubes to penetrate into the active site of the enzyme so direct electron transfer can occur. This work will primarily

focus on second-generation fabrication methods in both the solution state and polymer-supported state.

Examples of each generation of bioelectrodes used in biosensors and BFCs have been demonstrated in the literature. Some of these methods are more successful than others. In particular, glucose bioelectrodes and glucose/oxygen biofuel cells are some of the most thoroughly investigated systems, as both of these boast the strongest success and strong dynamic applications. Some of the most successful enzymes responsible for catalyzing the reactions of glucose and oxygen are GOx and Laccase, respectively. Both of these oxidoreductases boast high turnover rates and a tolerance to environmental conditions; however, their methods of catalyzing their respective reactions are quite distinct from each other, as their active sites have significantly different structures.

GOx, as described in Section 1.2, has an FAD in its active site. Electron mediation is normally achieved with GOx through the use of small mediators that can penetrate the active site and interact with the reduced $FADH_2$. Once electron transfer occurs, the mediator diffuses out of the electron sites and shuttles electrons to the electrode surface through Marcus-type collisions[24]. Thus, for glucose electrodes, a second-generation fabrication approach is best. By utilizing an approach of immobilizing GOx in a redox-active polymer, Heller first demonstrated the innovation of a polymer-supported GOx-based bioelectrode[25]. An organoosmium complex was used to shuttle electrons from the active site to the electrode surface. By covalently linking the organoosmium complex to poly(vinylpyridine) (PVP), his group was able to achieve mediation in a polymer-supported system. Since the initial discovery of this immobilization technique, a large number of systems have been developed on this model.

Laccase, however, is a blue copper oxidase that catalyzes the reaction of oxygen to form water.[26] The active site of Laccase consists of a cluster of three copper atoms with an additional type-1 copper (T1-Cu) center near the exterior of the enzyme[26]. The T1-Cu assists in electron transfer and is located next to a hydrophobic region of the active site. This allows organic complexes to interact with the T1-Cu rather easily to facilitate electron transfer. Because of the proximity of the T1-Cu to the surface of the enzyme and its location in the hydrophobic pocket, there have been examples of both second generation and third generation fabrication methods that have successfully been demonstrated[27-29].

1.2.2 – Second Generation Glucose Bioelectrodes

Glucose is an abundant renewable resource that reacts with the oxidoreductase GOx. At its active site, GOx has a Flavin Adenine Dinucleotide (FAD) unit that is responsible for electron transfer to molecular oxygen. First generation bioelectrodes made from GOx utilized the electrochemical detection of hydrogen peroxide[30-32], as demonstrated in **Figure 1.6**. However, there were some major drawbacks that included inactivation of the enzyme due to the production of H_2O_2. Inactivation comes from repeated catalytic cycles consistently producing hydrogen peroxide and activated transient species that are very difficult to identify damaging the enzyme[33]. When considering the structure of GOx, in particular the depth of the active site, it seemed logical that a redox mediator would be beneficial for the long-term stability of GOx[33].

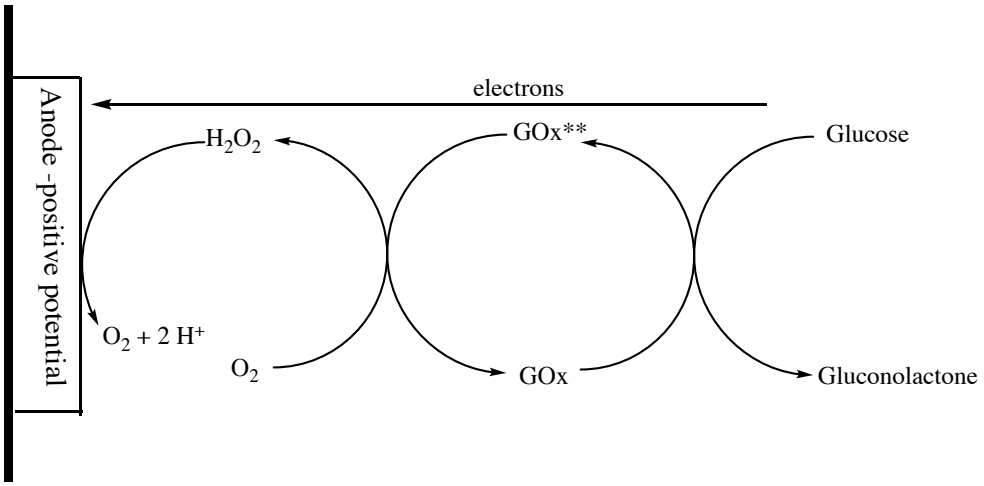

Figure 1.6 demonstrates production and detection of hydrogen peroxide in a 1st generation glucose bioelectrode.

The first example of an electron mediator compatible with GOx was a benzoquinone redox couple[34-35]. When GOx was immobilized at the surface of a graphite electrode, it was observed that with oxygen as a co-oxidant the system retained approximately 43% activity after approximately 7 x 10^6 catalytic cycles, while when using benzoquinone the system retained approximately 70% relative activity after 4 x 10^7 catalytic cycles[33]. This retention in reactivity led to a series of mediators being studied, including single and double electron mediators, such as hexacyanoferrate, a series of organic dyes, and a series of water-soluble ferrocene derivatives acting as co-oxidants for GOx[36-39]. **Figure 1.7** shows how a ferrocene molecule acts as a mediator in a second-generation bioelectrode with GOx. One of the major drawbacks to this electrode design, however, includes the diffusion limitations of the mediator to transport electrons to the electrode from the enzyme[19]. This diffusion limitation hinders the current output of a bioelectrode. To eliminate the diffusion limitation of the mediator, several different approaches to immobilize the mediator in close proximity to the electrode were made. Some of these methods included attaching the mediator to high molecular weight poly(ethyleneglycol) chains that were physically attached to the enzyme, trapping the enzyme and mediator behind a

semi-permeable membrane, and chemically modifying mediators directly to enzymes that are bound to the electrode surface[40-43].

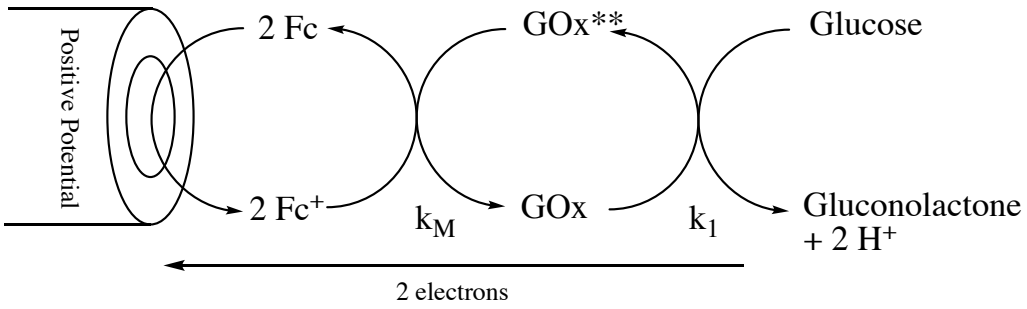

Figure 1.7 shows how a Ferrocene (Fc) derivative can act as a redox mediator for Glucose Oxidase (GOx).

One particularly innovative design to solve this diffusion issue came from the Heller group. This was the first example of using a polymer where the redox mediator is directly attached to immobilize the enzyme on the electrode surface[40]. Poly(vinylpyridine) (PVP) was functionalized with three different groups. The first group was an osmium bipyridine complex that acted as the electron mediator. The second group was a group to increase the hydrophilicity of the polymer, such as 2-bromoethanol or 3-bromopropionic acid. The final group was an ester group that forms bonds with a nitrogen-containing cross-linking agent and the lysine residues on the enzyme surface. Figure 1.8 shows the first PVP-Os materials used to immobilize GOx at an electrode surface. Other redox mediators for GOx include chromium and manganese half-sandwich complexes, a variety of functionalized ferrocenes, and assorted organic redox mediators[44-45].

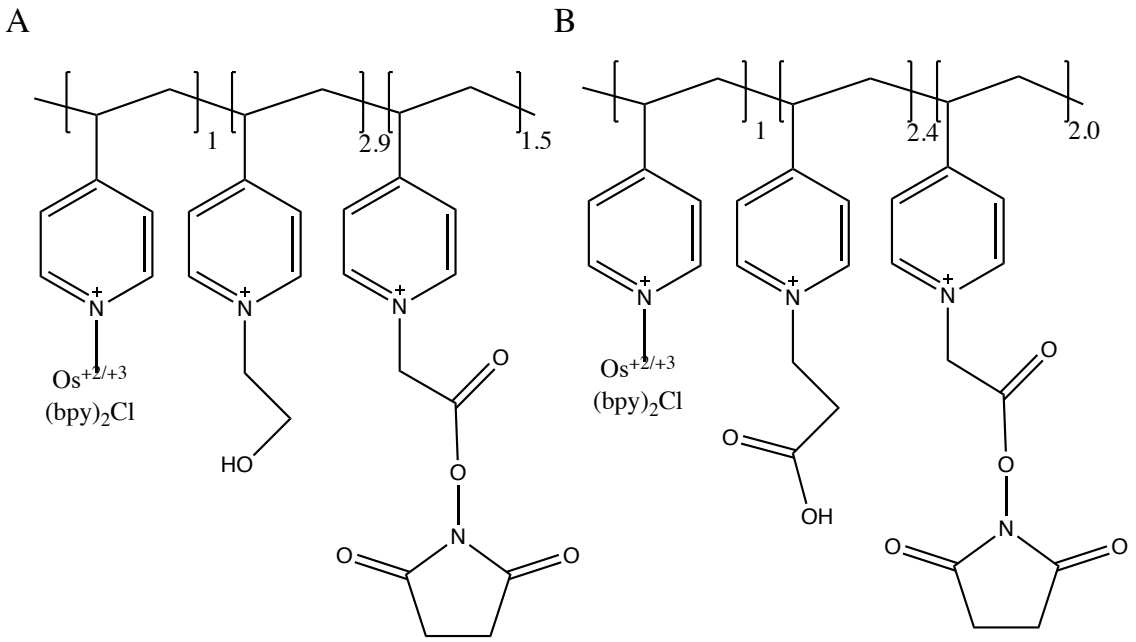

Figure 1.8 Show the first two electroactive materials used by Heller to immobilize GOx on an electrode surface[25].

Based on this original design, a series of other systems have been designed for enzymes, including fructose dehydrogenase, horseradish peroxidase, glucose dehydrogenases, and enzymes from the cytochrome P450 families[23, 46-48]. The PVP-Os system, however, is not without its inherent drawbacks. Osmium is rather toxic and quite expensive. In addition, the polymer must be thoroughly modified to become water-soluble. To address this issue other materials have been developed where the mediating species is either ruthenium or ferrocene-based, and more water-soluble polymers capable of forming hydrogels including poly(vinylimidazole) and poly(allylamine) have been used[49-56]. One of the most successful systems of interest that uses this approach to fabrication has been a linear poly(ethylenimine) (LPEI) system using a pendant ferrocene as a mediator[48]. The focus of this work will be largely pertinent to these LPEI-based ferrocenyl systems.

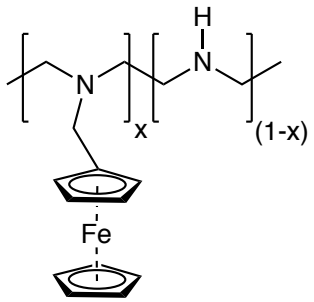

Figure 1.9 Ferrocene-momdified linear poly(ethylenimine) (Fc-LPEI)

1.2.3 – Ferrocene-Modified Linear Poly(ethylenimine) Bioelectrodes and Their Applications

The Glatzhofer group has attached ferrocene directly to linear poly(ethylenimine) (LPEI), creating a ferrocene-functionalized linear poly(ethylenimine) (Fc-LPEI). LPEI was an attractive candidate as the base polymer, as the material has been demonstrated to have a high degree of polymer flexibility, a large number of amino nitrogen atoms that can be functionalized, and is a polymer that hydrates well[57]. Initial studies of ferrocene functionalized LPEI and branched poly(ethyleimine) (BPEI) demonstrated electrochemically-reversible behavior that is appealing for a redox polymer to be used in bioelectrodes[57]. When these materials were used in fabricating a material for a glucose bioelectrode, it was noted that the Fc-LPEI material exhibited a higher maximum current density, J_{max}, than the PVP-Os system developed by Heller[57]. One interesting feature of the Fc-LPEI material made by the Glatzhofer group is that the electron-diffusion coefficient is approximately 40 times larger than the electron diffusion coefficient of a ferrocene-poly(allylamine) material that has been demonstrated for use in other GOx-containing bioelectrodes[50]. Combining this observation with the rather rigid backbone of poly(allylamine) suggested the LPEI is, indeed, a more flexible polymer than other amine containing polymers, allowing for a greater area of mobility for the ferrocene mediator[48].

From this initial design, other materials have been prepared, such as methylated ferrocene mediators and differing tether lengths that covalently link the ferrocene derivatives to the LPEI,

that aim to solve other conventional issues seen in bioelectrode materials. When applying these Fc-LPEI materials in a glucose biosensor or using them as bioanodes in glucose biofuel cells, these materials perform quite admirably. Biofuel cells are typically characterized by their power output in terms of absolute power output (mW), area-dependent power output (mW/cm^2) or volume –dependent power output (mW/cm^3). The power output of a typical fuel cell is dependent on the product of two components: E^o_{cell} and J_{max}. E^o_{cell} is defined as the difference between the peak reduction potential of the cathodic reaction (E^o_{ipc}) and the peak oxidation potential of the anodic reaction (E^o_{ipc}). J_{max} is the maximum current density of the electrode. **Equations 1.1 and 1.2** summarize these relationships.

$$P = E^o_{cell} \times J_{max} \qquad \textbf{1.1}$$

$$E^o_{cell} = E^o_{ipc} - E^o_{ipa} \qquad \textbf{1.2}$$

Theoretically, the limiting E^o_{cell} should be determined by the difference in the potentials of the enzymes used to make the electrode components of a biofuel cell. For example, in a biofuel cell composed of GOx and Copper Laccase, the potential generated by the fuel cell is 0.749 V[58]. The T-1 Cu center of Laccase at the cathode has a potential of 0.539 V vs SCE at pH = 7.0, while the FAD center of GOx has a potential of -.210 V vs SCE at pH = 7.0. In practice, however, the mediator is the species that is reacting at each electrode. A biofuel cell prepared from propionylferrocene-modified linear (polyethyleneimine)) (Fc-C3-LPEI) with GOx and PVP-Os with Laccase generated 100 uW/cm^2 with a peak potential of 0.135 V[48, 59]. One important observation is the decrease in the thermodynamic driving force of E^o_{cell} from the theoretical observation of 0.749 V based on the enzymatic calculation. This loss, further referred to as the "potential gap," motivated the development of "tuned" redox polymers whose potentials are pushed more favorably toward their respective enzymes to aid in minimizing this loss[48, 59-61].

Ferrocene, in this case, is an excellent candidate as a mediator that can be used in these bioelectrode materials. Ferrocene is very susceptible to electrophilic aromatic substitution[62]. By adding electron-donating groups or electron-withdrawing groups to the cyclopentadienyl ring of a ferrocene, the redox potential of the ferrocene species can be altered systematically[59, 62]. To address the need for a redox mediator whose potential closely resembles that of the enzyme it mediates, our research group has investigated methylating and chlorinating ferrocene to provide mediators whose potentials are closer to their corresponding enzymes[63-64]. By methylating ferrocene, it was demonstrated that the redox potential would change by approximately -50 mV per each methyl group added[48, 64]. When ferrocene is chlorinated, the redox potential shifts by approximately +100 mV[65]. By constructing a biofuel cell with a GOx/tetramethylferrocenyl(propionyl-modified linear poly(ethylenimine) (Me_4Fe-C_3-LPEI) bioanode and a Laccase/chloroferrocenyl(propionyl)-modified LPEI (ClFc-C_3LPEI), a maximum power of ca. 600 uW/cm^2 with a cell potential of ca 0.25 V was achieved[63]. This was the first example of a fuel cell constructed completely of ferrocene derivatives. This provided solutions to two objectives: the need for a tuned redox potential and a more environmentally friendly construction to the fuel cell by eliminating the need for an organoosmium complex in the biocathode. Figure 1.10 shows the structure of materials that are both ferrocene and osmium based.

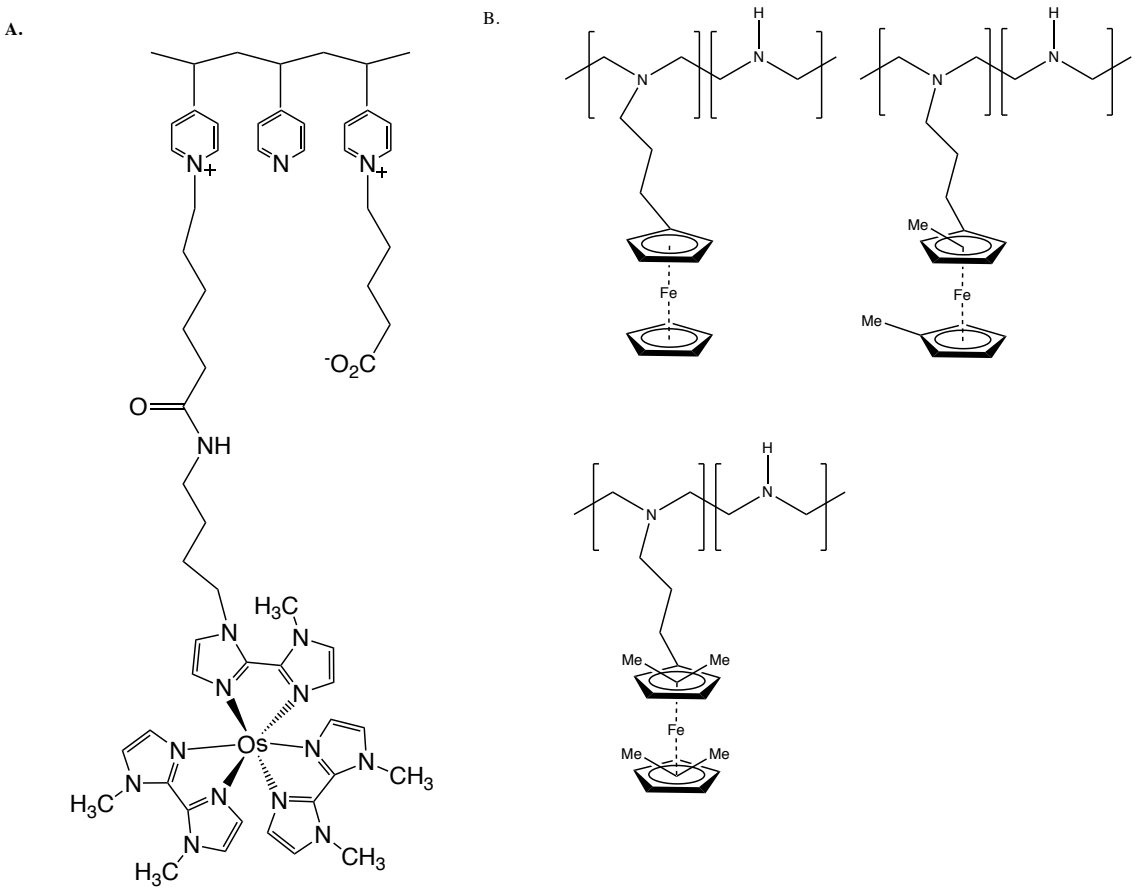

Figure 1.10 A depicts the Heller group's material, the osmium material bound to poly(vinylpryridine). B depicts the ferrocene-functionalized linear poly(ethylenimine) materials used by our lab group made from ferrocene, dimethylferrocene, and tetramethylferrocene.

1.2.4 – Bioelectrode Component Selection and Development Process

Previous sections of this chapter aimed at highlighting the impactful discoveries made in bioelectrode and biofuel cell development. One aspect that is yet to be addressed, however, is the development process that goes into making and developing new materials that act as bioelectrodes. For the sake of simplicity, the focus here will be targeted solely on the development of one material to be used bioelectrode (specifically the polymer and enzyme material), and not on making a full biofuel cell. In addition the type of electrode on which the polymer-enzyme material is immobilized has attracted a great deal of attention, by the Glatzhofer

group and by others[47, 64-66]. Materials like glassy carbon, carbon paper, and carbon felt are only some examples of materials that have been demonstrated to have an impact on the amperometric performance of bioelectrodes. This impact, however, is thought to be caused by the change in the effective surface area between the polymer-enzyme material and the electrode surface, and not due to changes in how the enzyme and mediator exchange electrons[42, 62-64]. Thus, the focus of this discussion will be limited to only the selection of compatible mediators and enzymes used to make polymer and enzyme materials.

There is a strong agreement in the biofuel cell community that the following requirements are necessary for an enzyme and mediator to pair successfully: 1) The mediator must be small enough to penetrate the enzyme's active site and interact with the redox center. 2) The mediator must exhibit a reversible redox behavior at the surface of the electrode. 3) The redox mediator must be able to effectively accept the electrons from the enzyme's active site to shuttle the electrons to the electrode surface[45]. It is in this final criterion, however, where a debate has arisen in the biofuel cell community, specifically in the methods characterizing how efficiently a mediator accepts electrons from an enzyme. Some choose to characterize the efficiency by a kinetic analysis of the exchange between the enzyme and the mediator. Others choose to characterize a mediator's efficiency by the maximum current generated when the bioelectrode is functioning. In order to fully understand the disagreement in characterization methods found in the literature, it is necessary to have a quick overview of the mechanism of how the enzyme catalyzes a reaction with the substrate and then exchanges the electrons with the mediator.

Figure 1.11 shows how an enzyme and mediator are thought to work together in a catalytic process to convert a substrate into an electrochemical response. In this catalytic process,

the activated enzyme and the substrate form an enzyme-substrate adduct. This adduct then reacts to form a product-enzyme adduct that decomposes into the deactivated enzyme and the product. The cosubstrate then enters the deactivated enzyme to form a deactivated enzyme-cosubstrate complex. This complex then reacts to form an activated enzyme-coproduct complex that decomposes back into the coproduct and the activated enzyme that can undergo this catalytic cycle again.

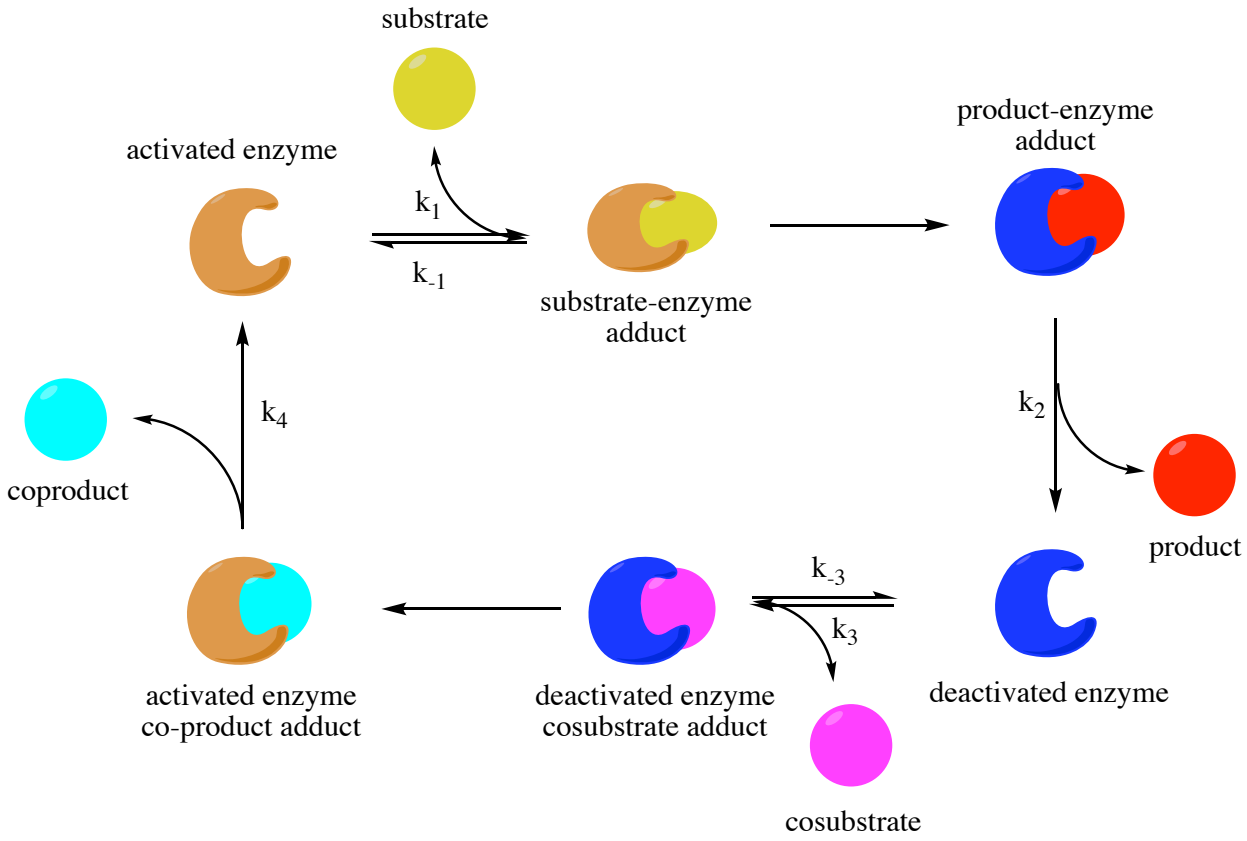

Figure 1.11 The steps wherein a substrate and a cosubstrate (either cooxidant or coreductant) are used by oxidoreductases in a catalytic cycle.

As mentioned previously, the first method that is used by a large number of research groups to determine how effective a mediator is at acting as a co-substrate with an oxidoreductase is determining the rate of reaction that occurs to reactivate the enzyme complex. When the kinetic

model is applied to an electrochemical detection method, the system behaves according the behavior shown in **Figure 1.11**. Ikeda has proposed a simplified model in analyzing the mechanism according to **Figure 1.12,**[67] which outlines a brief kinetic analysis of **Figure 1.11**[68]. Theoretically, as long as k_3 is larger than k_1 there should be an amperometric dependence on the magnitude of k_3.

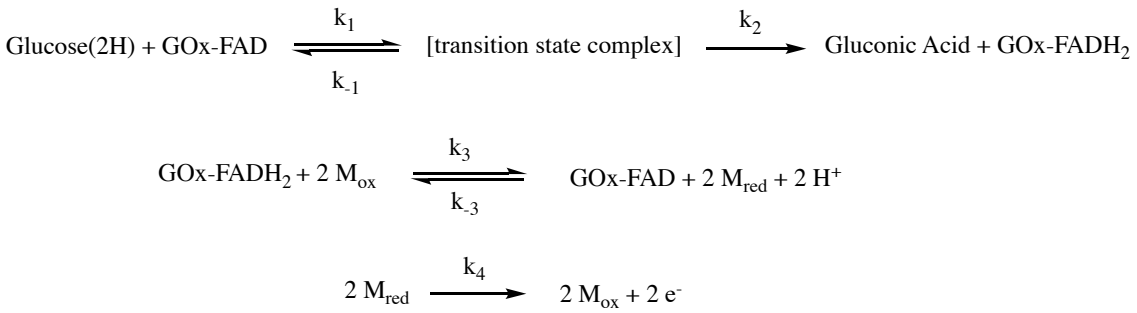

Figure 1.12 shows the kinetic model used to outline the kinetic details of the mechanism shown in Figure 1.10.

Analysis by Ikeda shows that, under steady state conditions, the rate of the enzyme-catalyzed reaction, v_e, is expressed by

$$v_E = \frac{k_{cat}[E]}{1+\frac{K_m}{[M_{ox}]}+\frac{K_S}{[S]}} \qquad (3)$$

where [E] is the concentration of the enzyme, k_{cat} is equal to $(k_2k_4/(k_2+k_4))$ and is called the catalytic constant, K_M is $(k_2(k_{-3} + k_4)/k(k_2+k_4))$ and K_S is defined as $(k_4(k_1+k_2)/k_1(k_2+k_4))$. K_M and K_S are the Michaelis constants for the oxidized mediator and the substrate, respectively. However, based on this model, there is a dual dependence on both mediator and substrate. This implies that more than one factor can limit the current[68]. However, as long as the substrate and enzyme do not change, then K_s should be a reasonable comparison of how efficiently the mediator accepts electrons from the enzyme, and thus be a predictor of the amperometric performance of a bioelectrode. As this method of kinetic analysis can be rather complicated, a

second method characterizing a mediator's efficacy has been developed in the literature, especially when screening multiple compounds as viable mediator candidates.

The second method that researchers use to characterize the efficiency of the electron exchange between the enzyme and the mediator is directly measuring the amperometric output of a bioelectrode under catalytic conditions[44]. By varying the concentration of glucose, the maximum current density, J_{max}, of the material can be determined. Michaelis-Menton kinetics can be applied to an electrochemical sensor to determine the maximum current density, J_{max}, and the Michaelis constant of the enzyme, K_M. K_M provides insight into the efficiency of the enzyme immobilized in the polymer-supported phase when compared to the K_M of a similar system in solution. In this second method of analysis, it should be noted that a direct measure of the exchange between a mediator and the enzyme is not the focus, but a measure of the performance of the entire system.

1.2.5 – Current State of Biofuel Cell Design and Performance

The discussion thus far has been focused on development and design of bioelectrode materials. However, very little of the discussion has been presented regarding the current state of the biofuel cell industry. For example, a large focus on the use of carbon nanotubes has been observed in the last decade, from both the Glatzhofer group and others[23, 69-71]. Carbon nanotubes, when incorporated into redox polymer films, have been found to greatly increase the amperometric performance of a bioelectrode. By incorporating Single Walled Carbon Nanotubes (SWNTs) into a dimethylferrocene-modified LPEI (Me_2Fc-C3-LPEI) film containing GOx, an optimized current of 11.2 mA/cm^2 was observed, whereas an electrode made from only Me_2Fc-C_3-LPEI and GOX produced approximately 0.6 mA/cm^2 [69]. When incorporated into a BFC using an air-breathing Pt cathode, a maximum power output was determined to be 340 μW/cm^2. It is

speculated that the incorporation of SWNTs into a polymer film increases the geometric surface area of the electrode, the conductivity of the electrode material, and nanotube network connectivity[69].

Other groups have used compressed carbon nanotubes to create entire electrode materials[70]. Reports by Zebda demonstrate a compressed material made from Multiwalled Carbon nanotubes (MWNTs) and GOx, and well as MWNTs and Laccase[70]. The reported current density for the current GOx-based bioanode was optimized to be 8 mA/cm^2, while the maximum current density for the Laccase-based biocathode was determined to be 5.8 mA/cm^2. When the two electrodes were connected to form a biofuel cell, the resulting power output was 1.25 mW/cm^2. While this design does provide an attractive alternative to a mediated biofuel cell, it should be noted that the MWNT electrode parameters, in particular the maximum current density, are still lower than those reported from mediated biofuel cell and bioelectrode systems described earlier in this section. However, there is some disagreement with the design of mediatorless biofuel cells[72]. Bartlett argues that most, if not all, evidence of direct electron transfer is a result of catalase and flavin impurities that are found in commercially available enzymes. While bioelectrodes prepared from MWNTs and GOx show that there is indeed electron transfer occurring between the GOx and the MWNT electrode surface, the operating potential of the electrode surface matches the potential of flavin impurities in GOx exactly. He claims that additional metal impurities may also alter the mediation occurring within the bioelectrode system, particularly with the reduction of oxygen[72]. It should be noted that this topic was introduced as a position that supports the further development of mediated systems, instead of taking the approach described by Zebda.

Other design schemes have been developed for mediated biofuel cells. For example, multiple enzymes have been immobilized in a Fc-LPEI material to perform more than one oxidation[63, 66]. Invertase catalyzes the hydrolysis of sucrose into glucose and fructose. Fructose Dehydrogenase (FDH) and GOx were immobilized with Invertase in Me_4Fc-C_3-LPEI to prepare anodic films that can harness electrons from two reactions simultaneously[63]. While the maximum current densities for this system are not very high (maximum current density = 640 μA at 37 ° C), it is a demonstration that a multiple enzyme cascade can be achieved for use in bioelectrode materials. Work by Zhu also utilized this approach with a multiple enzyme system that utilized the oxidation of glucose units in maltodextrins according to a synthetic enzyme pathway[73]. These enzymes, however, were not immobilized in a polymer matrix, but dissolved in solution. The benefit to this design, however, is that more than 2 electrons can harnessed from a glucose molecule. Their bioelectrode allowed 24 electrons to be harnessed[73]. A 13-enzyme cascade mediated by vitamin K_3 generated a maximum current density of 6 mA/cm^2, which suggests that enzymatic cascades could be a very useful design for glucose biofuel cells. It also demonstrates the limitation that most biofuel cells exhibit: only one reaction is utilized and the organic product still contains a large number of electrons to harness for use in the bioelectrode system.

Thus far, the discussion has centered on the oxidation of glucose at the anode and the organometallic mediators used to harness the electrons from GOx in this catalytic process. Bioelectrodes, however, can also serve as reduction sites. As a site for reduction, biocathodes have used laccase to reduce oxygen into water[55]. Platinum-based air breathing cathodes have also been used by the Glatzhofer group and others instead of biocathodes[57, 74-75]. The use of chemical reactions occurring at the cathode of a fuel cell has mainly been restricted to the reduction of oxygen, however, it could be imagined that other electrochemical reactions could be paired with

bioanodes. For example, an electrochemical or electrocatalytic reaction could be used to accept the electrons from the bioanode. In order for this pairing to work, however, there are a large number of factors to be considered, such as the potential at which the catalytic reduction occurs, the temperature of the reaction, and how well these parameters align with the bioanode. It could be envisioned that, theoretically, the reduction at the cathode and the oxidation of the anode of the cell could use the same substrate. This could be advantageous, as it could be imagined that both electrodes could be placed in the same solution, resulting in a compartmentless self-powered electrolysis, akin to a disproportionation reaction. Figure 1.13 outlines a general scheme of how this theoretical system would operate.

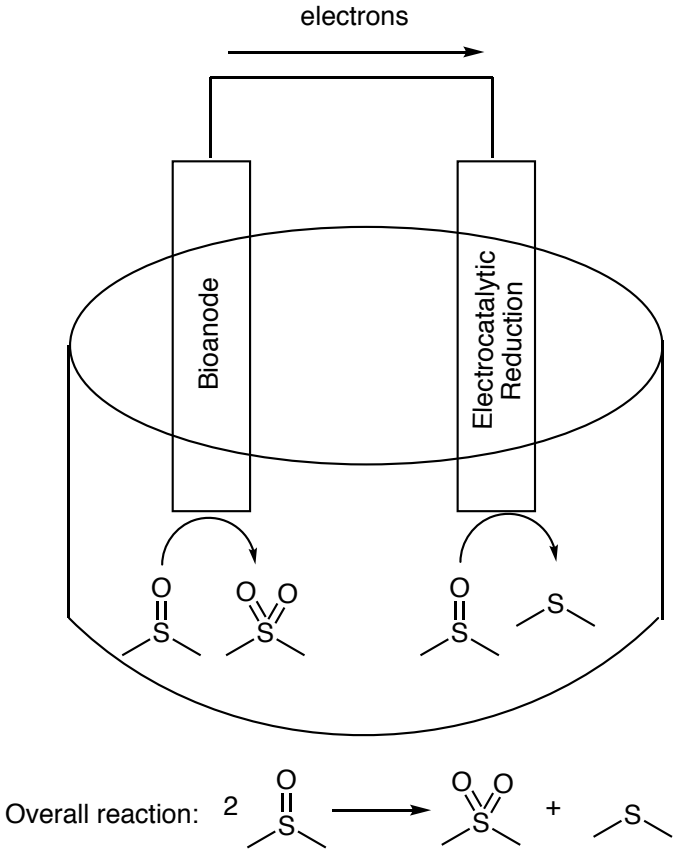

Figure 1.13 A theoretical schematic for a bioanode that oxidizes a substrate and uses the electrons harnessed from the reaction to power an electrocatalytic reduction on the same substrate.

Glucose bioelectrodes could be used as the bioanode in this example. A deoxydehydration reaction, where two neighboring hydroxyl groups are removed as water and an oxygen atom to generate an alkene, could serve as an attractive candidate for an electrocatalytic reduction occurring at the cathode[76]. Glucose contains five vicinal hydroxyl groups in its acyclic form, and could be considered a candidate for the DODH reaction. The remainder of this chapter will be focused on the fundamentals of the Deoxydehydration reaction.

1.3 Deoxydehydration Reactions

Deoxydehydration (DODH) reactions involve the removal of vicinal hydroxyl groups to form an alkene. In the process, the equivalent of an oxygen atom (deoxy) and a water molecule (dehydration) are removed from the vicinal diol.

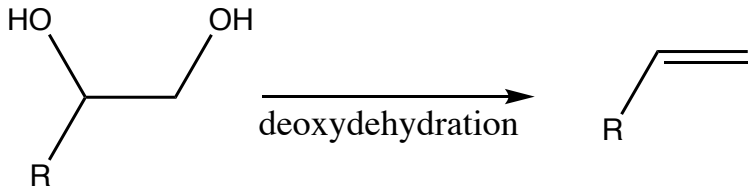

Figure 1.14 – The dexoydehydration reaction where a vicinal diol is converted to an olefin.

A catalytic DODH reaction was first reported by Cook and Andrews, utilizing a (η-5-pentamethylcyclopentadienyl)rhenium trioxo complex with triphenylphosphine as a chemical reductant[76]. Under these conditions, 1-phenyl-1,2-ethandiol was converted into styrene in approximately 95% yield. In addition to 1-phenyl-1,2-ethandiol, other polyols have been converted into their corresponding alkenes in excess of 80% yield. These reactions were run in chlorobenzene under high pressure for one to two days at 90 ˚C to 100 ˚C. One noteworthy effect lies in the use of coordinating solvents. The rate of reaction was hindered when coordinating solvents were used, suggesting a competition with the polyol by the solvent for the metal

complex. In addition, the rate of reaction was enhanced upon addition of p-toluenesulfonic acid (TsOH). This rate enhancement suggests that the acid favors formation of the metalloglycollate species shown in **Figure 1.15**. Since its initial discovery, multiple rhenium-based metal complexes and non-precious metal complexes have been demonstrated to be effective DODH catalysts[77-81].

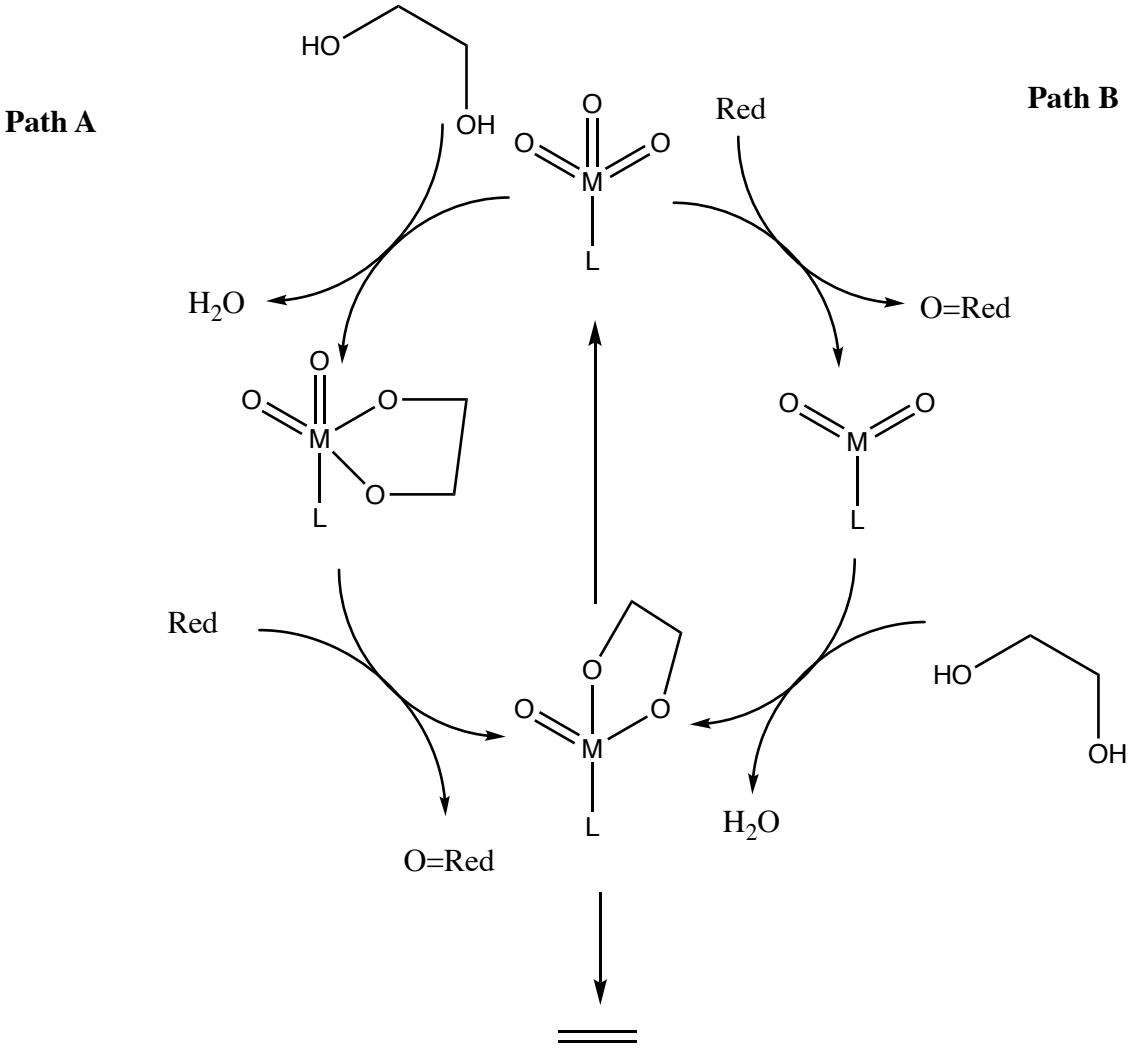

Figure 1.15 The two possible catalytic cycles proposed by the Cook and Andrews[76].

The mechanism is believed to proceed through one of two pathways, as shown in Figure 1.15: Pathway A – through metalloglycolate formation, followed by reduction, then fragmentation; or Pathway B – through catalyst reduction, metalloglycolate formation, then

fragmentation[76]. The Nicholas group has demonstrated that the mechanistic pathway of this reaction is dependent upon the nature of the metal catalyst and the reductant. We have yet to be able to predict the effects of a catalyst or reductant on the mechanism of the pathway[82-84]. Currently, these reactions are run under high temperature and high-pressure conditions. These conditions range from 100 °C to 150 °C for one to five days inside of sealed pressure reactors.

1.3.1 – Scope of Catalysts

Reports of one of the first catalysts for DODH other than Cp^*ReO_3 was published by the Gable group wherein they reported (tris-dimethylpyrazolylborate)trioxorhenium (Tp^*ReO_3) as a successful catalyst using triphenylphosphine as a stoichiometric reductant[78-79]. When compared to the Cp* ligand, the Tp* catalyst was found to be less active, but more robust. This catalyst also allowed more economically efficient and more environmentally-favorable solvents, such as toluene, but the reactions were run at 150 °C for one to five days using a substrate scope similar to that used by Cook and Andrews. For both systems, it was noted that the rate-limiting step for the catalytic cycle was alkene extrusion[76, 78]. Both studies noted that the rate of reaction, with respect to Cp^*ReO_3 or Tp^*ReO_3, was independent of metal complex concentration. When this reaction rate was compared to the rate of retrocyclization of the isolated rhenium glycolate species, they were found to be identical. This suggested that alkene extrusion is the rate-limiting step of the reaction.

Another notable catalyst in the DODH reaction is methyltrioxorhenium[85-86]. The Abu-Omar group demonstrated that with molecular hydrogen, the commercially available methyltrioxorhenium catalyst could be used for the conversion of epoxides to alkenes at 150 ˚ C. Their work hypothesized that a reduced rhenium glycolate species formed after prereduction of the catalyst[85]. However, by comparing the enthalpic penalties of the addition of molecular

hydrogen to methyltrioxorhenium, Nicholas and Lin concluded that the formation of a dioxorhenium (VII) glycolate seemed more energetically reasonable than a dihydroxomonooxorhenium (V) species[83]. This work further supports the implication that alkene extrusion is the rate-determining step in this reaction, as the alkene extrusion had the highest enthalpic barrier in the reaction[83].

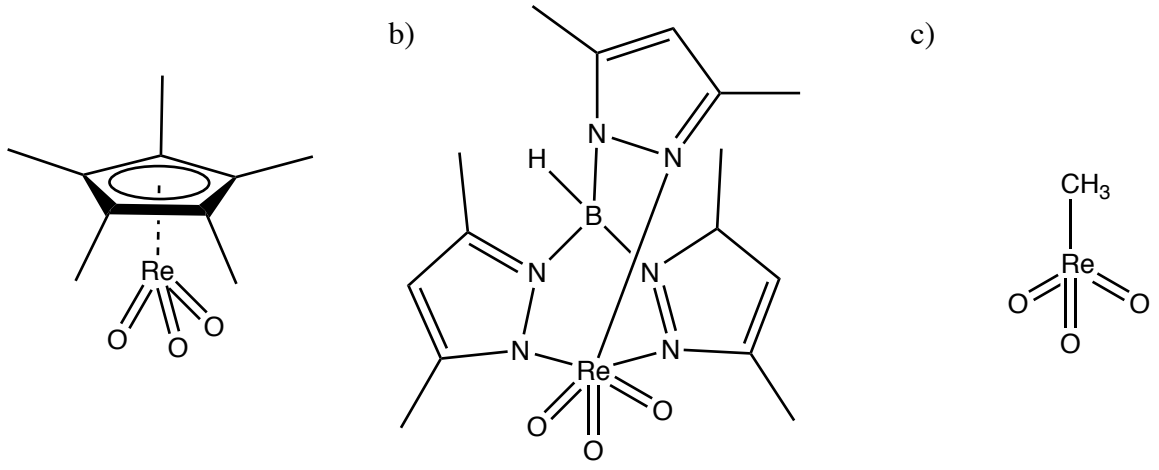

Figure 1.16 The structures of a) Pentamethylcyclopentadienyltrioxorhenium
b) (tris-dimethylpyrazolylborate)trioxorhenium c) methyltrioxorhenium

The Nicholas group has also reported that ammonium perrhenate, another commercially available substance, can be used successfully as a DODH catalyst[87]. Ammonium perrhenate was effective for converting a wide variety of diols and epoxides to the corresponding olefins with a large assortment of reducing agents. Effective reducing agents included assorted sulfites, benzyl alcohol, and other secondary alcohols. In addition, McClain demonstrated that a cationic rhenium species, *trans*-$[(py)_4ReO_2]^+Cl$ is capable of carrying out DODH reactions using elemental reductants[82]. This was the first demonstration of a cationic rhenium catalyst carrying out a DODH reaction.

1.3.2 Non-precious Metal Deoxydehydration Reactions

While there have been a large number of effective rhenium-based catalysts, rhenium is very expensive. This makes the commercial scalability of this reaction impractical. Work by Chapman and Nicholas recently demonstrated that oxovanadium complexes are capable of performing DODH reactions[88]. Assorted *m*-vanadate salts and chelated dioxovanadium complexes were investigated. Of the nine catalysts investigated, the species with the highest conversion and yield was [(butyl)$_4$N][pyridine-2,6-dicarboxylate)VO_2] with conversions at 100% and yields in excess of 95%.[88] Substrates in which these results were observed include 1,2-phenylethanediol, 1,2-octanediol, and 1,2-tetradecanediol. **Figure 1.17** shows the structure of the vanadium catalyst developed by Chapman et al.

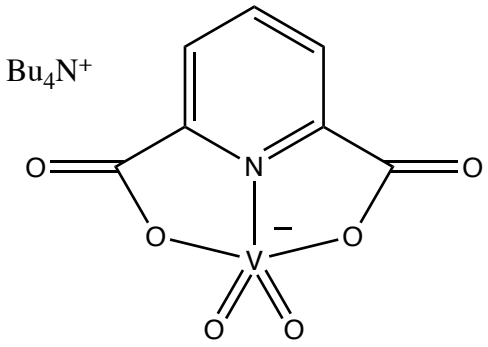

Figure 1.17 – Tetrabutylammonium [(pyridine-2,6-dicarboxylate)dioxovanadate]

For these reactions, both benzene and chlorobenzene were used as solvents, and triphenylphosphine and sodium sulfite were the best stoichiometric reductants. These conversions were conducted between 150 °C and 170 °C under high-pressure reaction conditions. In addition, our lab group reported solid-supported oxomolybdenum catalysis on similar substrates. While yields were limited, approximately 20%, and catalyst leaching was detected, this is one of the few reports where molybdenum oxide is reported as a solid-supported DODH catalyst[89-90].

1.3.3 – Effect of Reductant on Catalysis

The nature of the catalyst is not the only variable that must be considered in a DODH reaction. Phosphines appear to be the most commonplace reagent used in these systems[76, 88, 91]. Phosphines, however, are not easily separated from reaction mixtures, can be expensive, and are air-sensitive. Thus, these molecules are not ideal for commercial scale-up. Work from the Nicholas lab group demonstrated that sodium sulfite and tetra(N-butyl)ammonium sulfite can successfully be used as reductants[92]. When DODH reactions are run in a non-polar solvent, sodium sulfite and its oxidized form, sodium sulfate, remain insoluble and are easily separated. Their limited solubility, however, can still act as a potential limitation in the ability of sodium sulfite to be used as a commercial reducing agent.

A variety of primary and secondary alcohols have also been used as stoichiometric reductants for DODH reactions[86, 93]. Work by Boucher-Jacobs and Nicholas demonstrated that benzyl alcohol, used in combination with ammonium perrhenate, is an effective system for catalyzing DODH reactions of polyols[87]. This work investigated the capabilities of an ammonium perrhenate/benzyl alcohol system with a series of polyols and glycols at 150 °C in non-polar solvents. It was noted that the ammonium perrhenate was insoluble in non-polar solvents at room temperature. This allowed for facile catalyst recovery and reuse. Boucher-Jacobs *et al* showed not only catalyst recovery, but the ability of recovered ammonium perrhenate to catalyze DODH reactions through multiple cycles. In addition, the oxidized benzaldehyde could be easily precipitated with sodium bisulfite, leaving the desired olefin after a simple purification.

Recent work by McClain *et al* demonstrated elemental, heterogeneous reductants were effective reductants for both ammonium perrhenate and , *trans*-$[(py)_4ReO_2]^+Cl$[82]. These reactants

included elemental iron, zinc, manganese, and carbon. This removed the difficulty associated with removal of phosphine-oxides, the higher cost, and the increased toxicity and waste associated with phosphine usage, and eliminated the need for precipitation of aldehydes by allowing for facile purification by filtration. This also demonstrated the possibility of heterogeneous surface reduction of DODH systems, either in the reduction of the metallaglycolate, or of the catalyst itself.

The differing nature of these reductants suggest that there could be differing mechanisms of action for the reduction step in DODH. For reductants such as phosphines and sulfites, it is likely that direct oxygen atom transfer is the mechanism for the reduction step. For elemental reductants, it is possible that direct electron transfer can occur on either the catalyst, or the metaloglycolate species. Previous work by Hermann et al reports that a (N,N,N-1,4,7-trimethyltriazacyclononane)trioxorhenium (VII) metal complex can be reduced by elemental Zn in methanol to produce the corresponding dihydroxomonooxorhenium (V) species[94]. When primary and secondary alcohols act as reductants in a DODH reaction, it is likely that a proton transfer is required for reduction. This suggests that the mechanism of the reduction step, and the order of the mechanistic steps, may change between each set of reaction conditions. Electrochemical reductions for the DODH pathway have yet to be investigated.

1.4 Project Goals and Challenges

In order to establish a comprehensive scope to the work in the upcoming chapters, it is essential to include some fundamental questions in this section.

Can a bioelectrode power an electrochemical DODH reaction?

In considering what would allow for a DODH to be powered by a bioanode, the Gibbs' Free Energy of the reaction, ΔG_{rxn}, must be less than zero. Connecting the ΔG_{rxn} to the

electrochemical potential of the process, the free energy is dependent on the number of electrons transferred in the balanced electrochemical process, n, Faraday's constant, F, and the standard electrochemical potential of the fuel cell, $E°_{cell}$, according to Equation 4.

$$\Delta G = -nFE°_{cell} \quad (4)$$

A negative ΔG_{rxn} means that a positive standard electrochemical potential is required for an electrochemical cell to operate spontaneously. The electrochemical potential of the cell is the difference between the standard reduction potential of the cathodic process, $E°_{cathode}$, and the standard reduction potential of the anodic process, $E°_{anode}$, according to Equation 5.

$$E^o_{cell} = E^o_{cathode} - E^o_{anode} \quad (5)$$

Therefore, to obtain the desired overall positive potential, it is essential that $E°_{cathode} > E°_{anode}$. In this theoretical example of a bioanode-powered DODH, the $E°_{cathode}$ is the potential of the DODH and the $E°_{anode}$ of the bioanode.

How would the bioanode affect $E°_{cell}$?

In considering how this positive cell potential could be achieved, it will be necessary to consider the magnitude of the standard reduction potentials of each process. If a sufficiently strong oxidative process is used in the anodic reaction, the standard reduction potential is strongly negative. For example, the standard reduction potential of GOx catalyzing the oxidation of glucose is -0.210 vs SCE. This would mean that the cathodic reaction would need to have a standard reduction greater than -0.210 V vs SCE to keep the $E°_{cell} > 0$ V. One important note to consider in the bioaode is that the enzyme is not what determines the working potential of the electrode. It is the reduction potential of the mediator, not the enzyme, that would affect $E°_{cell}$, as discussed in Section 1.2.4 of this chapter.

How would the DODH affect the $E°_{cell}$?

The second influence on the $E°_{cell}$ is the reduction potential of the cathodic process. A sufficiently positive DODH reduction potential favors a positive $E°_{cell}$. For example, if the reduction potential of the DODH process is 0.5 V, then the reduction potential of the bioanode must be less than 0.5 V to maintain a positive $E°_{cell}$. However, if the reduction potential of the DODH is -0.5 V, then a reduction potential less than -0.5 V is needed in the anodic process to power the reduction.

Can DODH be turned into an electrocatalytic reaction?

In order for an electrochemical reaction to be carried out, a sufficient potential must be applied. Most examples of electrocatalytic reactions are currently powered by advanced electrochemical instruments, such as a potentiostat, instead of a bioanode[95-97]. Electrocatalysis, in the scope of DODH, could utilize an electrode surface to act as the electron source a reaction[95-97]. The benefits associated with electrocatalytic processes include, as a general rule, very high turn-over numbers, and often times lower temperatures than their thermally-based reaction analogues[98]. Theoretically, the chemical reductant used in the thermocatalytic process could be replaced with a proton source and an electron source, and it is reasonable to speculate that an electrocatalytic DODH can be developed.

Once the DODH reaction has been adapted, how can we find bioanode materials that will provide a sufficient working potential for the DODH reaction?

While there have been great advancements in the power and energy output of enzymatic biofuel cells, there has been minimal achievement in the fundamental understanding of the components that make an effective electrode material from the standpoint of the polymer components: the enzyme, and the electron-transport mediator. Further, there is not a connection

between the performance of a second-generation bioelectrode material when in the solution state versus in the polymer-supported state. There is also not an adequate method of mediator design targeted toward tuning redox potentials. Finally, it has been suggested that there is a specific interaction between GOx and a ferrocene mediator. Fc-LPEI materials displayed larger J_{max} values as compared to PVP-OS materials, however, the Fc-LPEI materials do not shuttle electrons as well as the PVP-Os materials, as noted in **Section 1.2.3**[25, 59]. Other methods that have sought to characterize these connections led to a very complex electrochemical kinetic analysis, or an overly-simplified analysis of i_{cat}. In order to tune the biofuel cell to a certain working potential sufficient for DODH, it is essential that a fundamental understanding of the interaction between the components is obtained. In addition, there must be an understanding of how these interactions translate to an immobilized state when the materials are trapped on an electrode.

To summarize the overall scope of this work, it can be said that there are two main objectives to be investigated: 1) Development of a simple, quantitative tool for determining if a mediator will be compatible with an oxidoreductase, using Fc and GOx as a specific tool for analysis. Extension of this method to development of polymer-supported bioelectrode material development will be carried out, if found; and 2) Developing an electrochemical version of the DODH reaction, and, ultimately, an electrocatalytic DODH process. This could lead to the development of a bioanode-powered DODH that could produce fuel additives in a disproportionation-like process, shown in Figure 1.15.

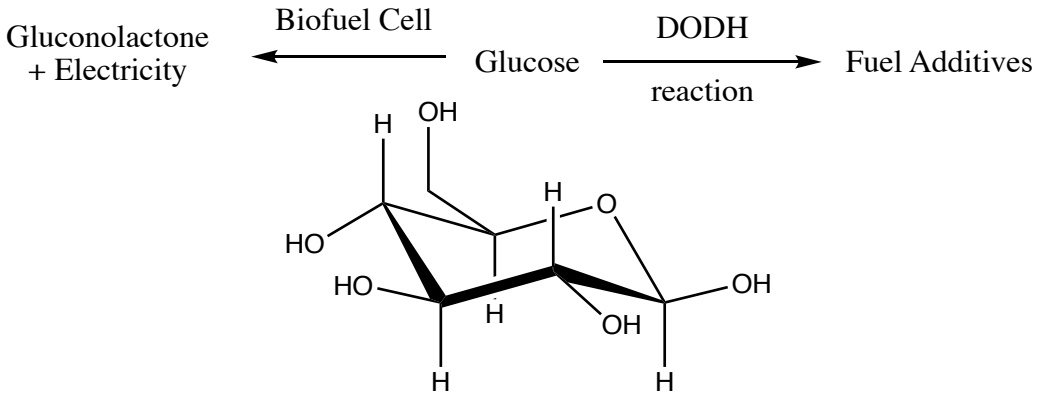

Figure 1.15 demonstrates how renewable material, glucose, could be used for both a biofuel cell and a DODH reaction. It should be noted that biofuel cells and DODH have been researched independently, and the attempt to bridge the two topics is largely theoretical.

1.5 Chapter Preview

In considering the path to achieving our aforementioned goals, there are two main focuses in this document. Chapters 2, 3, and 4 are focused on the development of a tool that allows for a method of screening appropriate mediators to make the potentials of the redox mediator in a biofuel cell align with the electrochemical potential of the enzyme. This would provide a more favorable potential for the anodic reaction. Chapter 5 is targeted toward identifying the reduction potential of a series of rhenium complexes that could be used in DODH reactions, with the goal of finding ways to reach a more favorable reduction potential in the cathodic process.

Chapter 2 - The Detection of a Ferrocene-Glucose Oxidase Binding Isotherm

Herein is reported a novel approach to detecting a binding isotherm observed electrochemically with ferrocene and Glucose Oxidase, where Glucose Oxidase is treated as an electrochemical inhibitor. A solution of ferrocene is titrated with different amounts of GOx and a decrease in the amperometric response of the ferrocene leads to the calcuation of K_a based on the

modeling of urea inhibiting the electrochemical activity of copper. From this isotherm, an association constant, K_a, is developed. The modeling and application of this binding isotherm is discussed. This isotherm suggests that there may be a unique interaction that is displayed when a mediator interacts with an enzyme. This could serve as a tool that could indicate the effectiveness of a compound to act as a mediator.

Chapter 3 –The Effects of Electron Donating and Electron Withdrawing Groups on a Langmuir Binding Isotherm Between Glucose Oxidase and Ferrocene

The binding isotherm from Chapter 2 is applied to a range of ferrocene derivatives, mainly focusing on the effects of the functional group on the magnitude of K_a. In addition, it will be discussed if this newly observed Ka value can be used to predict the mediative capabilities of a molecule in the solution state. A new ferrocene derivative, methoxy(ethoxy(ethoxy(methylferrocene))) (FcG2OMe), is determined to have potentially higher efficiency as an electron transport mediator for GOx, as evidenced by the highest K_a value. It could be envisioned that this binding might lead to more effective materials in the polymer-supported state, as the mediator may be better at "wiring" the enzyme into the electrode.

Chapter 4 – Synthesis and Characterization of a Ferroceny Glycol Ether-Containing Linear Poly(ethylenimine) for Use in Bioelectrode Materials Based on K_a of a Langmuir Binding Isotherm

A new bioelectrode material is prepared from LPEI and FcG2OMe is developed, based on the observation of the aforementioned isotherm. The new enzyme-containing material is characterized in the absence and the presence of glucose. The amount of cross-linking agent is varied to make a more stabile material.

Chapter 5 – Steps Toward a Rhenium-Catalyzed Electrocatalytic Deoxydehydration Reaction

A new rhenium catalyst is demonstrated to have thermal catalytic abilities, as both the perrhenate and hexafluorophosphate salts. The electrochemistry between these two salts is compared, as there are significant differences. A rhenium glycolate is prepared to investigate the likely mechanistic pathway, and to investigate the possibility of both an electrochemical and electrocatalytic deoxydehydration reaction using this new rhenium complex as a catalyst.

Chapter 2: The Detection of a Ferrocene-Glucose Oxidase Binding Isotherm

2.1 - Introduction

Biofuel cells (BFC) and biosensors have attracted a great deal of attention over the last two decades[99-102]. There is a vast array of applications for these bio-based electronic tools, ranging from detection methods for antibodies, cancer, in-vivo glucose monitoring, and environmentally-friendly electrical batteries[103-104]. Of particular interest in this field is the glucose bioelectrode, which uses glucose oxidase (GOx) to oxidize glucose to gluconolactone, and an electron transport mediator (ETM) to harvest the electrons from the Flavin Adenine Dinucleotide (FAD) at the center of the enzyme's active site. The number of electrons shuttled to the electrode surface can be used to quantify the amount of glucose in the sample. As mentioned in Chapter 1, second generation bioelectrode fabrication methods are attractive for oxidoreductases, such as GOx, as the enzyme's FAD unit is buried approximately 15 Å deep within the active site[22]. The pathway of the biocatalyzed oxidation process has been determined to proceed *via* the ping pong mechanism shown in Figure 2.01, where the substrate glucose diffuses to the active site of GOx and is oxidized to gluconolactone. The gluconolactone then diffuses away from the reduced active site. A co-oxidant molecule, in this case an electron transport mediator (ETM), diffuses to the active site to oxidize the $FADH_2$ in the active site back to FAD, and then diffuses away to the electrode surface. In characterizing how effectively a molecule can act as a mediator, kinetic analysis is commonly applied. Oxygen is the co-oxidant for GOx in nature, however, in the absence of oxygen, it has been demonstrated that ferrocenes, organoosmium complexes, and organoquinones effectively act as co-oxidants that can shuttle electrons to an electrode surface[25, 105-108].

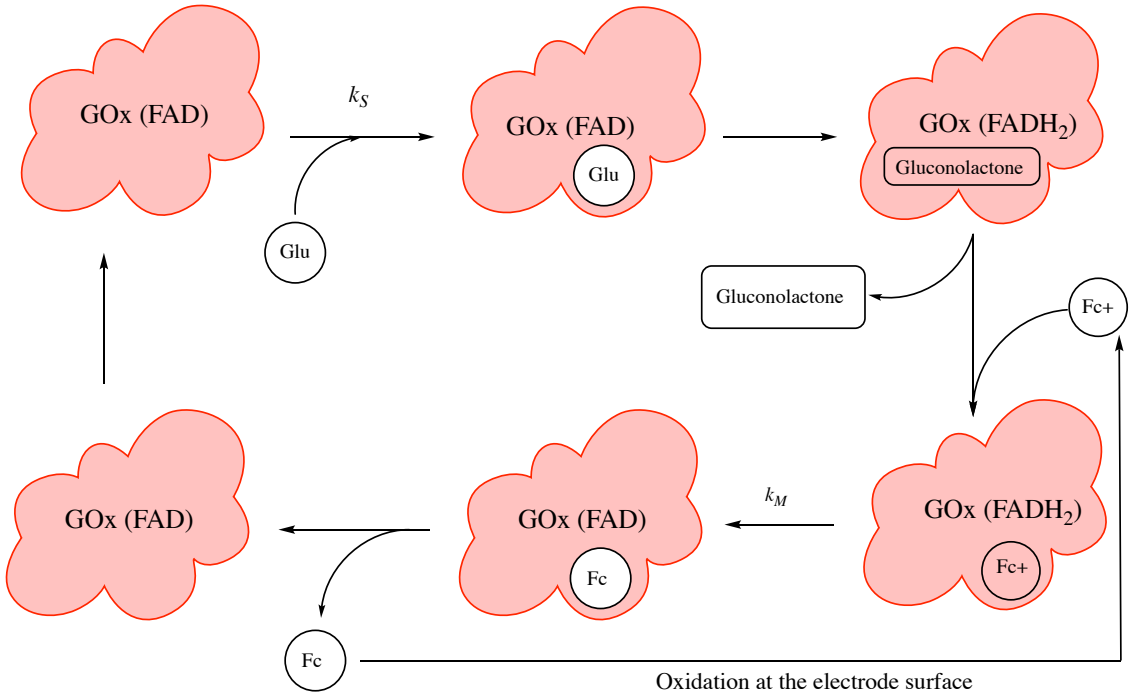

Figure 2.01 The catalytic cycle through which GOx oxidized glucose and is then reoxidized by ferrocenium ions in solution. Glucose (Glu) diffuses to the active site of GOx(FAD) and is oxidized by GOx(FAD) to gluconolactone. The reduced form of the enzyme, GOx(FADH$_2$), is then oxidized by ferrocenium ions (Fc+) to form ferrocene (Fc) and GOx(FAD). The ferrocene is oxidized by the electrode surface to regenerate the Fc+.

When comparing how effectively one molecule acts as a mediator compared to another molecule, it is common practice to characterize the rate of electron transfer, k_M, between the reduced $FADH_2$ and the oxidized mediator[67]. One of the first characterizations of an organometallic mediator by its rate constant for electron transport within the system, k_M, was conducted by Hill et al[36]. However, more recent characterization techniques have led to an increased efficiency in determining k_M. Traditionally, most laboratory groups have relied on this k_M to estimate a mediator's practicality in a biosensor. The current method, as characterized by Bartlett et al, utilized a linear plot of the catalytic current, i_{cat}, versus the square root of the enzyme concentration, $e_\Sigma^{1/2}$, to screen a variety of ferrocinium derivatives using the equation

$$i_{cat} = nFAD_M^{1/2} k_M^{1/2} m_0 e_\Sigma^{1/2} \qquad (1)$$

where *n* is the number of electrons transferred from FAD to the mediator, A is the surface area of the electrode, $D_M^{1/2}$ is the diffusion coefficient for the mediator (the accepted value for ferrocinium and a range of ferrocinium derivatives has been calculated to be 3.0 x 10^{-6} cm^2 s^{-1}), m_0 is the mediator concentration, and *F* is Faraday's constant[109]. This approximation, however, operates under the assumption of pseudo-first order conditions, when the concentration of glucose is significantly higher than the k_S, the rate constant of the reaction catalyzed by GOx where glucose is converted to gluconolactone. Since this method of analysis was developed, the kinetic constants, k_M, of a large array of ferrocene, organoosmium, and quinone mediator constants were determined. It was noted that, while the corresponding ferrocenium and oxidized salts of the molecules were sufficiently capable of acting as rapid oxidants for GOx($FADH_2$), the observed rate constants for the electron transfer from GOx($FADH_2$) to each oxidized salt were still lower than the electron transfer rate from GOx($FADH_2$) to oxygen[110]. Summaries of the rate constants and potentials for more commonly appearing ferrocene mediators are presented in Table. 2.1[36]. It should be noted that all ferrocene derivatives are sufficiently soluble to obtain a concentration of 0.5 mM to be considered a viable candidate for analysis.

Ferrocene Derivative	E_0 vs SCE (mV)	k_M (L mol^{-1} sec^{-1})
1,1'-dimethylferrocene	100	0.77 x 10^{-5}
Ferrocene	165	0.26 x 10^{-5}
Vinyl ferrocene	250	0.30 x 10^{-5}
Carboxyferrocene	275	2.01 x 10^{-5}
1,1'-dicarboxyferrocene	285	0.26 x 10^{-5}
(dimethylamino)methyl ferrocene	400	5.25 x 10^{-5}

Table 2.1 A summary of the redox potential (E_0) and the mediative rate constant, k_M, as reported by Cass et al for a series of ferrocene derivatives[36]

However, there are certain drawbacks to this method of analysis. As technology has advanced, there have been some issues discovered in the assumptions made by the original experimenters. It was noted that choosing the appropriate concentrations of glucose, enzyme, and mediator for

experimental conditions were not as simple as originally thought. Those experiments that use concentrations of mediator and enzyme that are 100 times less the concentration of substrate did not meet the conditions for pseudo-first order analysis. In fact, dual concentration dependence existed for both the mediator and the substrate. Some examples of conditions where pseudo first-order kinetics were applied did not sufficiently have their concentrations in the appropriate ranges[68]. In addition, the methods of analysis are rather complicated and involve a number of extensive calculations and simulations[67]. Conversely, the overly-simplified method where the i_{cat}, the catalytic current produced when the enzyme's substrate is introduced, is not a fair measure for a mediator's efficiency due to the aforementioned dual dependence on the concentration of the substrate and mediator[44]. It should be noted, however, that the electron transfer rate constants that have been discussed only refer to bioelectrode systems with the electron generating and transport species in solution. When analyzing systems where the mediator is "wired" to the enzyme, a different kinetic analysis is applied.

When enzymes and mediators are immobilized within a polymer material, a more traditional Michaelis-Menten model may be applied to the electrochemical system[111]. By incorporating the dependence on both the mediator and the substrate, equation 2 has been developed.

$$I = \frac{I_{max}}{1+{K_m}/{[M_{ox}]}+{K_S}/{[S]}} \qquad (2)$$

where K_M is the Michaelis constrant of the enzyme, $[M_{ox}]$ is the bulk concentration of the oxidized mediator, K_S is the Michaelis constant of the substrate, and [S] is the bulk concentration of the substrate, I is the observed current at a given substrate concentration, and I_{max} is the maximum current that the electrode can produce. Current methods of characterizing the "wired" bioelectrodes used bythe Glatzhofer group include looking at these parameters, I_{max} and $K_{m,}$ as

parameters of analyzing the overall polymer-supported material performance and enzyme performance, respectively. However, instead of I_{max}, the Glatzhofer group uses the maximum current density, J_{max} to help normalize material performance when using different types of electrodes[63-65].

A final method of analyzing a material's performance is by looking at the product of the concentration and the electron diffusion coefficient, $cD_e^{1/2}$. This method of analysis is helpful in analyzing the Marcus collisions between mediators that are generally accepted as methods of electron transfer from the enzyme to the electrode[112]. The Glatzhofer group has developed a bioelectrode material made from GOx and linear poly(ethylenimine) (LPEI) functionalized with a series of ferrocene derivatives[48, 59, 64, 75]. When compared to previous GOx-containing bioelectrodes, it was noted that our materials amperometrically outperformed organoosmium-based materials. One interesting note, however, is that our materials were not able to transport electrons as well as the organoosmium material[113]. It was speculated that, based on these results, there was a specific interaction between GOx and the ferrocene mediator that allows for ferrocene to accept electrons from GOx more effectively than the osmium complexes. Thus, it seems logical that there is need for a tool that can characterize a specific interaction, if it indeed exists, between an enzyme and a mediator. Microcalorimetry seems to be an ideal method for this method of detection, as very small changes in heat are detected when a new interaction is detected. However, this method appears to be best suited for slower processes that generate small amounts of heat. This method would not be applicable on a fast time scale, if that is indeed the time scale on which this interaction could occur. Further, unpublished observations report that when our Fc-LPEI polymer solutions are mixed with solutions of GOx, a precipitate forms. This has been observed when solutions of Cl-Fc-LPEI and Laccase are mixed, as well as Fc-C1-LPEI

and GOx during electrode fabrication. Microcalorimetry, however, requires that precipitates are not formed, or methods to correct for the enthalpy of phase change would have to be developed. Thus it is desirable to develop other screening tools that may also be more accessible to researchers in an electrochemical laboratory.

Hypothesis

If there is an interaction between ferrocene and GOx that is responsible for the aforementioned increase in amperometric current while there is an observed decrease in $cDe_{1/2}$, there may be a method of detecting it electrochemically *via* a change in redox potential. $E_{1/2}$ is altered by adding electron donating and withdrawing groups to the cyclopentadienyl ring on the ferrocene. Thus if there is a specific interaction between the enzyme and the mediator, the electronic properties of the ferrocene may be altered. As an additional possibility, it can be speculated that, since the electron-transport between ferrocene and the electrode is diffusion limited, a ferrocene-GOx adduct may diffuse at a different rate as compared to "free" ferrocene. This possible Fc-GOx interaction may also affect the amperometric response. Cyclic voltammetry is an attractive tool for analyzing both of these parameters, as both amperometric response and electrochemical potential can be observed. By titrating ferrocene with GOx, it seemed reasonable that one or both of these parameters may change.

2.2 Discussion and Results

2.2.1 Selection of Mediator

The Glatzhofer group has extended the scope of the optimization of ferrocene containing LPEI (Fc-LPEI) to realize that there are several factors that appear to affect maximum current density, including the length of the tether connecting the mediator to the polymer, the degree of methylation or other functionalization on the ferrocene ring, and the amount of cross-linking

agent used in preparing the Fc-LPEI films[48, 57, 64, 75, 113]. To simplify the effects of the aforementioned parameters, we will use an unmodified ferrocene molecule that is analogous to the original (ferrocenyl)methyl- modified linear poly(ethyleminime) (Fc-C1-LPEI) material first characterized by Meredith et al[57, 113], as shown in Figure 2.02.

When building a small molecule analogue of this material, it seemed reasonable to begin these studies with (dimethylamino)methylferrocene (DMAFc). In addition, this molecule has been demonstrated to have an excellent kinetic constant when used as a mediator in the free solution state with GOx[114]. It was noted by Meredith, however, that the DMAFc exists between the amine and the ammonium salt at physiological pH. This competing process could only act to complicate the analysis, as both the amine and ammonium species have different electrochemical potentials. To eliminate the complication of this pH-dependent equilibrium, a third methyl group was added to the nitrogen to remove the basic lone pair on the nitrogen atom.

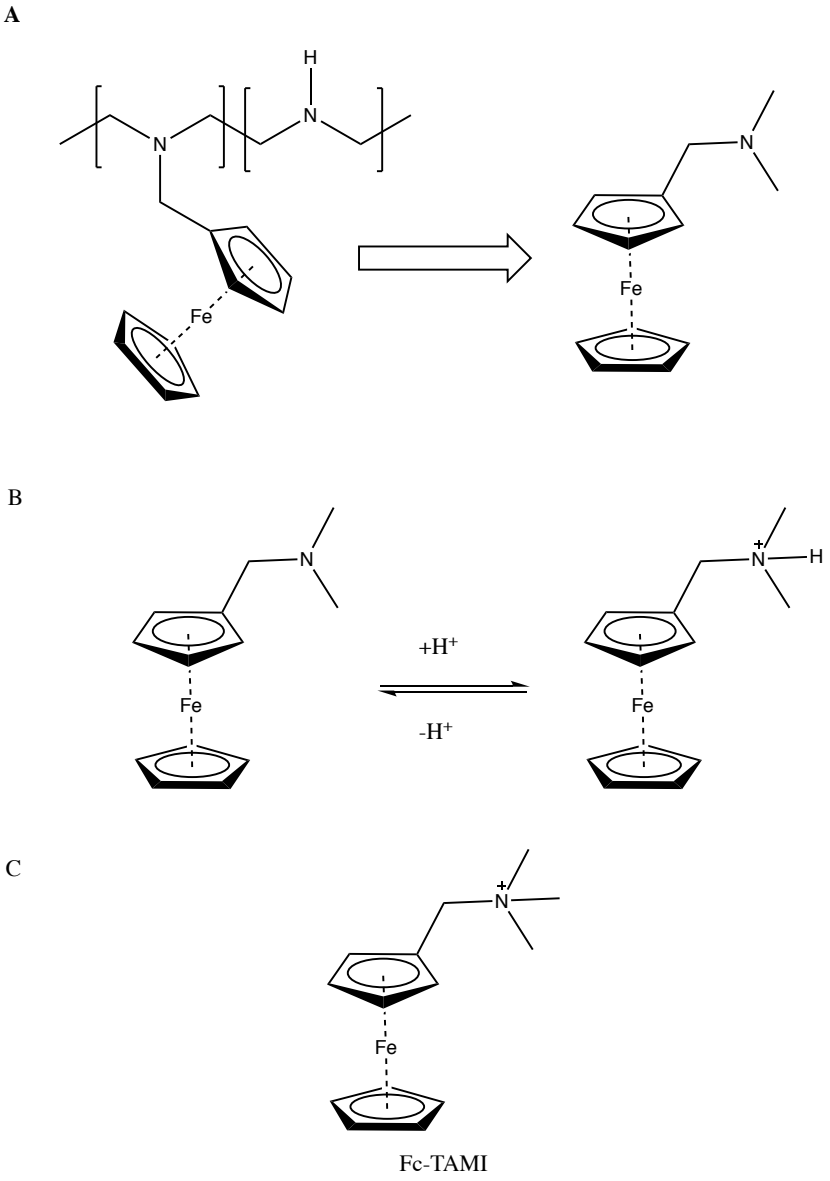

Figure 2.02 A. The structural similarities between the DMAFc and the Fc-C1-LPEI material developed by Meredith. B demonstrates the acid-base equilibrium occurring at physiological pH, and C shows the trimethylammonium salt used in this set of experiments.

It should be noted that this same equilibrium behavior is also observed in the polymer-supported state in the Fc-C1-LPEI material made by the Glatzhofer group[57, 113]. Under physiological conditions, more than one ferrocene signal is observed at ferrocene substitutions higher than 5%. This suggests that the amine backbone of the LPEI is protonated, and the positive charge on the

cationic nitrogen acts as an electron-withdrawing group for the ferrocene attached to the LPEI. At low pH values around 2, LPEI can have up to 50% of its nitrogen atoms protonated[57]. As pH increases, the percentage of protonated nitrogens decreases and the protonated nitrogen becomes undetectable, as evidenced by Meredith et al. This pH dependence is shown in Figure 2.03.

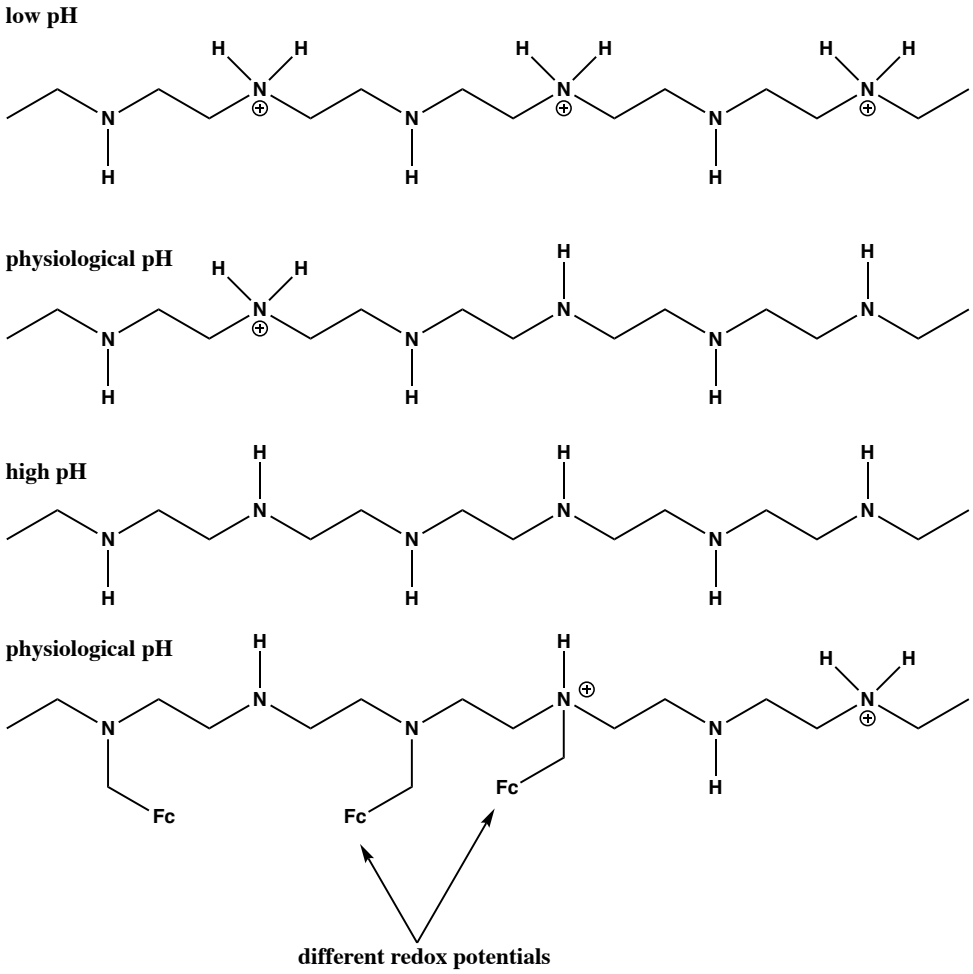

Figure 2.03 shows the effects of pH on the protonation of LPEI. At lower pH values, the polymer can have up to 50% protonation. Higher pH values leave the polymer deprotonated. Upon substituting LPEI with ferrocene there is a mixture of possible protonation states, as observed by two different Fc signals in the cyclic voltammogram.

2.2.2 – Titration of FcTAMI with GOx

Cyclic voltammograms of (ferrocenylmethyl)trimethylammonium iodide (FcTAMI) in phosphate buffered saline (PBS) were recorded using a glassy carbon working electrode, a

saturated calomel reference electrode (SCE), and a platinum wire auxiliary electrode at 150 mV/sec, as shown in Figure 2.04. The voltammogram showed two initial signals in the oxidative wave: one at 510 mV vs SCE and a second signal at approximately 690 mV vs SCE. In the reductive wave, a small shoulder appeared at 560 mV vs SCE, and a large reductive wave at 340 mV vs SCE. The ratio of the peak current response at $E_{1/2}$ = 420 mV vs SCE (i_{pa}/i_{pc}) was 0.96. Presumably, the redox couple at $E_{1/2}$ = 420 mV corresponds to the ferrocene/ferrocinium redox couple, and the second reductive wave is the iodide/iodide complex. When a mixture of FcTAMI and GOx was analyzed using cyclic voltammetry, the voltammogram changed significantly. A new oxidative shoulder appeared at 420 mV vs SCE while the oxidative peaks at 510 mV and 690 mV were depressed. In their place, a new oxidative peak at 580 mV vs SCE formed. The reductive shoulder at 560 mV was depressed and the final reductive wave remained unchanged. The formation of new oxidative waves suggested that a new redox species had formed, presumably from the addition of GOx. It was speculated that this new species was evidence of a GOx-Fc interaction, however, the ferrocene was not the only species that appeared to change. The redox waves corresponding to the iodide reduction process also changed. This suggests that the iodide ion could also be interacting with GOx. To investigate the exact nature of these changes, separate solutions of the iodide and ferrocene ions should be titrated with GOx. **Figure 2.04** shows the peaks discussed above as GOx is titrated into the FcTAMI solution.

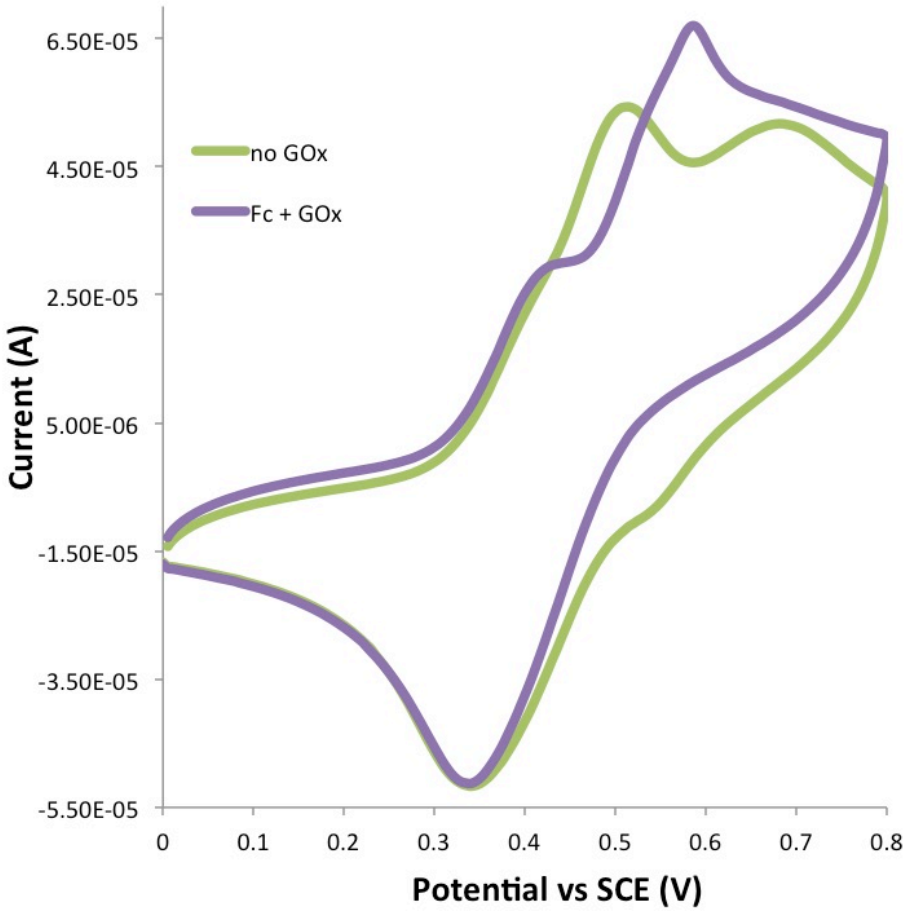

Figure 2.04 Cyclic voltammograms of 1.0 mM FcTAMI in the presence (purple line) and absence (green line) of GOx in PBS, pH=7.4, collected using a glassy carbon working electrode, a Pt wire reference electrode, and a saturated calomel electrode (SCE) for reference.

Iodide is known to be redox-active as it transitions through the tri-iodide anion, and finally to elemental iodine[115]. Iodide is first oxidized to the tri-iodide cation and then oxidized again to make elemental iodine. This suggests that the electrode could detect more than just the ferrocene or a ferrocene-GOx complex. To determine if any of the observed electrochemical phenomena were due to the oxidation of the iodide ion, a 1 mM sodium iodide solution was analyzed using cyclic votammetry in the absence and presence of GOx. The voltammogram of sodium iodide in the absence of GOx showed the two same oxidative peaks as the FcTAMI, as well as the same

two reductive features as the FcTAMI. This suggests that the electrochemical species in Figure **2.05** is the iodide oxidation pathway on both peaks, instead of the ferrocene at the lower potential peak as originally believed.

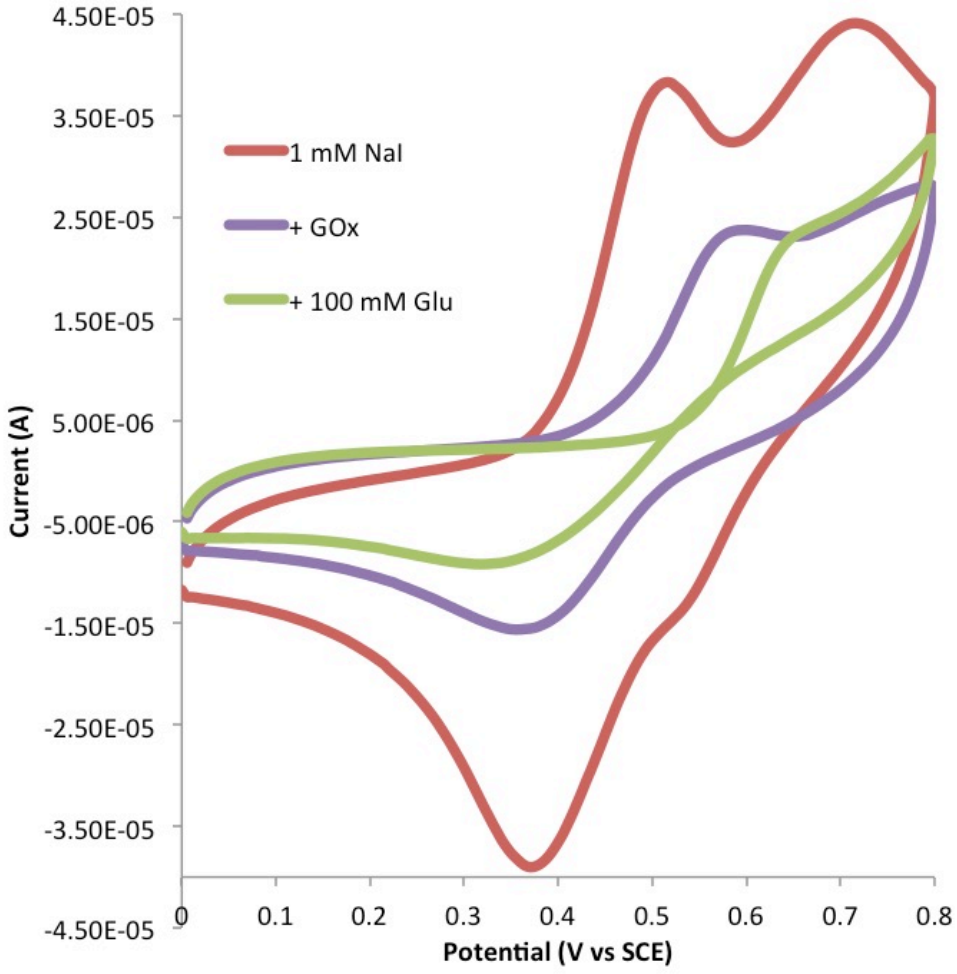

Figure 2.05 Voltammograms of 1.0 mM NaI in the absence (red) and presence of 100 µM GOx (purple), and in the presence of 100 µM GOx and 100 µM gluose (green), collected at 150 mV/sec in PBS pH=7.4.

Upon addition of GOx to a solution of sodium iodide, a change in the cyclic voltammogram of the iodide anion is observed. The voltammetric peaks at approximately 480 mV and 700 mV vs SCE are diminished, and a new peak at approximately 580 mV appears, suggesting a new redox species was formed in solution. These studies suggest that iodide has a direct interaction with the

GOx. And, upon the addition of 100 mM glucose to the solution of NaI and GOx, the oxidative peak potential shifts approximately 80 mV. Based on the observations in the voltammograms in the absence and presence of GOx with and without glucose, it appears that the iodide interacts with GOx in some capacity. In the presence of glucose, the FAD center could be reduced by the iodide ion instead of by glucose.

$$\text{No GOx} \quad I^- \xrightarrow{E} I_3^- \xrightarrow{E} I_2$$

$$\text{With GOx} \quad I^- \xrightarrow{FAD} I_3^- \xrightarrow{E} I_2$$

This is supported by the decrease in the amperometric response when glucose is added to a solution of NaI and GOx. This indicates that the iodide ion will compete with the glucose for the FAD center in the mediation process, and possibly be deactivated in the process. This has been previously observed where iodide altered the mediative voltammograms, indicating iodide is a competitive substrate for Horseradish Peroxidase[116]. Since it is observed that iodide could greatly alter the activity of the FcTAMI in the presence of GOx, it was necessary to remove the iodide from the system. It is important to note, however, that this does suggest that iodide has the capability of acting as an electron transport mediator (ETM) for GOx. To our knowledge, this is the first evidence that iodide could act in a mediative capacity.

2.2.3 – Titration of (Ferrocenylmethyl)trimethylammonium chloride with GOx

By performing an ion exchange on an Amberlyte-400 ion exchange resin using methanol as an eluent, ferrocenylmethyl(trimethylammonium) chloride (FcTAMCl) was prepared. Upon analysis of the FcTAMCl using cyclic voltammetry in PBS, a single oxidation wave and a single reductive wave with an $E_{1/2}$ = 380 mV vs SCE, ΔE_p = 60 mV, and i_{pa}/i_{pc} = 0.98, was observed. The presence of only one reversible peak in the voltammogram indicates that iodide has been

removed from the mixture during ion exchange. This suggested that a reversible, single electron transfer process is occurring, as is typically observed with ferrocene species[117-118]. Upon addition of GOx to FcTAMCl, E_{pa} and E_{pc} remained unchanged. However, there is a noticeable change in the i_{pa} and i_{pc} as the concentration of GOx is increased. It should be noted that i_{pc}/i_{pa} remained constant near 1, suggesting the reversibility to the ferrocene redox couple did not change. It is important to note that separate solutions were prepared for each analysis at a specific GOx concentration to ensure that the change in electrochemical response was not due to dilution.

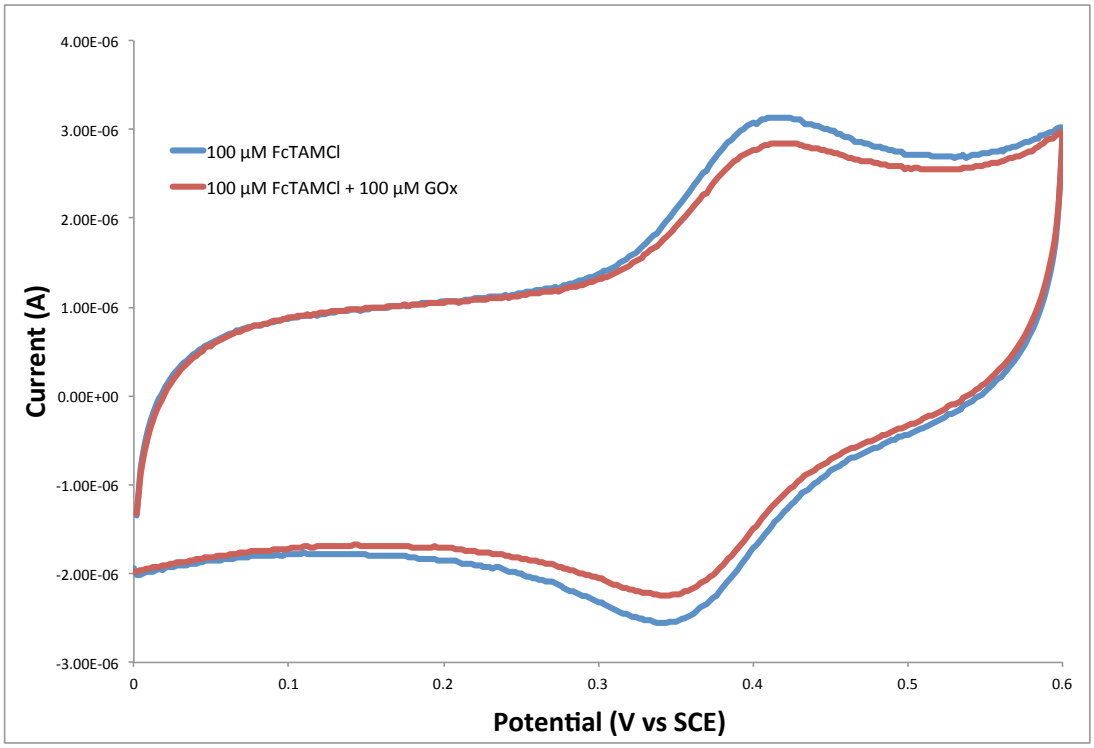

Figure 2.06 Cyclic Voltammograms of 100 µM FcTAMCl in the absence (blue) and presence (red) of 100 µM GOx.

Plotting the amperometric response (i_{pa}) of the anodic wave as a function of GOx generates an asymptotic curve. This trend has been previously observed in a system described by Atlaf where a copper electrode was inhibited by urea, as monitored using cyclic voltammetry[119]. When urea was bound to the surface of the copper electrode, the amperometric current was inhibited. There

was a direct correlation between the amount of copper inhibited and the amperometric response, allowing them to develop a binding isotherm, wherein an adsorption coefficient could be determined. Treating GOx as an electrochemical inhibitor to ferrocene allowed a similar application of the model for our ferrocene/GOx system. Figure 2.07 shows the behavior of i_{pa} as a function of the concentration of GOx.

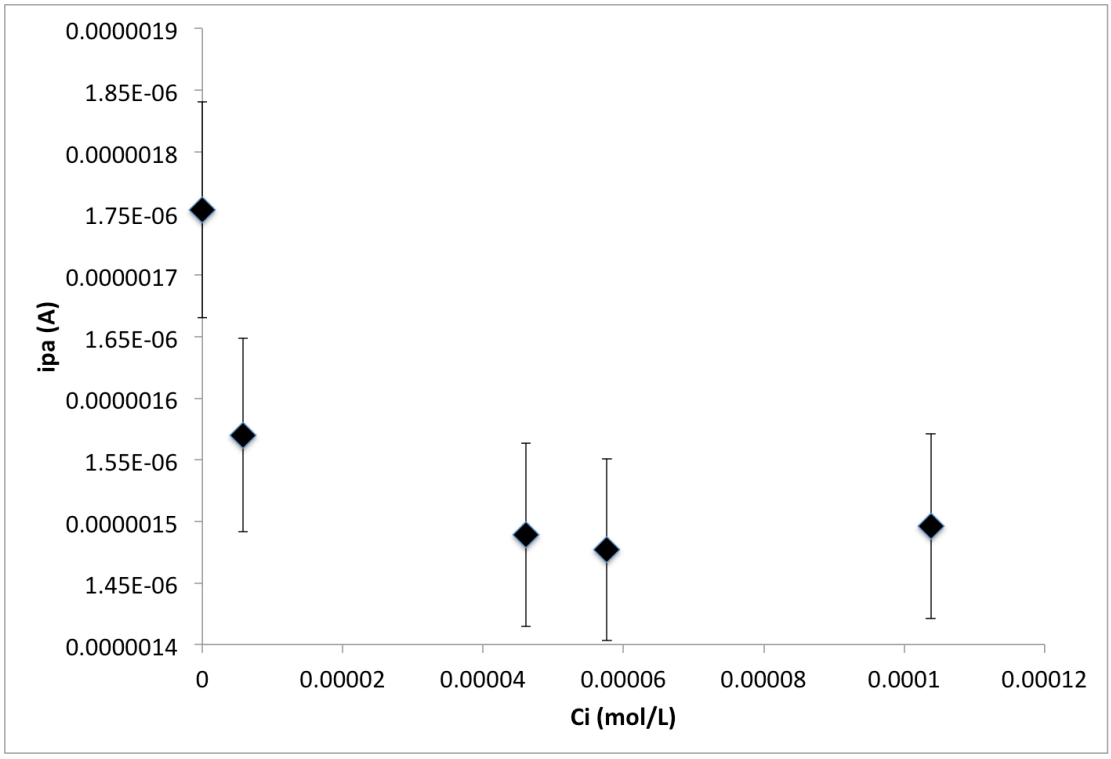

Figure 2.07 – A plot of the amperometric response as a function of [GOx]

The model for the isotherm is described below in equations 2-4.

$$\theta = 100\times\left[1-\frac{(i_a)_i}{(i_a)_0}\right] \qquad (2)$$

$$\frac{\theta}{1-a\theta} = K_a C_i \qquad (3)$$

$$\frac{C_i}{\theta} = \frac{1}{K_a} + aC_i \qquad (4)$$

where C_i is defined as the concentration of the GOX (as an inhibitor), $(i_a)_I$ is defined as the amperometric response of the ferrocene at the designated concentration of GOx, $(i_a)_0$ is defined as the amperometric response of the ferrocene in the absence of GOx, a is an adjusting parameter giving the slope of C_i/θ, and K_a is the association constant of any resulting GOx-Fc complex. By plotting C_i/θ vs C_i, a linear regression can be applied to determine the association constant of the complex K_a, as described in equation 4.

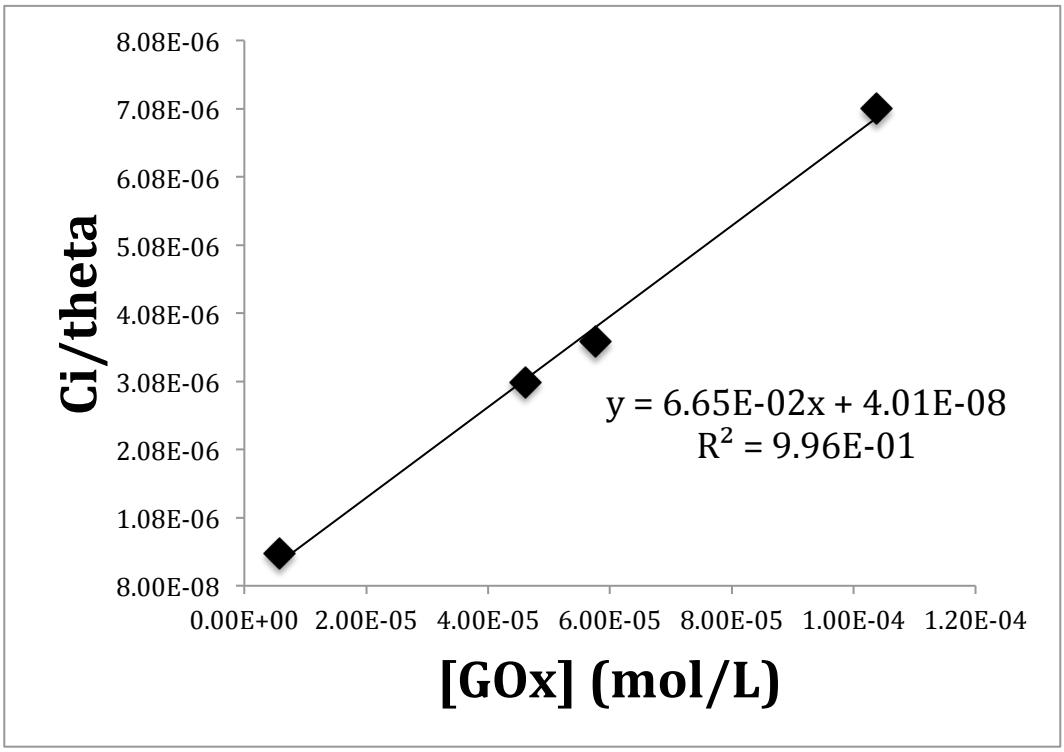

Figure 2.08 A plot of Ci/θ vs Ci, where Ci is the concentration of GOx (mol L^{-1}).

The value of K_a is determined by taking the inverse of the y-intercept, as described by the binding model. The binding constant, K_a, was determined to be 2.49 x 10^7. Assuming this binding constant is similar to an equilibrium constant, the large magnitude suggests that the interaction that is occurring between FcTAMCl and GOx is a thermodynamically favorable

interaction. Based on this association constant value, the free energy of FcTAMCl interacting with GOx can be determined according to equation 5[120-122].

$$\Delta G = -RTlnK_a \qquad (5)$$

where R is the ideal gas constant, T is the absolute temperature, and K_a is the adsorption constant. ΔG was calculated to be -42.2 kJ/mol at 25° C. With this quantitative characterization, a descriptive model that explains how the model behaves can be developed.

2.2.4 – Describing the Model of the Observed Interaction

When considering the possibilities that can qualitatively describe the nature of this observed interaction, it is possible that one of two scenarios occur as outlined in Figure 2.09: 1 (bottom diagram): When FcTAMCl adsorbs to GOx, the resulting Fc-GOx adduct is electrochemically active, but the increase in the size of the Fc-GOx makes it move more slowly through the solution. 2 (top diagram): When FcTAMCl adsorbs to GOx, the resulting Fc-GOx adduct is electrochemically inactive or electrochemically less active, which causes the observed decrease in amperometric response.

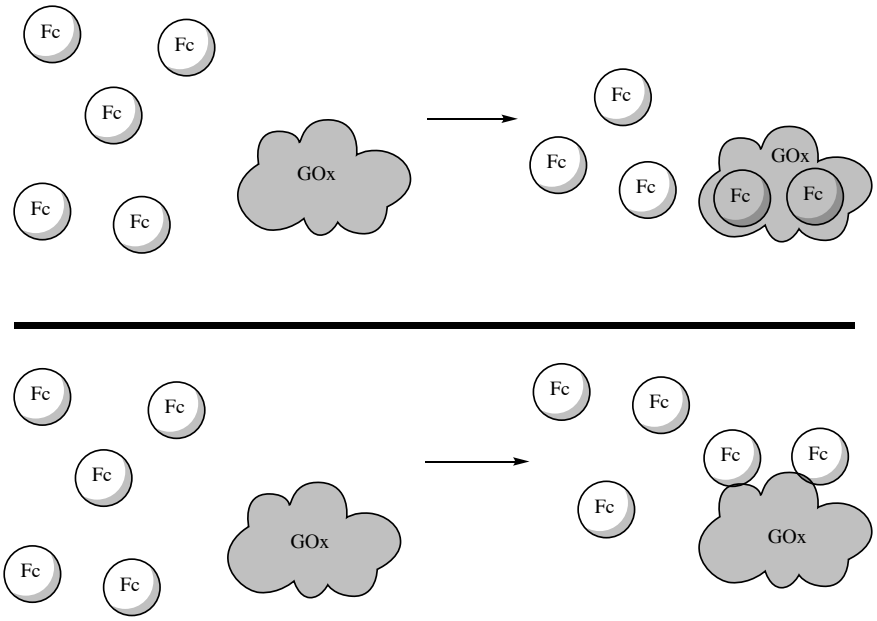

Figure 2.09 Two possible scenarios that could describe the nature of the interaction with the ferrocene and GOx in the binding scenario. The top figure shows GOx fully inhibiting the electrochemical response of the ferrocene, while the bottom figure shows a surface adsorption of ferrocene to GOx causing a slower-diffusing ferrocene species.

In considering the first scenario, the possibility of an electrochemically active Fc-GOx adduct is proposed. If this adduct is the electrochemically-active species, a reasonable way of investigating this model is by analyzing the diffusion coefficient. The Randles-Sevcik equation (6) describes the amperometric response (i_p) as a function of the diffusion coefficient, D. By plotting the amperometric response as a function of the square root of the scan rate, a linear plot is generated and the slope is used to calculate D_{app}. It is important to note that D_{app} is used in lieu of D, as it is still uncertain of the exact nature of the system's behavior, as the reality of the situation could be a composite of free and bound ferrocene.

$$i_p = 0.4463nFAC\left(\frac{nFvD}{RT}\right)^{1/2} \qquad (6)$$

where n is the number of electrons transferred, F is Faraday's constant, A is the electrode area in cm^2, C is the concentration of the electrochemical species in mol/cm^3, *v* is the scan rate in V/s, R is the ideal gas constant, and T is the temperature.

By creating a plot of the amperometric response vs the square root of the scan rate used to record the voltammograms of the samples used in the previous analysis, straight lines were observed, implying the system was diffusion-controlled. The slope was then used to calculate the diffusion coefficient of each sample. When plotting the diffusion coefficient as a function of the enzyme concentration, an asymptotic behavior was observed. The apparent diffusion coefficient, D_{app}, decreased by up to half as the concentration of the enzyme was increased. By monitoring the diffusion coefficient as the enzyme concentration increases, it appears that the ferrocene species is diffusing more slowly through solution when more enzyme is present. The diffusion coefficient drops precipitously upon a small addition of GOx. The diffusion coefficient, D_{app}, of the free FcTAMCl in the absence of GOx was determined to be 8.5×10^{-6} cm^2 sec^{-1}. This is in good agreement with other studies that have measured electrochemically the diffusion coefficient of assorted ferrocene derivatives. An average diffusion coefficient for ferrocene and its derivatives is between 5.0×10^{-6} cm^2 sec^{-1} and 8.0×10^{-6} cm^2 sec^{-1} [123].

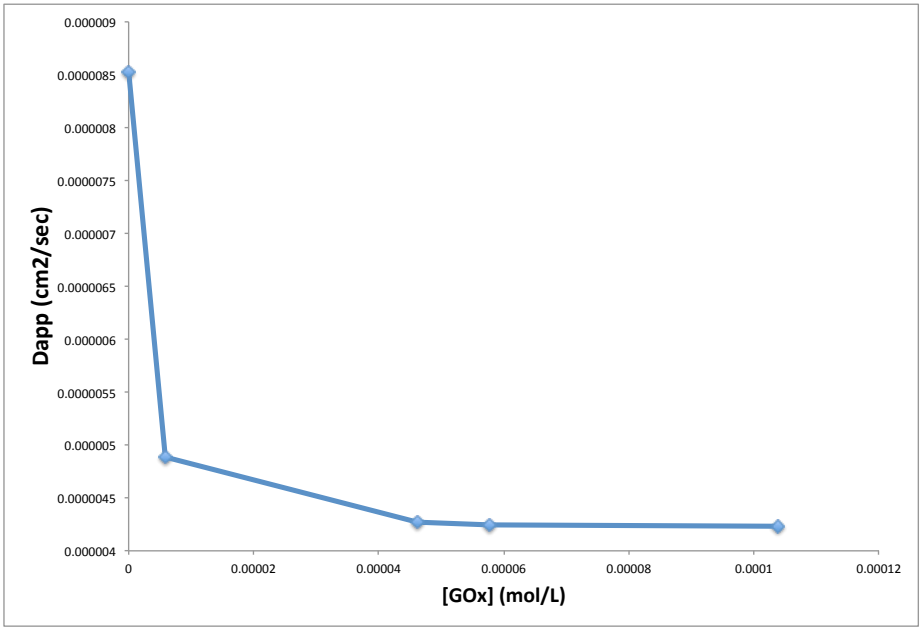

Figure 2.10 A plot of D_{app} vs enzyme concentration for a series of ferrocene-GOx mixtures containing 0.1 mM ferrocene and between 0 and 110 mM GOx (activity = 107,000 units/g). Diffusion collected using peak current Epa= 420 mV vs SCE at varying scan rates between 50 and 250 mV/sec.

In a solution of 5 µM GOx, the D_{app} of the ferrocene species dropped to 4.8 x 10^{-6} cm^2 sec^{-1}. Between 46 µM and 100 µM GOx, however, the D_{app} decreases slightly to 4.2 x 10^{-6} cm^2 sec^{-1} and does not change measurably, suggesting that the ferrocene in solution saturates the enzyme. It could be interpreted that the significant drop in the diffusion coefficient could be due to a Fc-GOx complexation, as the D_{app} is decreasing. This is supported by the Stokes-Einstein equation (7) that states an indirect relationship between the D_{app} and the hydrodynamic radius of a species moving through solution[124].

$$D_{app} = \frac{k_B T}{6\pi\eta r} \qquad (7)$$

where k_B is the Boltzmann constant, T is the absolute temperature, η is the mobility of a charged particle, and *r* is the hydrodynamic radius of the spherical particle.

According to the Stokes-Einstein relationship, when the D_{app} is cut in half, it suggests that the radius of the electrochemically-active species doubles. This implies that the diameter of the electroactive species is four times that of the ferrocene. When comparing the unit dimensions for the crystal structure of GOx, the unit cell dimensions are a = 57.6 Å, b= 132.1 Å, and c = 215.4 Å[22]. For simplicity sake, the unit cell dimensions of an unmodified ferrocene molecule are a =10.50 A, b = 7.63 A, and c = 5.95 A when n=1 in the unit cell.[125] By looking at the smallest gap between the dimensions, it appears that the smallest possible difference in radius, or the difference between the a dimensions, it shows that the smallest possible ratio of the radii is 5. According to the Stokes-Einstein equation, the change in the diffusion coefficient suggests a four-fold change. For such an approximation a change in the radius of four is pretty close to a change of 5. This agreement suggests that the ferrocene is locked into the active site, and becomes electrochemically inactive.

While one model proposes that the ferrocenes adsorbed in the Fc-GOx are electrochemically active and the other model proposes that the ferrocene in the Fc-GOx adduct is active, both models include a Fc-GOx adduct. To further characterize this adduct, and possibly gain some insight as to which model is more representative of the phenomenon occurring, an investigation into the stoichiometry of the adduct could be beneficial. If the adsorption of the ferrocene to the enzyme completely eliminated the electrochemical response of ferrocene, as described in the second scenario, it would seem reasonable that, at an inhibitor concentration equal to the concentration of ferrocene, there wouldn't be a detectable response using CV. However, this initial prediction is dependent on an assumption of a binding model where one ferrocene adsorbs to one GOx. Other stoichiometric ratios, such as two ferrocenes adsorbing to one GOx, or three ferrocenes adsorbing to one GOx could be possible. To investigate all of

these possibilities, a simple equilibrium expression can be used to model the amount of unbound FcTAMCl remaining in solution, using the binding constant, K_a. According to the Randles-Sevcik equation, there should be a directly proportional response to the concentration of unbound ferrocene and the observed amperometric response in the voltammogram. To model these predictions, the conditions where the highest concentrations of GOx will be used. The concentration of both GOx and FcTAMCl at these conditions is 100 μM. By predicting the amount of available ferrocene using the equilibrium expression below and the measured K_a, the stoichiometry should be able to be calculated by matching the predicted amperometric response to the experimental amperometric response.

$$\text{GOx (aq)} + \text{Y FcTAM} \rightleftharpoons \text{GOx(FcTAM)}_y$$

$$K_a = \frac{GOx(FcTAM)_y}{[GOx][FcTAM]^y}$$

When the simulation is set to 1 GOx to 1 FcTAMCl, it is calculated that the concentration of FcTAMCl in solution at equilibrium, $[\text{FcTAMCl}]_{eq}$, is 2 μM. Using the Randles-Sevcik equation to build a simple proportion, the amperometric response at this concentration can be predicted. The predicted response is 0.35 μA at 2 μM FcTAMCl. If the stoichiometry is set to 1 GOx per 2 parts FcTAMCl, then the equilibrium concentration of FcTAMCl is calculated to be 85 μM. The expected current for 85 μM FcTAMCl is 1.49 μA, When the stoichiometry is 1 GOx to 3 FcTAMCl, there is approximately 99 μM FcTAMCl, suggesting the current should not significantly change from 1.75 μA, as summarized in **Table 2.2**.

y	$[FcTAM]_{eq}$	Expected i_{pa}
1	2 μM	0.035 μA
2	85 μM	1.49 μA
3	> 99 μM	1.75 μA

Table 2.2 Predicted equilibrium concentrations and amperometric response of FcTAMCl using different stoichiometric ratios, assuming $K_a = 2.49 \times 10^7$.

The observed current at 100 μM GOx and 100 μM FcTAMCl is 1.50 μA. This is in excellent agreement with the prediction where the stoichiometry between FcTAMCl and GOx is 2:1. Based on the agreement with our observed results and the changes in the apparent diffusion coefficients, it is reasonable to speculate that the second scenario, where adsorbed FcTAMCl is electrochemically inactive, is more appropriate. In this adsorption, two ferrocene molecules adsorb to one GOx. This is reasonable, as two ferrocenium molecules are needed to oxidize the $FADH_2$ center of GOx* in the catalytic cycle, as was previously described in **Figure 2.01**. This also suggests the observed change in D_{app} is due to the decrease in concentration of the electrochemically active FcTAMCl, instead of directly detecting a Fc-GOx interaction. It is believed that, based on the ability of GOx to catalyze glucose oxidation in the presence of ferrocenes, these GOx-ferrocene adducts decompose when glucose is introduced into the system. This interaction could also prove useful in improving the design of the polymer materials used in the bioelectrodes. The stoichiometry of the 2:1 ferrocene to GOx ratio could suggest that constructing the polymer in such a way that two ferrocene molecules are in close proximity to one another. This approach could lead to an improved amperometric performance in a polymer-supported bioanode, as the two ferrocene molecules could more easily access the active site.

2.3 - Conclusions

A binding interaction between a ferrocene derivative, FcTAMCl, and Glucose oxidase was detected using cyclic voltammetry. To our knowledge, this interaction is the first of its kind to be detected using this method. When GOx is treated as an electrochemical inhibitor, the interaction can be quantified using a Langmuir binding isotherm. The stoichiometry of this interaction is believed to be two ferrocenes to one GOx, as evidenced by calculation of unbound ferrocene using a predictive equilibrium expression. This excellent agreement between calculated aperometric response at equilibrium concentration and observed amperometric response suggests that once the ferrocene molecules adsorb to GOx, they are no longer electrochemically available to the electrode. These adducts remain intact until glucose is introduced into the system. In addition, the first interaction between sodium iodide and GOx was demonstrated using the same method, but was not quantitated. This suggests that the iodide could compete with the ferrocene or other electrochemical mediator for positions in the active site of GOx, as has been reported with Horse Radish Peroxidase. This interaction could be used as a tool for screening mediators in biofuel cells, however further work into the interaction with other ferrocene derivatives is necessary.

2.4 - Experimental

All reagents and enzymes were purchased from Sigma-Aldrich and used without further purification. FcTAMI was synthesized using previous literature methods[126]. All cyclic voltammetric data was obtained using a Chemical Instruments 280 bipotentiostat. Electrochemical experiments were carried out in phosphate-buffered saline (PBS) at a pH of 7.4 using a saturated calomel electrode as a reference electrode, a Pt wire auxiliary electrode, and a glassy carbon working electrode.

Ion exchange to Prepare FcTAMCl

A column of Amberlyte ion exchange resin (3.87 mEq/g) was flushed with DI water thoroughly and then charged with 2.0 M NaCl solution that was allowed to slowly drain through the resin. The column was subsequently flushed with fresh DI water to remove excess NaCl from the column. Methanol was then flushed through the column until convection lines were no longer present in the eluent. A concentrated solution of FcTAMI in MeOH was prepared and loaded onto the column. The ion exchange resin was loaded at 1.8 mEq per g of amberlyte. The FcTAMCl was eluted with fresh methanol. Once eluted, the methanol was removed under reduced pressure to afford pure FcTAMCl as a yellow powder in greater than 95% yield. To check that all iodide was removed, a small amount of the product was dissolved in 3 mL of water, and one drop of silver nitrate afforded a white precipitate, suggesting that only chloride was present. If iodide was present in the solution, a yellow precipitate would have formed.

Enzymatic Titration of Ferrocenyl-methyl trimethylammonium derivatives with GOx

A FcTAMCl stock solution was prepared using pure FcTAMCl derivative in PBS. Each analyzed mixture contained 0.100 mM FcTAMCl, and varying amounts of GOx ranging from 6 – 120 μM, (MM= 160,000 g mol^{-1}). Cyclic voltammetric measurements were conducted at a scan rate of 150 mV/sec using a 3 mm glassy carbon electrode as the working electrode.

Investigating iodide as a potential mediator

A solution of 1.0 mM NaI was prepared. Two solutions were prepared from the NaI stock: a 2.00 mL solution of NaI in PBS, and a 2.00 mL solution 0.100 mM NaI solution was prepared by adding in sufficient GOx and NaI solution to make 2.00 mL of solution in PBS. After an initial scan of GOx and NaI in the absence of glucose, 50.0 uL of 2.00 M glucose solution was added to the solution, and the cyclic voltammogram was recorded at 150 mV/sec using a circular

3 mm diameter glassy carbon electrode, a saturated calomel reference electrode, and a platinum wire auxiliary electrode.

Chapter 3: The Effects of Electron Donating and Electron Withdrawing Groups on a Langmuir Binding Isotherm Between Glucose Oxidase and Ferrocene

3.1 Introduction

Enzymatic biofuel cells utilize redox-active molecules and enzymatic reactions to generate electrical currents. Oxidoreductases are a class of enzymes used in the bioelectrodes to convert the chemical energy into electrical energy for use in a biofuel cell[127]. When a substrate diffuses into the active sit of an oxidoreductase, it is converted into a product that diffuses away from the active site. A co-substrate then diffuses into the active site and reacts again in order to regenerate the active form of the enzyme. Glucose oxidase (GOx) is one such enzyme used in the fabrication of bioanodes[128-129]. GOx has been used to make solution-state sensors, as well as polymer-supported materials containing organoosmium compounds and ferrocene compounds that are cross-linked to form hydrogels[48, 75, 113, 130].

GOx catalyzes glucose oxidation using a "ping-pong" mechanism. In the solution state, glucose diffuses into the active site of GOx where it is oxidized to gluconolactone by the FAD in the active site and FAD is reduced to $FADH_2$. The newly reduced $FADH_2$ is then oxidized by a co-substrate diffusing into the active site to regenerate the FAD as the reduced co-oxidant diffuses away. For those bioelectrodes fabricated by polymer-supported materials, a cross-linked polymer brings the metal complexes in close proximity to the enzyme and effectively "wires" the metal complexes to the enzyme. As glucose diffuses through the redox hydrogel, GOx converts glucose to gluconolactone and the Flavin Adenine Dinucleotide (FAD) active site of GOx is reduced to $FADH_2$. The close-proximity metal complexes react with the reduced $FADH_2$ to regenerate the active GOx(FAD)[45, 114, 118]. The reduced mediators then pass electrons to an

electrode surface through a series of Marcus collisions[24, 49, 131]. This process is shown in Figure 3.1.

3.1 A

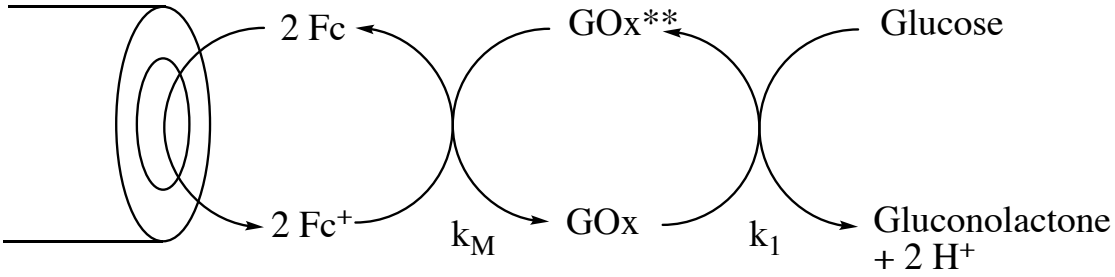

3.1 B

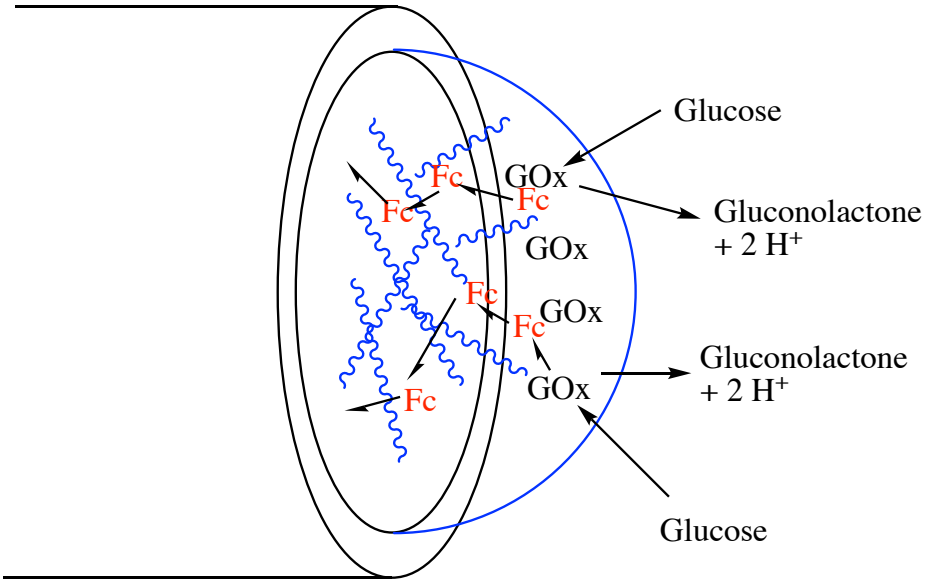

Figure 3.1 A) A simple mechanism that shows how electrons are transferred from glucose being oxidized to gluconolactone by GOx and the reduction of ferrocinium by GOx*. B) A diagram of the polymer-supported bioelectrode where ferrocene (Fc) is attached to a polymer material that is cross-linked to entrap GOx. The Fc shuttles the electrons from the enzyme's active site.

In considering which components go into making an effective bioelectrode, there have been a number of methods used, including determining the kinetic constant, k_M, of the electron

transfer between the enzyme and the mediating organometallic complex, and by the maximum current density, J_{max}, of a bioelectrode[40, 45, 68, 117]. Of these methods, comparing the kinetic constants of assorted ferrocenium salts has drawn the most attention, as it provides a direct measure of the efficiency of electron transfer between an enzyme and the mediator[68, 109, 117]. Theoretically, k_M could be used to predict which mediators perform best in GOx-based systems, leading to the development of more efficient mediators for use in bioelectrode materials. Most researchers can be hesitant to this approach, however, as the mathematical models can be very complex[68]. While there are assortments of potential mediators that can shuttle electrons from GOx to an electrode surface, the discussion will be limited to GOx-based electrodes that use ferrocene to mediate the electron transfer between GOx and the electrode.

In choosing the appropriate ferrocene derivative for use in these GOx-based electrodes, it is unclear as to which structural features on the ferrocene produce the highest current densities in polymer-supported bioelectrodes[68]. GOx-based bioelectrodes have been used as model systems for investigating the structural effects of a mediator on its ability to mediate, as mediators containing osmium, iron, manganese, chromium, and other organic compounds have been demonstrated to act as mediators for GOx[19, 44-45, 105]. It is also noted that most kinetic analyses have not determined any significant correlation between structure and k_M[44, 132-133]. In addition, there is not a direct correlation between the redox potential, $E_{1/2}$, and k_M[108, 133]. Regarding the "rules" for selecting mediator components for GOx, three major structural attributes have been accepted as necessary for successful mediation in the literature: 1) The mediator must be small enough to fit inside the active site of GOx. 2) The mediator must contain an aromatic pi moiety, such as a cyclopentadienyl or benzene ligand, so it can interact with the $FADH_2$ in the active site and 3) The compound must exhibit a rapid, reversible electrochemical reaction at an

electrochemical potential below the potential of $FADH_2$ in the active site of GOx[19, 44-45, 105]. These vague rules, however, do not indicate any specific functional groups to yield superior performance when they are incorporated in the ferrocene and are used in a bioelectrode.

While there has not been much progress in using a molecule's specific functional groups to predict a molecule's ability to mediate by comparing each molecule's k_M, some general structural features have been shown to affect the k_M. By utilizing a series of micelles made from cetyltrimethylammonium bromide, Triton 100X, and sodium dodecyl sulfate around an alkyl ferrocene, the "charge" on the mediator was varied from positive to neutral to negative, respectively[134]. The rate constant, k_M, was measured as a function of the charge using a series of alkyl ferrocene derivatives that partition into the charged micelles. When the charge was varied from neutral to negative, k_M decreased by a factor of 1000. However, k_M did not change significantly when the charge was changed from positive to neutral. This suggested the charge on the mediator only affects the rate constant, k_M, of the electron transfer between GOx and the ferrocene, if the ferrocene derivative has a negative charge. This is reasonable, as the isoelectric point of GOx from Aspergillus Niger is approximately 4.1[134]. By calculating the charge based on the amino acid residues of the protein the charge at a neutral pH of the enzyme is close to -58[135].

In addition to the effects of charge, the size of a mediator has been demonstrated to affect its ability to mediate, as measured by k_M and the maximum current density in a polymer-supported system. For example, the Glatzhofer group has used methylated ferrocenes in GOX bioelectrodes constructed from linear poly(ethyleneimine) (LPEI), as the methylation of a ferrocene reduces the redox potential of the bioelectrode material by approximately 50 mV per methyl group[48, 59, 64]. In comparing the maximum current density of the electrode materials in 100 mM glucose, the dimethylferrocene-based material had a higher performance. However,

when tetramethylferrocene was used, the maximum current density decreased, as shown in Table 3.1. This observation matches the observations of Forrow et al, where dimethylferrocene derivatives showed significantly reduced k_M values, from 6.9 x 10^{-5} M^{-1} s^{-1} in an unmethylated hydroxyaminoferrocene to 1.5 x 10^{-5} M^{-1} s^{-1}.

Redox polymer	***J_{max} (mA/cm^2) 25 ° C (37 ° C)***	**$E_{1/2}$ vs SCE (V)**	**K_M (mM)**
Fc-C_3-LPEI	1.01 ± 0.06 (1.96 ± 0.07)	260 mV	20.7 ± 2.3
Me_2Fc-C_3-LPEI	1.16 ± 0.05 (2.09 ± 0.04)	170 mV	21.7 ± 1.9
Me_4Fc-C_3-LPEI	0.606 ± 0.04 (0.983 ± 0.05)	80 mV	10.4 ± 3.4

Table 3.1 A summary of the characterization of different ferrocene-modified linear poly(ethylenimine) materials characterized by Hickey et al[48].

Many factors have been determined to affect how well a ferrocene molecule can transfer electrons between GOX and the electrode surface, such as the size of the mediator and the charge associated with the mediator[24-27]. One factor that has not been predictable, however, is the effect of the redox potential of the redox mediator on its mediative capability.[44-45] It has been demonstrated that electron donating and withdrawing effects of different functional groups can affect the redox potential of a ferrocene mediator[44-45]. As such, it is reasonable to infer that the redox potential may correlate to the kinetic constant, k_M, of the electron transfer between GOx and a mediator. As was discussed in Chapter 2, k_M has been used to assess a molecule's capability to act as a mediator for GOx. In an attempt to connect the $E_{1/2}$ of the mediator to its effectiveness as a mediator, Forrow conducted a kinetic study on over fifty ferrocene derivatives with GOx in order to discern if there are any additional trends in the ferrocene mediator's functional groups and side chains, electrochemical potential, and kinetic constant, k_M[44]. It was also observed that the potentials of the ferrocene mediator varied with the functional group. By

comparing the potential against the functional group of the ferrocene, it was determined that certain groups affected the potential of the ferrocene in the following order: $+NMe_3 > NH_2 > CONH_2 > OH > CO_2H$[44]. This is most likely due to the effects of electron donating and withdrawing functional groups on the ferrocene altering the redox potential. When comparing the electrochemical potential ($E_{1/2}$) of a ferrocene to the kinetic constant, however, there was not an observed trend when considering all of the fifty mediators used in this study. Most ferrocene mediators were determined to interact with GOx at rate between 3.0×10^{-6} M^{-1} sec^{-1} and 8.2×10^{-5} M^{-1} sec^{-1} [44]. This lack of correlation between $E_{1/2}$ and k_M was believed to be due to the fact that $E_{1/2}$ is only one of many factors that can affect a molecule's k_M[44, 132-133, 136].

One interesting feature, however, was the observable trend between k_M and $E_{1/2}$ when grouping the compounds together by functional group. By varying the length of the tether between the functional group and the ferrocene, a series of experiments that measured the $E_{1/2}$ and k_M of a series of functional groups was conducted. Ferrocene mediators containing alcohol and carboxylic acid functional groups showed the strongest correlation between $E_{1/2}$ and k_M, while mediators containing amino alcohols, amines, and amides showed the weakest correlations. There was not a rational explanation provided for this phenonmenon, except that functional group and the distance of the functional group on a mediator were speculated to play a role. For example, when in comparing the k_M of ferrocenemethanol to 1-ferrocenyl-1-methylmethanol, the k_M decreased significantly from 8.2×10^{-5} M^{-1} s^{-1} to 3.0×10^{-5} M^{-1} s^{-1}. This change was originally suspected to be caused by the increased volume due to the addition of the methyl group. When the methyl group on the latter species was replaced with an ethyl amino group, k_M only changed slightly from 8.2×10^{-5} M^{-1} s^{-1} to 7.6×10^{-5} M^{-1} s^{-1}. This suggested that the reduction in k_M was not purely due to steric hinderance. In addition, changing the length of

the side chain was shown to alter the k_M. Changing ferrocenyl methanol to ferrocenyl ethanol resulted in a significant reduction in k_M. This suggests that the side chain of the ferrocene may assist in positioning the ferrocene near the $FADH_2$ in the active site of GOx, as shown in Figure 3.3. When combining this observation with the aforementioned correlation between the size of the mediator and the mediator's capability, the "black magic" of mediator selection was not really clarified.

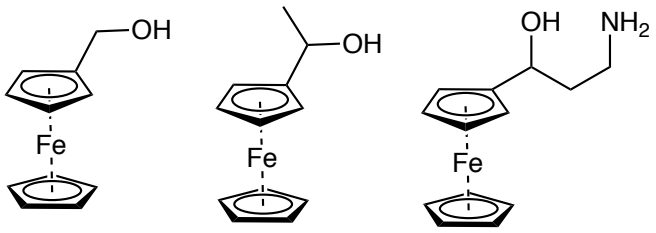

Figure 3.2 The structure of ferrocenylmethanol (left), 1-ferrocenyl-1-methylmethanol (middle), and 1-amino-1-ferrocenylmethanol (right) used by Forrow to demonstrate that more than sterics can affect the mediative capability of a molecule[44-45].

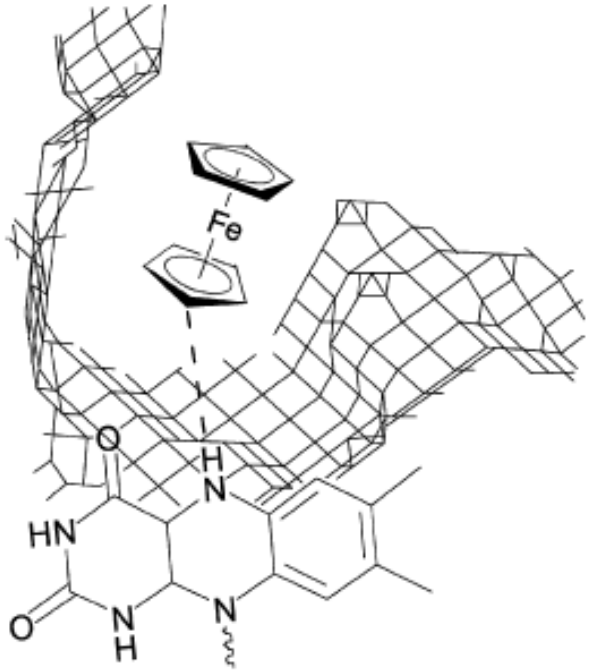

Figure 3.3 A model of Ferrocene binding to the $FADH_2$ deep in the active site of GOx. Reproduced from Forrow et al[44].

Hypothesis

Chapter 2 of this work describes a binding isotherm that can be characterized electrochemically using cyclic voltammetry. Based on the aforementioned discussion surrounding structure and its effects on the kinetic constant k_M, it is reasonable to speculate that the structure of a molecule could impact the magnitude of the binding constant, K_a. By titrating a series of ferrocene derivatives GOx and treating GOx as an inhibitor, it is likely that a K_a can be determined for each species. If the magnitude of K_a varies between ferrocene derivatives, then further information regarding the effects of K_a on a molecule's ability to act as a mediator can be discerned.

3.2 Results

3.2.1 - Experimental Design

In order to investigate the effects of structure on the binding constant, three additional molecules were chosen in addition to the (ferrocenylmethyl)trimethylammonium chloride: 1) ferrocenecarboxylic acid (FcCOOH); 2) ((methoxy)ethoxy)ethoxymethylferrocene (FcG2OMe); and 3) bis(trimethylammoniummethyl)ferrocene chloride (FcTAMCl2), as shown in **Figure 3.4**. FcCOOH has been demonstrated to act as a mediator for GOx previously, and holds a negative charge at physiological pH. FcG2OMe is a neutral species with a long water-soluble tail that is much more hydrophilic than the corresponding alkyl chains that have been used in studies with surfactants. FcTAMCl2 is a dicationic species that could theoretically bind more efficiently than FcTAMCl to the negatively charged GOx due to increased electrostatics. This, however, may not increase the K_a, as the aforementioned studies using differently-charged surfactants only demonstrated a significant effect on charge if the mediator has an overall negative charge.

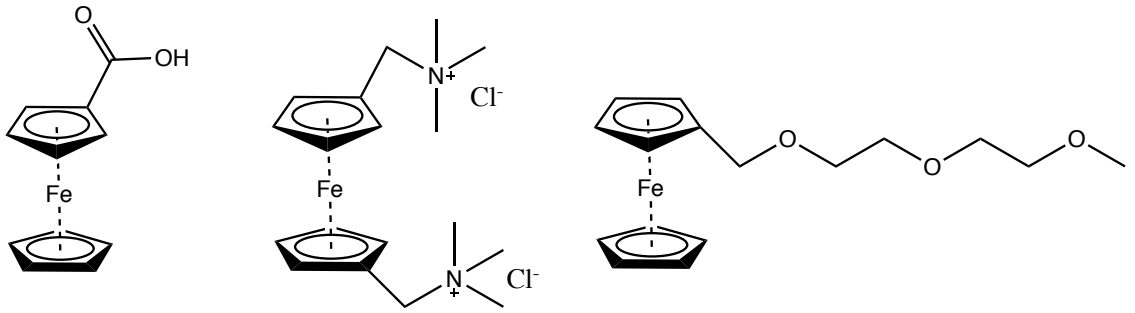

FcCOOH FcTAMCl2 FcG2OMe

Figure 3.4 Structures of Ferrocene carboxylic acid (FcCOOH), 1,1'-Bis(trimethylammoniummethyl)ferrocene (FcTAMCl2) and ((methoxy)ethoxy)ethoxymethylferrocene (FcG2OMe).

3.2.2 -Synthesis of ((methoxy)ethoxy)ethoxymethylferrocene (FcG2OMe) *from FcTAMI*

Previous methods have utilized ferrocenyl methanol as a precursor for this type of structure by deprotonating the ferrocenyl methanol with a strong base, and then nucleophilically attaching the resulting ferrocenyl alkoxide to an alkyl chloride, according to **Figure 3.5**.

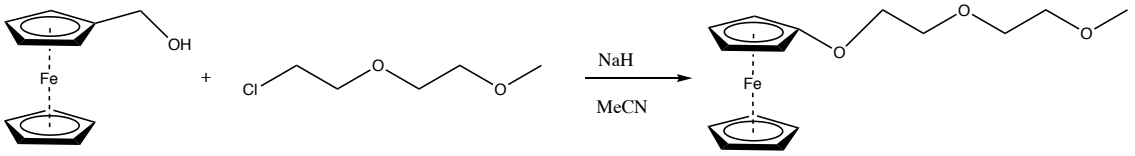

Figure 3.5 Synthetic pathway used by Cui et al to synthesize FcG2OMe[123].

Our route, however, utilizes the FcTAMI as a precursor. Using the glycol monomethylether as a solvent and the addition of a weak base, K_2CO_3, affords 85% yield of FcG2OMe after heating to reflux for 24 hours. This eliminates the need for a strong base in the synthesis, and affords a more simplified synthetic route. In considering the applications for this pathway, this provides a ferrocene tether that has hydrogen bonding acceptors in the chain. Previously used tethers in ferrocene functionalized LPEI only contain carbon spacers, which are quite hydrophobic. Using

these new glycol-ether tethers could increase the water solubility of Fc-LPEI materials, making materials that are more attractive for implantation.

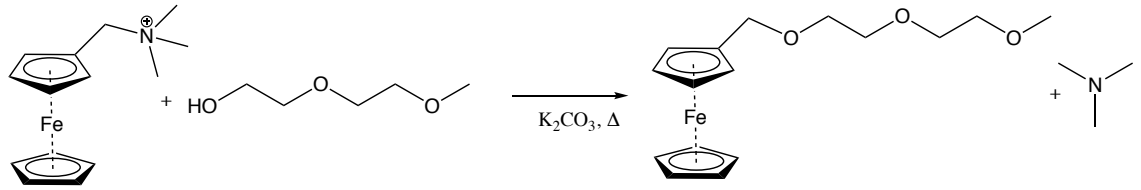

Figure 3.6 Our one-pot synthetic route that uses FcTAMI as a precursor and the glycol ether as a solvent.

3.2.3 – Electrochemistry of Mediators

Solutions of each ferrocene derivative (0.100 mM) were prepared and analyzed via cyclic voltammetry at 150 mV s^{-1} in Phosphate Buffered Saline (PBS) with a pH = 7.45. The resulting voltammograms are shown in **Figure 3.7**. FcCOOH exhibited an $E_{1/2}$ of 270 mV vs SCE. The resulting i_{pa} was 1.90 µA and the i_{pc} was 1.80 µA. The ΔE_p for FcCOOH was 50 mV. FcG2OMe exhibited an $E_{1/2}$ of 209 mV vs SCE with an i_{pa} of 0.6 µA and an i_{pc} of 0.58 µA. The ΔE_p was 58 mV. The FcTAMCl exhibited an $E_{1/2}$ of 385 mV vs SCE, with an i_{pa} of 0.81 µA, and an i_{pc} of 0.78 µA. The ΔE_p of the FcTAMCl was 53 mV. The FcTAMCl2 exhibited an $E_{1/2}$ of 402 mV vs SCE with an i_{pa} of 0.50 µA and an i_{pc} of 0.51 µA. The ΔE_p was 47 mV. The differences in $E_{1/2}$ follow the same trend observed by Forrow et al, as the trimethylammonium substituent affected the potential most. One interesting note, however, is that the addition of a second trimethyl ammonium group on the other cyclopentadiene ring did not further alter the potential by more than 20 mV. This shows that the second trimethylammonium group does not further alter the electron withdrawing effects of the trimethyl ammonium groups. Each potential gave a ratio of i_{pc}/i_{pa} equal to approximately one with a ΔE_p between 47 to 50 mV. These two observations suggest that a single electron is transferred reversibly between the ferrocene and the electrode for each derivative used in the analysis, which is consistent with other ferrocene derivatives.

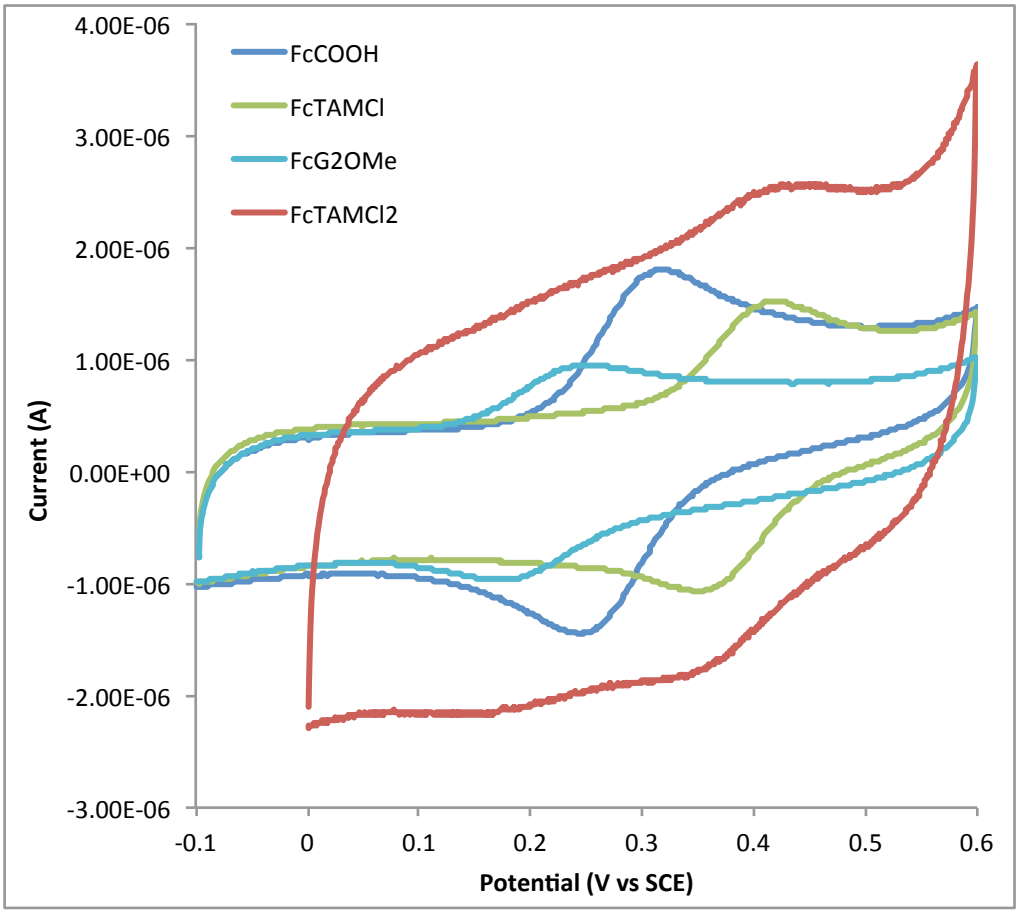

Figure 3.7 Cyclic Voltammograms of 0.1 mM solutions of each ferrocen derivative: FcCOOH, FcTAMCl, FcTAMCl2, and FcG2OMe taken in PBS at pH = 7.4. Recorded at a scan rate of 150 mV s^{-1}.

3.2.4 – Determination of K_a for each ferrocene derivative

0.100 mM solutions of each ferrocene derivative were prepared containing between 0 and 0.100 mM GOx in PBS. Each solution was analyzed via cyclic voltammetry using a glassy carbon working electrode, a saturated calomel reference electrode (SCE), and a platinum auxiliary electrode. Upon addition of GOx to each ferrocene derivative, the $E_{1/2}$ and ΔE_p did not change. However, the i_{pa} decreased as the concentration of GOx increased. One interesting feature, however, is that the i_{pa} of the ferrocene derivatives did not decrease linearly. This behavior matched the binding isotherm behavior observed between FcTAMCl and GOx. An asymptotic

decrease was observed for FcCOOH, FcG2OMe, and FcTAMCl2. Treating these data according to the binding isotherm from Chapter 2, linear behavior was observed for each derivative, which led to the determination of a K_a for each, as shown in Figures **3.8** and **3.9**. It was determined that the K_a for the FcCOOH was 1.54 x 10^6. The K_a for the FcG2OMe was determined to be 4.33 x 10^7, and the K_a for the FcTAMCl2 was determined to be 4.08 x 10^6.

$$2\,Fc + GOx \leftrightarrow (Fc_2GOx)$$

$$\theta = 100\times\left[1 - \frac{(i_a)_i}{(i_a)_0}\right] \quad (1)$$

$$\frac{\theta}{1-a\theta} = K_a C_i \quad (2)$$

$$\frac{C_i}{\theta} = \frac{1}{K_a} + aC_i \quad (3)$$

By comparing the K_a values to one another, it was observed that the K_a value for each ferrocene derivative was ranked from lowest to highest: FcCOOH < FcTAMCl2 < FcTAMCl < FcG2OMe. This ranking seems reasonable, as the FcCOOH has a negative charge at physiological pH of 7.4. The pKa of ferrocenecarboxylic acid is 4.2. Since the pH of the PBS is 7.4, it is safe to assume that the primary form of the FcCOOH is the anionic carboxylate salt. Using the Henderson-Hasselbalch equation, 99.9 % of the FcCOOH is in the anionic form at pH = 7.4. It has been previously observed that FcCOOH has a smaller k_M value than other ferrocene derivatives and anionic micelles attached to alkylferrocenes exhibit reduced k_M values in the presence of the anionic GOx[44-45]. One interesting feature, however, is that the K_a of dicationic ferrocene derivative FcTAMCl2 was only slightly higher than that of FcCOOH and lower than that of the monocationic FcTAMCl. This could suggest that the addition of the second trimethyl ammonium group either increased the size of the ferrocene too much to fit as well in the active site or that too many positive charges are an electrostatic hindrance with the additional amino acid residues in the active site. One interesting observation regarding the $FcTAMCl_2$, however, is

the magnitude of the current against the background noise of the system. This could be caused by the positive potential of the electrode surface repelling the dicationic species, causing a more significant background.

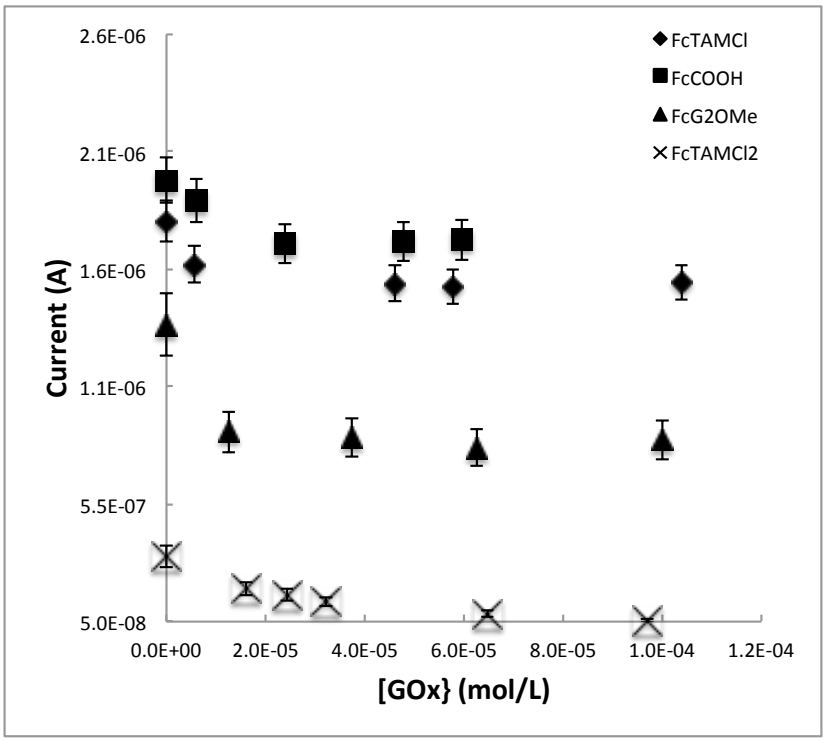

Figure 3.8 Plot of amperometric response (i_{pa}) as a function of concentration of GOx.

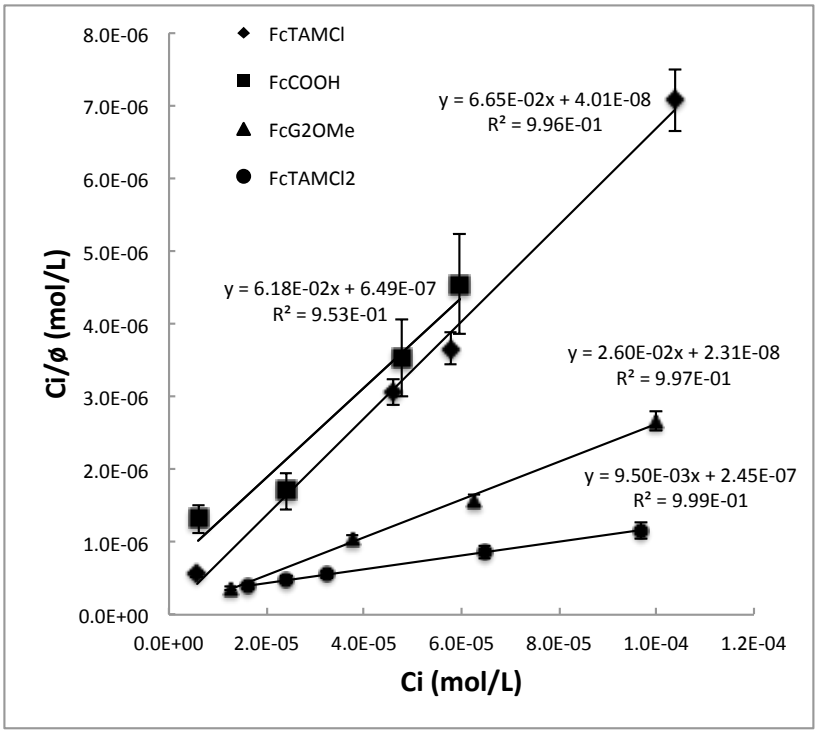

Figure 3.9 A plot of C_i/θ vs C_i for each ferrocene derivative, according to the binding isotherm developed by the Glatzhofer group.

3.2.5 – Correlation Between Binding Constant, K_a, and Catalytic Currents, i_{cat}

All binding experiments were conducted in the absence of glucose. However, the relevance of this binding coefficient is not necessarily related to the ability of a mediator to transfer electrons between the active site of GOx and the electrode surface. In order to investigate any potential connection between the binding constant, K_a, and the mediative ability of each ferrocene derivative, the increase in i_p was investigated to determine if any correlation exists. Solutions containing 0.100 mM mediator and 0.100 mM GOx were analyzed using cyclic voltammetry in the absence and presence of 100 mM glucose.

This document has already discussed the issues surrounding the use of k_M as a measure of mediative capabilities in Chapter 2. In considering these issues, it is reasonable to decide on a comparison for determining the application of the binding constant. Based on the different

magnitudes of the amperometric responses of the four mediators, it is reasonable to speculate that the resulting i_{cat} would not be a reasonable measure for directly comparing one molecule's mediative capability against another. A more appropriate measure for comparison could be the ratio of i_{cat}/i_{pa}. By using this ratio, the difference in the amperometric response in the absence of glucose, i_{pa}, can be compared to the catalytic response, i_{cat}, to provide a more appropriate measure of a molecule's efficacy as a mediator. It should be noted that additional concerns, such as diffusion of the mediator between the enzyme and the electrode surface, should be taken into consideration. However, by stirring the solution, the diffusion dependence can be eliminated. Thus, the increase in current should be due solely to the interactions between the mediator and the enzyme.

Each ferrocene derivative, upon the addition of glucose, yielded different voltammograms than in the absence of glucose. When glucose was added, a flat, wave shape is observed in the voltammogram of each ferrocene derivative, except for FcTAMCl2. Upon addition of glucose, FcTAMCl2 showed an increase in the current, and the sharp "spike" at the end of the electrochemical window was still observed, as demonstrated in **Figure 3.10**. This spike was observed in the absence of glucose, as well. The results of the amperometric analyses in the absence (i_{pa}) and presence of glucose (i_{cat}) are summarized in **Table 3.2**. The i_{pa} of FcTAMCl was 0.81 μA, and the i_{cat} was 12.6 μA, leading to a ratio of i_{cat}/i_{pa} of 15.5. The i_{pa} of FcCOOH was 1.31 μA, and the i_{cat} was 4.63 μA, leading to a ratio of i_{cat}/i_{pa} of 3.5. The i_{pa} of FcG2OMe was 0.50 μA, and the i_{cat} was 2.74 μA, leading to a ratio of i_{cat}/i_{pa} of 5.5. The i_{pa} of FcTAMCl2 was 0.25 μA, and the i_{cat} was 1.50 μA, leading to a ratio of i_{cat}/i_{pa} of 6. When comparing these data, there is not an observable trend between $E_{1/2}$ and K_a, or between i_{cat}/i_{pa} and $E_{1/2}$, as initially suspected. This is most likely caused by a specific functional group interaction

with the binding site on the enzyme. While it has been demonstrated that electron-donating and withdrawing groups can alter the potential of a ferrocene ring, there are amino acid residues in the binding site of ferrocene on GOx. These functional group interactions could be caused by hydrogen bonding, or other intermolecular forces. It could be imagined that if both electron donating and electron withdrawing groups can interact in this site, then it would be expected that there may not be a trend between $E_{1/2}$ and K_a. In considering why there is not an observable trend between the ratio of i_{cat}/i_{pa}, it could be due to the nature of the binding between ferrocene and GOx. In considering the mechanism of how GOx catalyzes the oxidation of glucose into gluconolactone, a strong K_a could inhibit the release of ferrocene from GOx which could slow down the overall process. It is notable that FcTAMCl exhibited the second highest K_a, and yielded the highest i_{cat}/i_{pa}, and FcCOOH exhibited the lowest K_a and yielded the lowest i_{cat}/i_{pa}. The derivative that exhibited the strongest binding did not exhibit the highest i_{cat}/i_{pa}. This model is consistent with the observed data, but further investigation into the effects of a broader array of functional groups on K_a should be conducted.

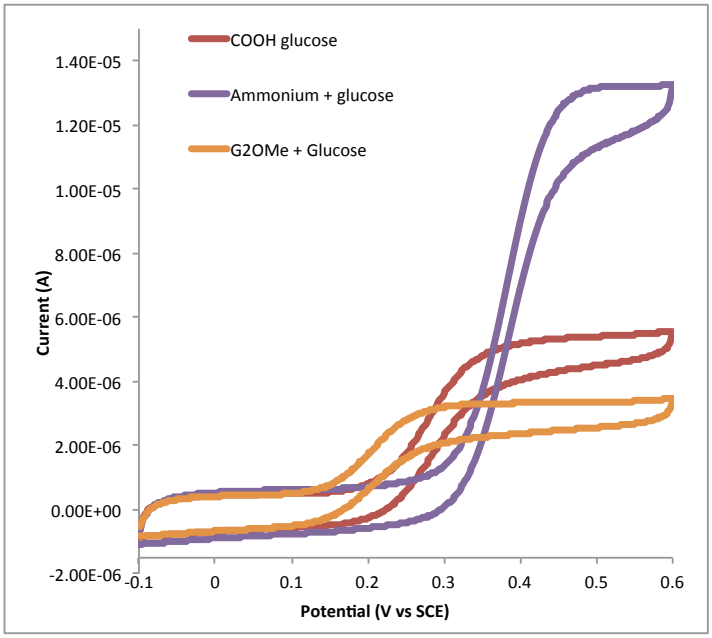

Figure 3.10 Cyclic Voltammograms of 0.1 mM FcCOOH, FcG2OMe, FcTAMCl, and FcTAMCl2 in the presence of 0.1 mM GOx and 100 mM glucose in PBS at pH = 7.4. Each voltammogram was recorded at 150 mV s^{-1} while stirring.

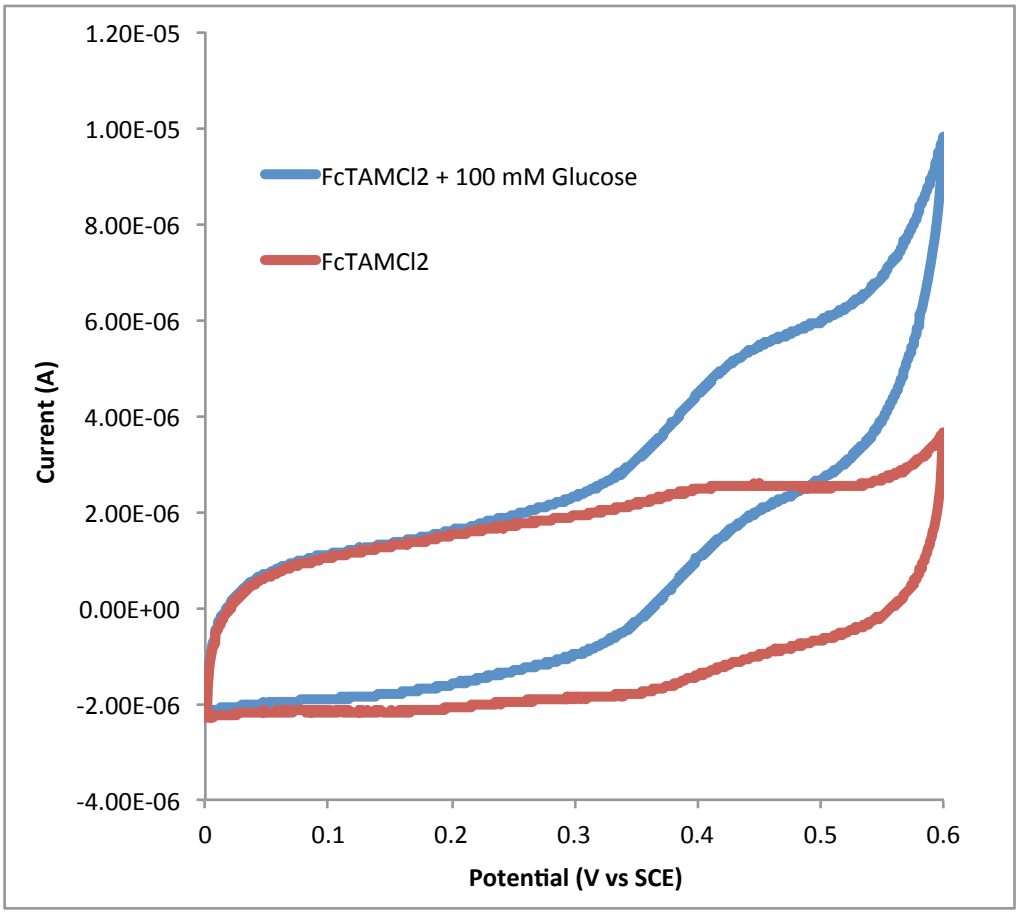

Figure 3.11 Cyclic Voltmmograms of FcTAMCl2 in the absence and presence of 100 mM glucose in PBS at pH = 7.4 collected at 150 mV s^{-1}.

Mediator	ip_a (μA)	i_{cat} (μA)	i_{cat}/i_{pa}	*Ka*
FcTAMCl	0.81	12.6	15.5	2.49×10^7
FcCOOH	1.31	4.63	3.5	1.56×10^6
FcG2OMe	0.50	2.74	5.5	4.33×10^7
FcTAMCl2	0.25	1.50	6	4.08×10^6

Table 3.2 The amperometric responses in the absence (i_{pa}) and presence of glucose (i_{cat}), the ratios of i_{cat}/i_{pa}, and the binding constant, K_a of each ferrocene derivative.

It should be noted that the weak correlation between K_a and i_{cat}/i_{pa} is only applicable to those electrodes in solution state. By immobilizing GOx in a redox-active polymer, it could be envisioned that a strong complexation may be favorable for communication between the redox polymer and the enzyme. Solution-state analysis relies on not only interaction between the

ferrocene and the enzyme, but the movement of the ferrocene to the electrode. In order determine the effect of the binding constant, Ka, on a mediator's ability to work in the polymer supported state, polymer-supported systems must be fabricated.

3.3 Conclusions

In summary, we have developed a simplified method for the synthesis of (((methoxy)ethoxy)ethoxy)methylferrocene (FcG2OMe). In addition, it has been demonstrated that three additional ferrocene derivatives, ferrocene carboxylic acid, FcG2OMe, and bis(trimethylammonium methyl) ferrocene chloride, bind to GOx, according to the binding isotherm developed by our lab group. The isotherm appears to be affected by electrostatic repulsions, as evidenced by the lowest value demonstrated by the smallest binding value associated with the anionic carboxylate derivative, but it could also be imagined that interactions from other intermolecular forces like hydrogen bonding could be at work. This could be investigated by probing the K_a of a larger array of functional groups on additional ferrocene derivatives. It was also demonstrated that a ferrocene glycol ether successfully acted as a mediator for GOx in the presence of glucose oxidase. There does not appear to be a direct correlation between the strength of the binding isotherm and a mediator's efficacy in shuttling electrons, as evidenced by the lack of correlation between the ratio of catalyzed to uncatalyzed amperometric response (i_{cat}/i_{pa}). Investigation into any correlation between Ka and the performance of polymer-supported 2nd generation biofuel cell may be beneficial in applying this observed isotherm. A large K_a could mean a larger current density, due to the mediator interacting favorably with the enzyme and harvest the electrons at a faster rate. Conversely, a large K_a could mean a smaller maximum current density in the polymer-supported material, as it could mean that the mediator is harder to release from the enzyme. New materials analogous to

the FcG2OMe must be designed to determine if the magnitude of K_a would impact the performance of analogous materials.

3.4 Experimental

All reagents and enzymes were purchased from Sigma-Aldridge and used without further purification. FcTAMCl, and FcTAMCl2 were synthesized usin previous literature methods, as described below[126]. All cyclic voltammetric data was obtained using a CV 50 bipotentiostat. Electrochemical experiments were carried out in phosphate-buffered saline (PBS), where 1M HCl was used to adjust the pH to 7.4 All electrochemical experiments were taken using a glassy carbon working electrode, a AgCl reference electrode, and Pt wire auxiliary electrode. Measurement taken in the absence of glucose were taken without stirring. Measurements taken in the presence of glucose were taken while each solution was stirred.

Synthesis of Methoxy(ethoxy(ethoxy(methylferrocene))) (FcG2OMe)

In a round bottom flask, 400 mg (1.42 mmol) of (ferrocenylmethyl)trimethylammonium iodide were dissolved in 10 mL of diethyleneglycol monomethyl ether. The solution was heated overnight to solvent reflux under nitrogen. The solution was extracted with dichloromethane and the solvent was removed under reduced pressure to afford a yellow oil. The yellow oil was passed through a silica column in 5:1 hexanes/dichloromethane. The yellow band was recovered and the solvent removed under reduced pressure to afford a yellow oil. The yellow oil was charachterized using NMR spectroscopy, and good agreement was observed with other literature reports[123]. ^{1}H NMR: δ4.28 (5 H, s); δ4.19 (4 H, br s); 4.11 (2 H s); 3.63-3.53 (8 H, m); 3.37 (3 H, s)

Synthesis of bis(trimethylammoniummethyl)ferrocene iodide

This procedure was adapted from Lednicer[126]. A mixture of 25 mL of glacial acetic acid and 3 mL of 85% phosphoric acid was prepared in a 125 mL Erlenmeyer flask, and the flask was placed in an ice bath. To this mixture, 0.645 g of N,N,N',N'-tetramethyldiaminomethane (6.3 mmol) was added dropwise and allowed to stir for 1 hour. Afterwards 400 mg (2.2 mmol) of ferrocene were added to the mixture and the round bottom flask was purged with nitrogen. The mixture was heated to solvent reflux for 8 hours under nitrogen. The flask was removed from heat and placed in an ice bath. Sodium hydroxide pellets were added slowly to the reaction mixture with stirring until the pH was much greater than 10. The mixture was extracted with 3 aliquots of diethyl ether in a separatory funnel. The organic layer was concentrated under reduced pressure to afford an amber liquid. The amber liquid was passed over a silica column in a 9:1 hexane/chloroform mixture. Two bands eluted from the column: The first was (dimethylaminomethyl)ferrocene, as characterized by NMR analysis. The second band was characterized to be bis(dimethylaminomethyl)ferrocene. The second band was methylated with 3 equivalents of methyl iodide (6.6 mmols) in methanol. Upon the addition of ether, a yellow precipitate formed. NMR analysis confirmed the synthesis of bis(trimethylammonium methyl) ferrocene iodide.

Ion exchange of iodide to synthesize Bis(trimethylammoniummethyl)ferrocene chloride

Amberlyte ion exchange resin was flushed with DI water thoroughly and then charged with 2.0 M NaCl solution. The column was subsequently flushed with fresh DI water to remove excess NaCl from the column. Methanol was then flushed through the column until convection lines were no longer observed when the eluent from the column was added to pure methanol. A concentrated solution of FcTAMI2 in MeOH was prepared and loaded onto the column. The ion exchange resin was loaded at 1.8 mEq per g of amberlyte. The FcTAMCl2 was eluted with fresh

methanol. Once eluted, the methanol was removed under reduced pressure to afford pure FcTAMCl2 as a yellow powder in greater than 95% yield. To ensure the removal of iodide from the system, a small amount of each compound were dissolved in separate solutions and treated with 0.1 M AgCl. The resulting white precipitate, and not yellow, indicated that only chloride was present.

Enzymatic Titration of ferrocene derivatives with GOx

A Ferrocene stock solution was prepared using pure ferrocene derivative derivative in PBS. Each analyzed mixture contained 0.100 mM Fc derivative, and varying amounts of GOx ranging from 6 – 100 μM. Cyclic voltammetric measurement were conducted at a scan rate of 150 mV/sec using a 3 mm glassy carbon electrode as the working electrode without stirring.

Amperometric Enzymatic Investigations of Glucose in the ferrocene mixtures

To the mixtures above, 2 M glucose in PBS was added to make the concentration equal to 100 mM. Mixtures were prepared so that the final volume would not be different than the final volume of the control solutions.

Chapter 4 – Synthesis and Characterization of a Ferrocenyl Glycol Ether-Containing Linear Poly(ethylenimine) for Use in Bioelectrode Materials Based on K_a of a Langmuir Binding Isotherm

4.1 Introduction

Oxidoreductases are enzymes that harness electrons from or provide electrons to the chemical reactions they catalyze[137]. This class of enzymes, in particular Glucose Oxidase (GOx), has received a great deal of attention as they have been used in the fabrication of bioelectrode materials[23, 45, 69, 100, 105-106]. Second generation bioelectrodes utilize a mediator to transfer electrons harvested by oxidoreductases to an electrode surface. These mediators are small, electrochemically-active molecules that can: 1) penetrate the active site of an enzyme, 2) accept electrons from the active site of the enzyme and 3) release[44-45] electrons to the electrode. In the case of GOx, glucose diffuses into the active site of GOx, where the FAD center in the active site oxidizes glucose into gluconolactone, and the FAD is reduced to $FADH_2$. The $FADH_2$ is the oxidized back to FAD by the mediator, and the reduced mediator carries the electron to the electrode, where the electrode oxidizes the mediator. This cycle then repeats on a rapid time scale, approximately 1900 times per sec[138-139]. In solution, diffusion of each component from one to another and then to the electrode can limit the amperometric response of the bioelectrode[19]. In order to overcome these limitations, Heller developed an immobilization technique that is still used as a bioelectrode design[25].

Heller's design used an osmium bipyridine complex that is covalently linked to poly(vinylpyridine) to entrap GOx inside of a polymer material. This material effectively "wired" the enzyme to the polymer, enabling a means to overcome the diffusion limitation of one substrate to another[25]. The Glatzhofer group has used Heller's technique as a means to develop a

material based on ferrocene and linear poly(ethyleneimine)[48, 57, 75, 113]. Linear poly(ethyleneimine) (LPEI) has a low glass transistion temperature (T_g) of -35 ° C, which was thought give the material a high segmental mobility, compared to Heller's poly(vinylpyridine)–Osmium marterial (PVP-Os), as poly(vinylpyridine) exhibits a T_g of 142 ° C[57]. Our material outperformed Heller's material, as evidenced by a higher maximum current density, J_{max}, of 480 μA/cm^2 in the ferrocene-modified LPEI (Fc-LPEI) and a J_{max} of 21 μA/cm^2 in the PVP-Os[57]. Since Fc-LPEI had such a higher J_{max} and lower T_g, it was reasonable to suspect that electrons moved through the Fc-LPEI films at a higher rate, measured by the electron diffusion coefficient D_e. For these Fc-LPEI films, however, D_e was on the magnitude of 10^{-8} mol cm^{-2} sec^{-1}, while the D_e of Heller's PVP-OS material was on the magnitude of 10^{-6} mol cm^{-2} sec^{-1} [57, 140]. The electron diffusion coefficients are not in agreement with the observed J_{max} for each material. This suggested that the superior performance of the Fc-LPEI material against the PVP-OS material was caused by either the unique flexibility of the LPEI or due to a unique, uncharacterized interaction between Fc-LPEI and GOx.

The Glatzhofer group has electrochemically detected a binding isotherm that occurs between GOx and ferrocene (Fc), described in Chapter 2 of this document. By titrating a ferrocene solution with varying concentrations of GOx (C_i), the changes in amperometric response allowed a binding coefficient, K_a, to be detected. The value of θ, the ratio of the amperometric response in the presence and abense of GOx, was plotted as a function of the molarity of GOx to determine the K_a of the ferrocene derivative.

$$2\,Fc + GOx \leftrightarrow (Fc_2GOx)$$

$$\theta = 100\times\left[1 - \frac{(i_a)_i}{(i_a)_0}\right] \quad (1)$$

$$\frac{\theta}{1-a\theta} = K_a C_i \quad (2)$$

$$\frac{C_i}{\theta} = \frac{1}{K_a} + aC_i \qquad (3)$$

This K_a is on the magnitude of 10^5 to 10^7, depending on the particular derivative of ferrocene. This binding isotherm indicates how strongly a ferrocene molecule binds to GOx. ((Methoxy)ethoxy)ethoxymethylferrocene (FcG2OMe) exhibited the highest K_a value of all ferrocene derivatives tested, $K_a = 4.33 \times 10^7$. However, when used as a mediator in the presence of glucose, the catalytic current only increased five-fold from the noncatalytic system, whereas (ferrocenylmethyl)trimethylammonium chloride (FcTAMC) exhibited a $K_a = 2.49 \times 10^7$ exhibited a 15-fold increase in the catalytic current in the presence of glucose. This left some uncertainty as to whether this tool could be useful as a screening tool for mediators that could be used to develop high-performance bioelectrode materials. However, it could be imagined that when these strongly-binding mediators are attached to a redox polymer, the interaction may help draw the polymer and other redox tethers closer to the enzyme and increase the efficiency of electron transfer between the active site and the electrode surface, as shown in Figure 4.1.

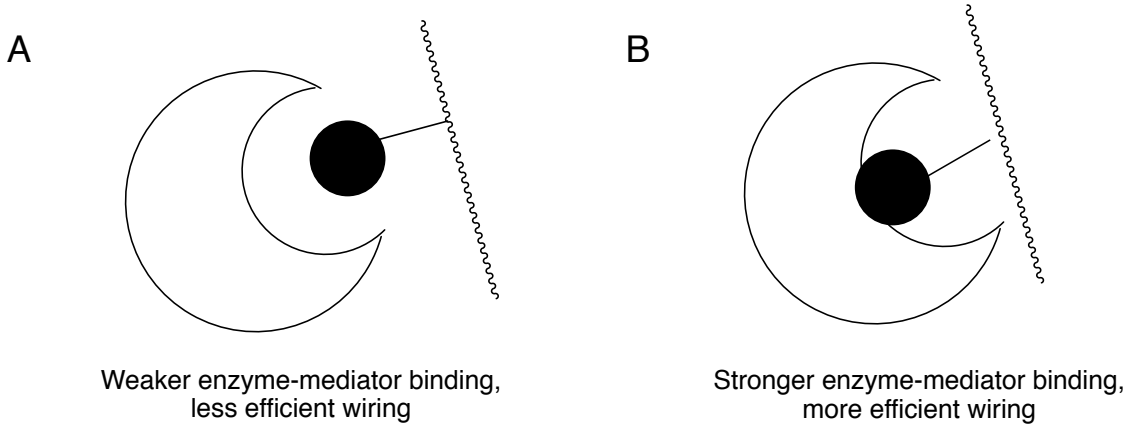

Figure 4.1 A) A weak enzyme-mediator binding, as measured by a smaller K_a value, could suggest that the enzyme is not as efficiently wired to the polymer support, while B) shows a stronger enzyme-mediator binding. A stronger mediator interaction could result in a higher performing bioelectrode material than a weaker enzyme-mediator interaction.

Hypothesis

Using the Ka of the enzyme and ferrocene binding interaction measured in Chpater 3 as a guide, a bioelectrode material can be synthesized by attaching moieties of ((Methoxy)ethoxy)ethoxymethylferrocene (FcG2OMe) to linear poly(ethylenimine) (LPEI). This material would serve as an analogous polymer material that can be used to investigate the effect of the binding constant K_a has an impact on the amperometric performance of a bioelectrode. If this detected enzyme-mediator interaction is effective in creating a stronger "wiring" of the enzyme to the polymer support, then the performance of the LPEI material made with FcG2OMe -type ethers should have a higher maximum current density, $J_{max,}$ than a LPEI material made with (ferrocenylmethyl)trimethylammonium moieties (FcTAM).

4.2 Results and Discussion

4.2.1 Polymer Synthesis and characterization

In considering the ferrocenyl glycol ether, FcG2OMe, there are three oxygen atoms in the chain. In order to make an analogous LPEI material, it is reasonable to speculate that the terminal methoxy group could be where the material attaches to the LPEI, as shown in figure 4.2.

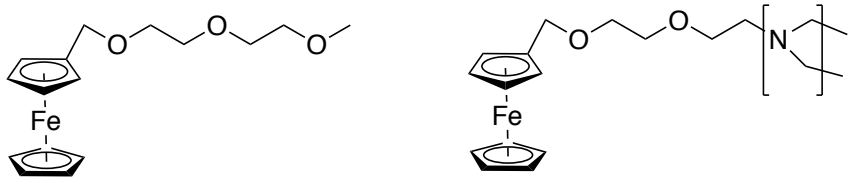

Fc-G2-OMe Fc-G2-LPEI

Figure 4.2 Ferrocenyl glycol material (FcG2OMe) used in chapter 3 that exhibited the highest K_a value and the analogous material made from the mediator and LPEI, Fc-G2-LPEI.

In order to synthesize this material, however, a different ferrocene molecule must be used. In order to synthesize the corresponding LPEI-functionalized ferrocene material, the Glatzhofer group has used both bromo- and iodo- groups to attach ferrocene derivatives at the terminal carbon to LPEI[48, 63, 75]. The necessary 2-(2-haloethoxy)ethanol is commercially available as a chloride. Using the trimethylammonium FcTAM as a starting material, the hydroxyl group should be sufficiently nucleophilic to attach to the alpha-carbon of the ferrocene ring to produce the halogenated glycol ether. The chloride can then undergo a Finkelstein reaction and produce a molecule that can attach to LPEI to produce the desired Fc-G2-LPEI, as shown in figure 4.3 below.

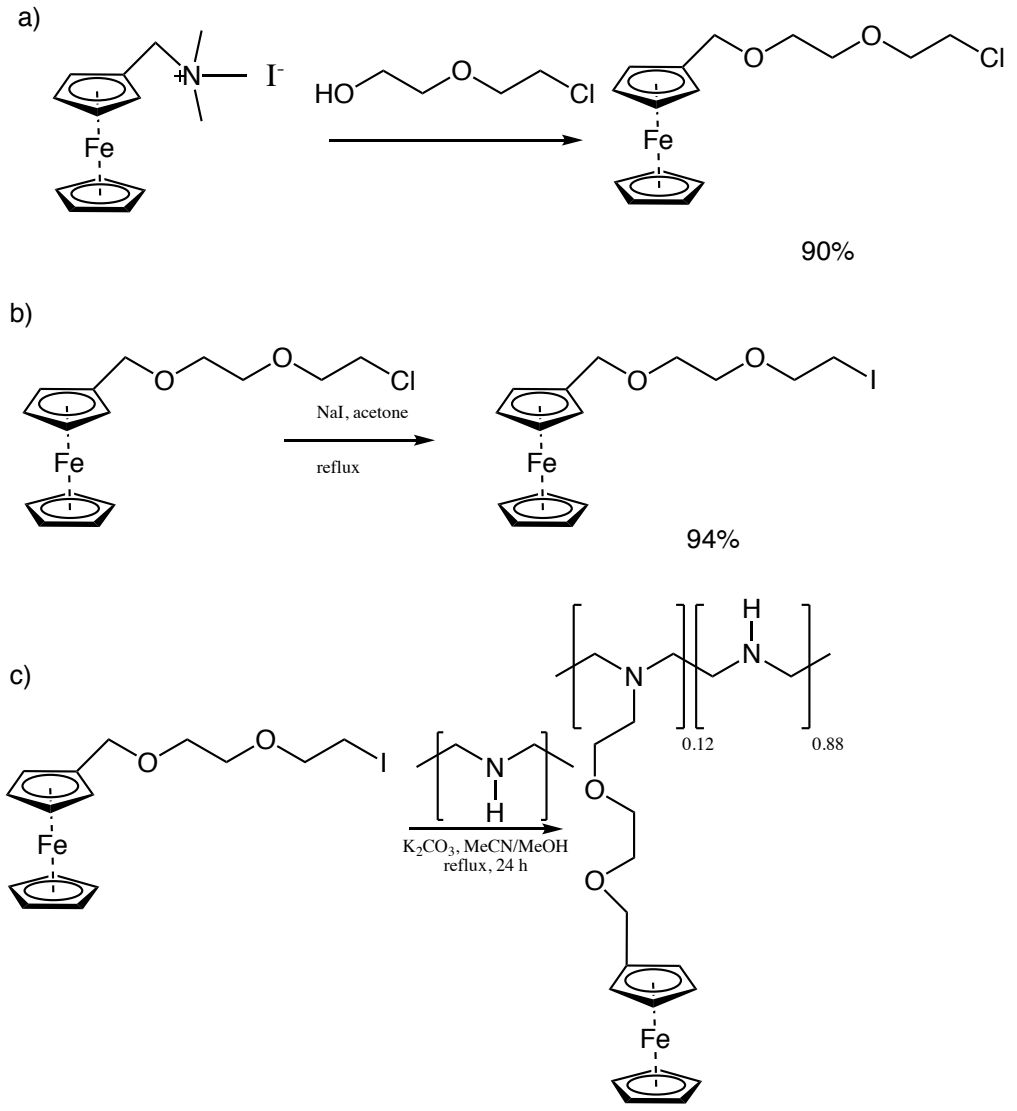

Figure 4.3 The synthetic scheme used to prepare the Fc-G2-LPEI material from FcTAM. The synthetic design in figures b and c were adapted from Meredith et al[59]

The polymer was synthesized in good yields. The percent substitution was characterized to be 12% ferrocene by NMR**.** To characterize the percent substitution of ferrocene attached to the polymer, the integration of the ferrocenyl hydrogens was set to 9. LPEI has four non-exchanging hydrogen atoms in a standard repeat unit. By this method, at 100% substitution, the LPEI hydrogen atoms should integrate to 4. Thus, setting the integrations of the ferrocenyl

protons to 9, the resulting LPEI backbone integration divided by four should lead to a percent substitution of ferrocene on the LPEI backbone.

Equation 4.1

$$\text{Fc-G2-LPEI ferrocene substitution percentage} = \frac{Measured\ H\ atom\ integration}{4}\ x\ 100\%$$

A ferrocenylmethyl-modified LPEI (Fc-C1-LPEI) (15% Fc) was also prepared as a method for comparison, according to a method outlined by Meredith. It is important to note that this Fc-C1-LPEI material was the same material used in Chapter 2 that inspired the use of (ferrocenylmethyl)trimethylammonium chloride to detect the binding isotherm. This Fc-C1-LPEI material will be used as a basis for comparison, as the FcTAM compound exhibited the second strongest binding constant, K_a.

4.2.2 – Electrochemical Characterization of Fc-G2-LPEI/GOx films

Once the polymer was made, a 10 mg/mL solution of the polymer was prepared, using small amounts of 1 M HCl (aq) to aid in dissolution. Once dissolved, the polymer was mixed with varying concentrations of a solution of ethylene glycol diglycidyl ether (EGDGE) and a consistent amount of Glucose Oxidase (GOx). The mixture was cast onto glassy carbon electrodes and allowed to cure for 24 hours at room temperature, according to a procedure developed by the Glatzhofer group[48, 63, 75]. Fc-C1-LPEI electrodes made from the material containing the ferrocenylmethyl moiety were prepared according to a procedure reported by Meredith[48, 63, 75]. The percent substitution of the ferrocene on the LPEI was 14%. All electrodes were placed in phosphate buffered saline (PBS) pH = 7.4 for 20 minutes to allow any residual iodide ions to diffuse out of the polymer. All films remained on the electrode and did not detach from the electrode surface, suggesting a mechanically stable film.

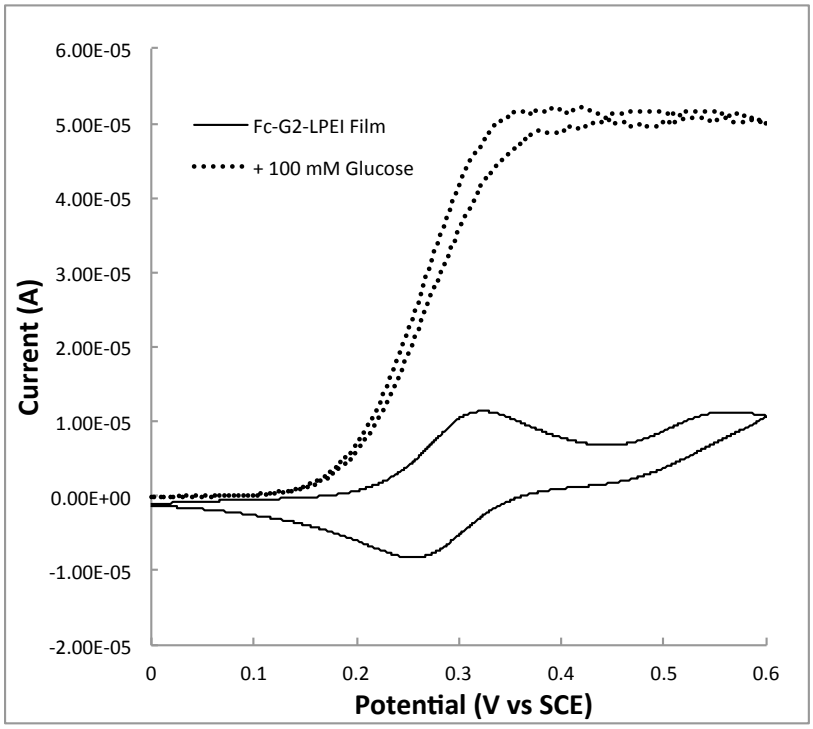

Figure 4.5 – Cyclic voltammograms of the glycol ether ferrocene-functionalized LPEI (Fc-G2-LPEI) films made using a 10 %(v/v) solution of ethylene glycol diglycidyl ether (EGDGE) with GOx in the absence (solid line) and presence (dotted line) of glucose. The voltammograms were obtained using a glassy carbon working electrode, a staturated calomel electrode (SCE) reference electrode, and a platinum wire auxiliary electrode at a scan rate of 5 mV/sec.

The resulting voltammograms of the film are shown in Figure 4.5. In the absence of glucose, there is an oxidative wave with an anodic peak potential, E_{pa}, at 310 mV vs SCE that shows a peak current, i_{pa}, of 7.1 μA. There is a reductive wave with a cathodic peak potential, E_{pc}, at 266 mV vs SCE that exhibits a peak potential, i_{pc}, of 6.9 μA. The ratio of i_{pa}:i_{pc} is 1.03, and the difference between the peak potentials, ΔE_p, is 44 mV, suggesting that these peaks are indicative of a reversible one electron transfer. This aligns with other ferrocene species that have acted as mediators for GOx in the polymer-supported phase. One interesting feature, however, is the redox potential of the ferrocene in the film is approximately 100 mV higher than that of the corresponding mediator studied in Chapter 3, the FcG2OMe. There is a second oxidative event

occurring around 560 mV vs SCE without a corresponding reduction event. This observed potential is similar to the potential of the reduction of iodide seen Chapter 2, suggesting that residual iodide may be present in the film, even after pre-soaking the electrode films in PBS prior to analysis.

In the presence of glucose, the voltammogram changed shape. There is no longer a reductive wave observed, and the secondary oxidative event at 560 mV vs SCE is no longer observed. There is a single oxidative peak at 310 mV vs SCE with a catalytic current, i_{cat}, of 52 μA. The increased current and lack of reduction waves indicate that the enzyme is acting as a catalyst in the presence of glucose.

To determine if a potential connection between K_a and the performance of a polymer-supported material designed using the corresponding mediators, films of ferrocenylmethyl-functionalized LPEI (Fc-C1-LPEI) were prepared according to a procedure used by Meredith[59]. Voltammograms of the Fc-C1-LPEI film in the absence and presence of glucose at a scan rate of 5 mV/sec are shown in Figure 4.6. An oxidative wave is observed with a E_{pa} of 330 mV vs SCE and an i_{pa} of 20.2 μA. There is a reductive wave observed with a E_{pc} of 295 mV vs SCE that exhibited an i_{pc} of 16.5 μA. The ratio of i_{pa}:i_{pc} was 1.22 and the ΔE_p was 35 mV. While this is not aligned exactly with a ΔE_p of 59 mV and a ratio of i_{pa}:i_{pc} equal to 1, this is still indicative of a single electron transfer due to the ferrocene. In the presence of glucose, a sole catalytic oxidative wave is observed in the voltammogram, with a catalytic current of 42.3 μA.

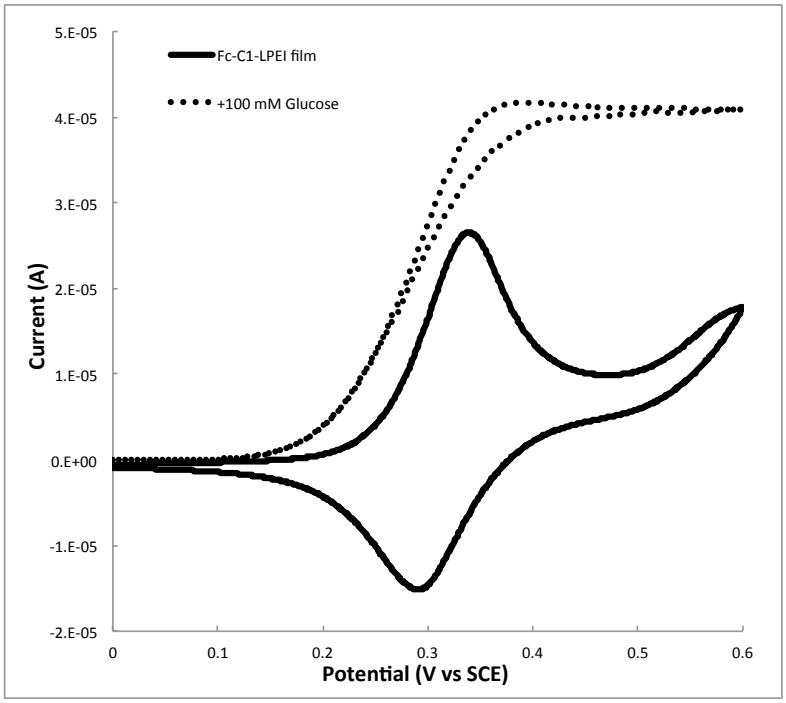

Figure 4.6 – Voltammograms of the Fc-C1-LPEI films in the absence (solid line) and presence (dotted line) of glucose. All films were immobilized on glassy carbon working electrode, and voltammograms were recorded using an SCE refence electrode and a platinum auxiliary electrode at a scan rate of 5 mV/sec.

In order to obtain a more quantitative analysis of the materials, and to check the efficiency of the enzyme, a glucose titration was performed to determine a maximum current density, J_{max}, and a Michaelis constant, K_m, of GOx immobilized in each film. The Michaelis constant represents the concentration of substrate at which half of the maximum rate is obtained, while the J_{max} represents the current produced at the electrode. These parameters can be used to relatively evaluate how efficiently the enzyme is operating within the material. When the Fc-G2-LPEI and Fc-C1-LPEI materials were titrated with glucose at 350 mV vs SCE and 390 mV vs SCE, respectively, a plot of current vs time shows a step-like behavior, as shown in Figure 4.7. Each step on the plot represents an increase in glucose concentration of 5 mM.

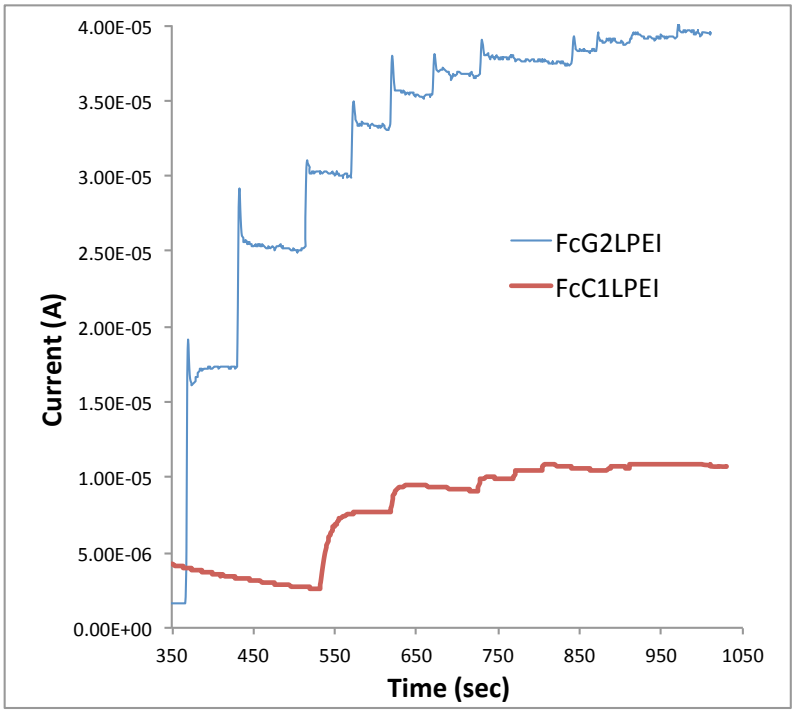

Figure 4.7 – A titration of FcG2LPEI (blue) at 350 mV vs SCE and FcC1LPEI (Red) at 390 mV vs SCE as the concentration of glucose increased by 5 mM while stirring.

When plotting the amperometric responses from the data Figure 4.7 as a function of glucose concentration, an asymptotic behavior is observed for both the Fc-C1-LPEI material and the Fc-G2-LPEI material. It is important to note that the geometric current density, *J*, is used instead of the absolute current to allow for comparison to other bioelectrode materials. The data was treated similarly to a Michaelis-Menton analysis and Lineweaver-Burke plots were prepared for both materials, as shown in Figure 4.8. The Lineweaver-Burke method of analysis allows for the treatment of non-linear data into a linear fashion from which the K_m and J_{max} could be determined. Testing three electrodes of each material, the K_m and J_{max} of the glycol based Fc-G2-LPEI material were calculated to be 9.8 ± 0.9 mM and 608 ± 60 µA cm^{-2}, respectively, while the K_m and J_{max} of the Fc-C1-LPEI material were calculated to be 1.94 ± 0.4 mM and 320 ± 40 µA cm^{-2}, respectively. The improved amperometric performance observed in the Fc-G2-LPEI material compared to the Fc-C1-LPEI material suggests that the original hypothesis regarding K_a

was correct. It appears that the K_a of the mediator in the solution state can be used as a predictor of performance in the polymer-supported state.

The observed results regarding the Fc-C1-LPEI material used within this experiment were not consistent with results reports by Meredith and Merchant when a similar material was used[59, 75, 113]. At pH=7, Merchant reports a J_{max} value of 237 μA cm^{-2}, while Meredith reports a value of ca. 750 μA cm^{-2} at 15 % ferrocene substitution[59, 75, 113]. However, it is more likely due to the difference in the % EGDGE used in each experiment. This work utilized a 10 %(v/v) of EGDGE as a cross-linking agent, while Merchant used a 30 % (v/v) EGDGE solution as a cross-linking agent. In addition, the percent substitution of the ferrocene in this work is different than the percent substitution of ferrocene used by Merchant (40%) and Meredith (5-40%). Hickey also noted that the % (v/v) EGDGE used in film preparation had a significant effect on the electron diffusion coefficient, $cD_e^{1/2}$ [64]. With all of these reports of varying amperometric values, it is difficult to make a direct comparison of materials using an optimized amount of EGDGE. In order to more thoroughly investigate the effects of the % (v/v) EGDGE used in preparing the films on the performance of the Fc-G2-LPEI material, and to investigate the effects on the Fc-G2-LPEI films, additional films were prepared using varying amounts of EGDGE.

4.2.3 – Varying the amount of EGDGE in the Fc-G2-LPEI films

Films of Fc-G2-LPEI material were prepared using between 15 % (v/v) and 30 % (v/v) EGDGE in the solution mixture, according to the method described above. Cyclic voltammograms of each new film in both the absence and presence of glucose, as well as Michaelis Menton titrations with glucose are shown in Figure 4.9.

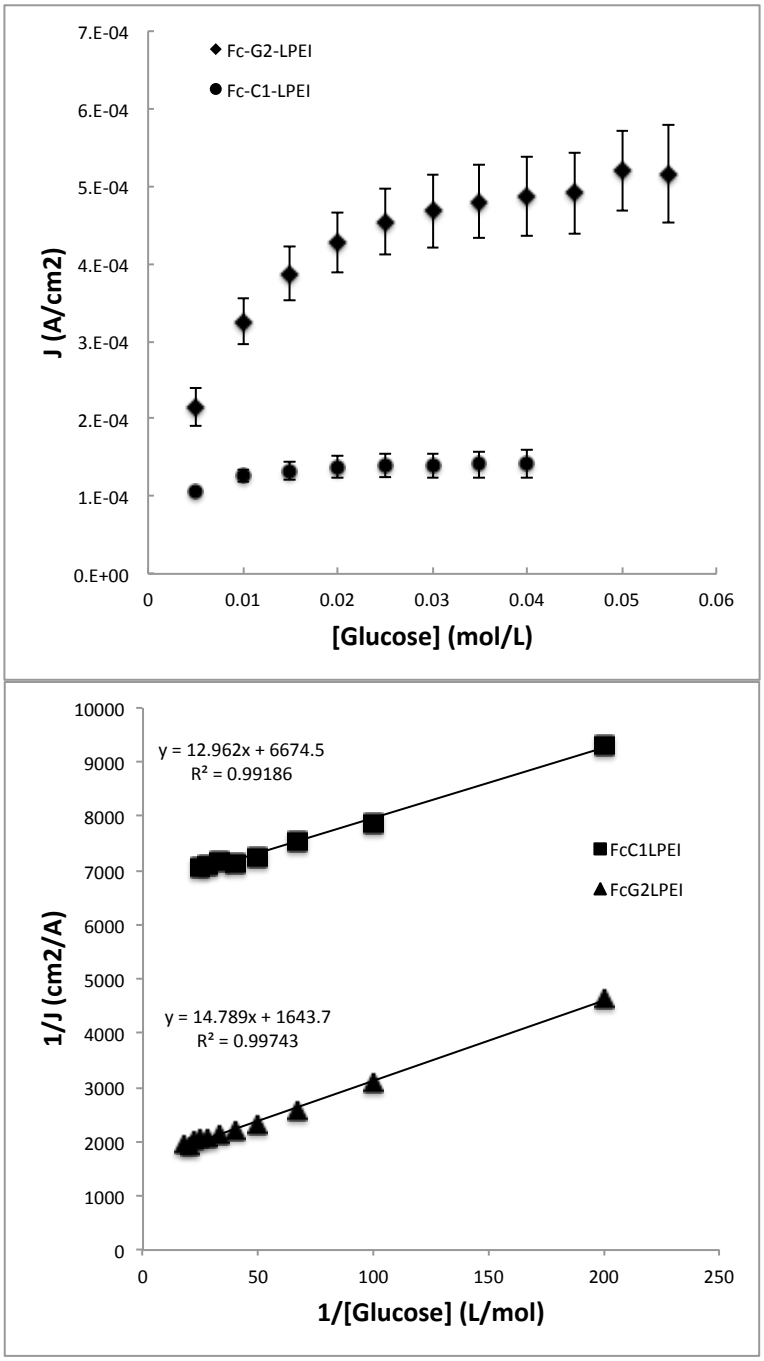

Figure 4.8 – Plots of the current density, *J*, as a function of glucose concentration as both Michaelis-Menton style plots (top figure) and Lineweaver-Burke plots of the data gathered in Figure 4.7.

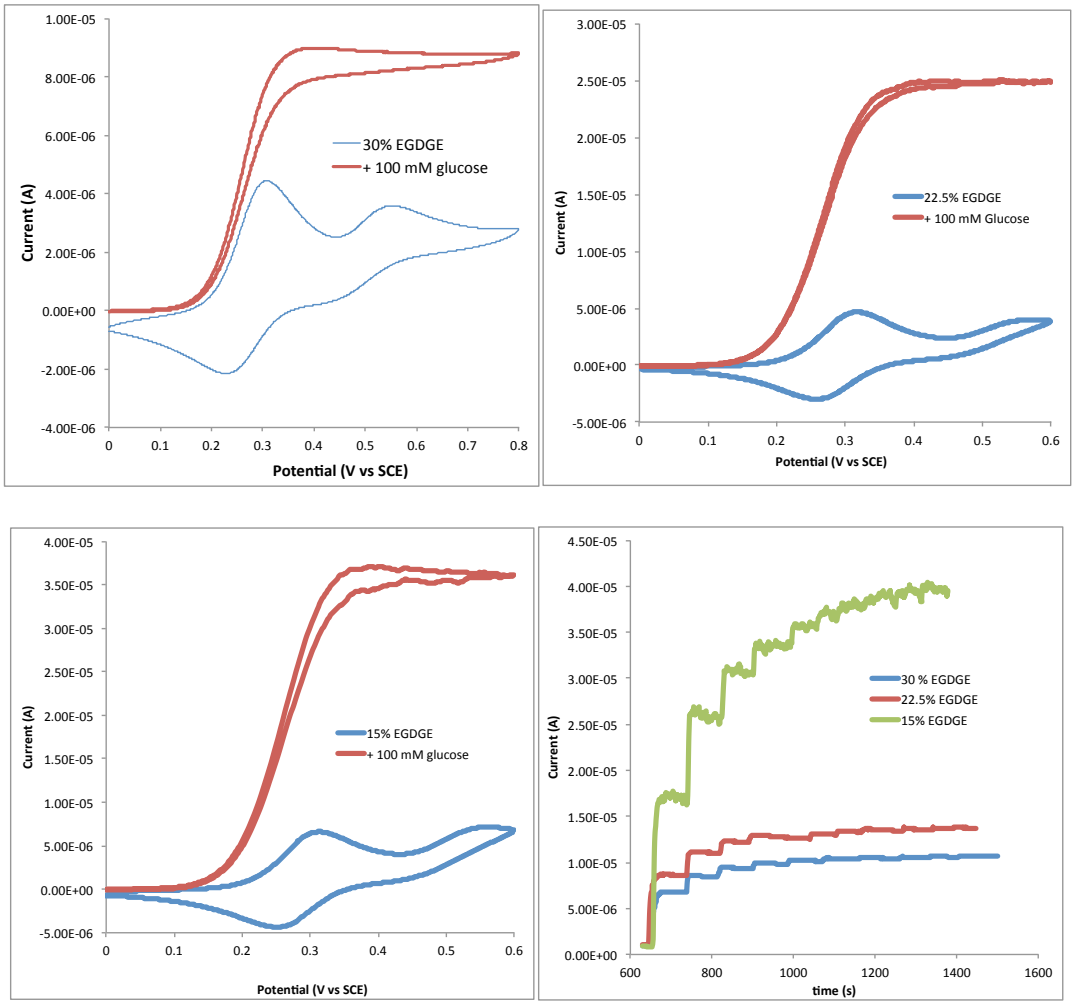

Figure 4.9 – Cyclic voltammograms of Glycol ether-based Fc-G2-LPEI using 30 % (v/v) EGDGE (top left), 22.5% (v/v) EGDGE (top right), 15 % (v/v) EGDGE (bottom left) in the absence and presence of glucose, collected at 5 mV/sec using a glassy carbon working electrode, SCE working electrode, and a Pt wire auxiliary electrode. The bottom right figure is a plot of the amperometric response as a function of time as the concentration of glucose is increased by 5 mM increments.

The voltammogram of the film made from Fc-G2-LPEI prepared with 30 % (v/v) EGDGE exhibits two oxidative waves at 298 mV vs SCE and 540 mV vs SCE with i_{pa} values of 3.4 μA and 0.8 μA, respectively. The reductive waves at 459 mV vs SCE and 242 mV vs SCE exhibits i_{pc} values of 0.7 μA and 1.4 μA, respectively. The difference between the lowest potential oxidative and reductive peaks is ΔE_p = 56 mV and the ratio of *ipa/ipc* = 2.42. In the presence of glucose, a single irreversible oxidative wave at approximately 350 mV vs SCE that exhibits a catalytic current, i_{cat}, of 9.2 μA. Based on data collected during the glucose titration shown in Figure 4.9, the J_{max} of the film was 232 ± 45 μA cm^{-2} and the calculated K_m was 5.3 ± 0.9 mM

The voltammogram of the Fc-G2-LPEI film prepared using 22.5% (v/v) EGDGE exhibited two waves, as well. There were two oxidative waves at 307 mV vs SCE and 546 mV vs SCE with an i_{pa} of 4.1 μA and 0.7 μA, respectively. There is only one reductive wave at 273 mV vs SCE with an *ipc* of 3.1 μA. The first oxidative wave and the reductive wave exhibit a ΔE_p of 34 mV, and a ratio of ipa:ipc of 1.3. In the presence of glucose, a single irreversible wave is observed with an E_{pa} of 347 mV vs SCE and an i_{cat} of 24.9 μA. Based on amperometric data collected during a glucose titration, the J_{max} of the film was 502 ± 67 μA and the K_M was calculated to be 8.9 ± 0.4 mM.

The voltammogram of the Fc-G2-LPEI film prepared using 15 % (v/v) EGDGE exhibited two oxidative waves at 300 mV vs SCE and 544 mV vs SCE that exhibited *ipa* values of 6.1 μA and 1.5 μA, respectively. There is one reductive wave at 266 mV vs SCE that exhibits an *ipc* of 4.5 μA. The ΔEp of the reversible peaks is 34 mV and the *ipa/ipc* = 1.5. In the presence of glucose, a single irreversible wave at 347 mV vs SCE with *icat* = 38.4 μA is observed. The value of *Jmax* for this material was 698 ± 57 μA cm^{-2} and the K_M was calculated to be 9.0 ± 0.8 mM.

When considering the efficiency of the enzyme as the percentage of cross-linker was varied, the K_M values remained approximately constant at 10% (v/v) and 22.5 %(v/v) EGDGE, suggesting that the activity of the enzyme was unchanged until the %of EGDGE reached 22.5% (v/v). K_M indicates how closely the enzyme performs in the polymer-supported state as compared to the free state in solution. The closer the value of K_M in the polymer-supported state is to the value of K_M in the solution state, 22 mM, the more the enzyme performs as if it is in solution. This could be explained by the higher concentration of cross-linking agent creating a network that has "cavities" in the network that are too small for the enzyme to catalyze the reaction. When comparing the J_{max} values of each, the 15% (v/v) film demonstrated the highest J_{max}, followed by the 10% (v/v) film, then the 22.5% (v/v) film, and the 30% (v/v) film. This suggests that there is an optimum amount of cross-linking agent that creates a network that is large enough for the enzyme to move around, but the films must be in close enough in proximity to each other so that a "relay" mechanism can be achieved in electron transport.

When comparing the values of i_{cat} for each film, the magnitude of the catalytic current increased as the % EGDGE (v/v) decreased. The film made from 10% EGDGE exhibited the highest *icat* of 52 μA. The film prepared from 15% (v/v) EGDGE exhibited the next highest i_{cat} of 38.4 μA. The film prepared from 22.5% (v/v) EGDGE exhibited the next highest i_{cat} of 24.9 μA, and the film prepared from 30% (EGDGE) exhibited the lowest i_{cat} of 9.2 μA. This observation is contrary to previous studies focusing on the effects of the amount of cross-linking agent. A study by Hickey using propionyltetramethylferrocene-functionalized LPEI (Me_4-C3-LPEI) with GOx demonstrated a non-linear trend between J_{max} and % EGDGE, that exhibited a maximum J_{max} of approximately 1000 μA cm^{-2} at approximately 30% (v/v) EGDGE added[64].

The maximum value of J_{max} in this work at 10 % (v/v) EGDGE could be indicative that this material performs better with a smaller degree of cross-linking agent than other ferrocene-containing LPEI materials. There are a potential list of factors that could cause this difference, as shown in prior reports by the Glatzhofer group, including the longer tether length, and the degree of methylation[48, 64, 75]. Since methylation of the ferrocene was not a part of this work, however, these data will not be considered in the discussion. To better understand the impact of each of these effects, previous data from published studies and this study have been compiled in Table 4.1. Previous data reported by Meredith, Hickey, and Merchant are all reported in values of J_{max} and K_M.

Table 4.1 – Values of Jmax and Km for different Fc-containing LPEI materials. Data from this work are in bold.

Material	% Fc	% EGDGE (v/v)	Atoms in Tether	Km (mM)	*Jmax* (μA cm^{-2})	ref
Fc-C1-LPEI	40	10	1	9.8	902	[75]
Fc-C3-LPEI	15	10	3	21	1020	[75]
Fc-C6-LPEI	15	10	6	21	655	[75]
Fc-G2-LPEI	12	30	7	5.3	**232**	
Fc-G2-LPEI	12	22.5	7	8.9	**501**	
Fc-G2-LPEI	12	15	7	9.0	**698**	
Fc-G2-LPEI	12	10	7	9.0	**603**	
Fc-C1-LPEI	14	10	1	1.9	**320**	

Of the materials listed in table 4.1, the Fc-G2-LPEI was not the highest performing film. The next highest performing material was the propionyl ferrocene-functionalized LPEI (Fc-C3-LPEI), as evidenced by the largest values of K_M and $J_{max.}$ The next best performing material was the Fc-C1-LPEI material prepared by Meredith, with a J_{max} and K_M of 902 μA and 9.8, respectively. This could suggest that the Fc-G2-LPEI material is not optimized in terms of ferrocene substitution. In comparing trends observed with other ferrocene-based LPEI materials

used in bioelectrode fabrication, it may be necessary to investigate the effects of the ferrocene substitution on the film, as both Hickey and Meredith noted that there appears to be an optimal percentage of ferrocene in films prepared from LPEI modified with ferrocene, dimethylferrocene, and tetramethylferrocene[48, 64, 141-143]. The methylferrocene and tetramethylferrocene modified LPEI material show maximum peak current densities at 20% ferrocene substitution. This work's ferrocene-substitution was approximately 14%. Additional factors should also be considered in attempting to correlate the structure of each film to the amperometric performance, such as tether length and enzyme loading. When comparing the length of the spacer, the Fc-G2-LPEI material is the best basis for comparison. There are six carbons in the hexanylferrocene-modified LPEI (Fc-C6-LPEI) and 7 atoms in the diethyleneglycolferrocene-modified LPEI (Fc-G2-LPEI). Meredith's Fc-C6-LPEI material exhibited both a higher J_{max} and a higher K_m than the Fc-G2-LPEI material. While the Fc-C6-LPEI material outperformed the Fc-G2-LPEI material amperometrically, there is not a noticeable difference in the $K_{m,}$ as shown in table 4.1. Large differences in K_M are often noted when the difference in K_M are near magnitudes of greater than 1000[75]. This indicates that the enzyme is performing with approximately the same efficiency in both the Fc-C1-LPEI and the Pc-G2-LPEI. Since the enzyme is not performing differently in either materials, this suggests that the Fc-G2-LPEI material is interacting more efficiently with the enzyme to transfer electrons to the electrode. This increase in current density supports that a higher K_a between a ferrocene derivative and GOx can be used to predict the amperometric performance of a polymer-supported electrode material.

4.3 Conclusions

A new polymer material was made using a glycol ether-based tether. This is the first material that incorporates a glycol ether-based tether into a ferrocene-containing LPEI electrode. In addition, this new material out-performed a material made using a one-carbon spacer and a similar ferrocene substitution. When the amount of cross-linking agent was varied, it was noted that 10 mol-% EGDGE yielded the optimum performance, as evidenced by J_{max}. In addition, it was noted that the work from Chapter 3 appears to have a significant impact by linking a binding constant to a mediator's performance when incorporated into a polymer-supported state. This is the first work to relate a mediator's binding capability to the relative performance of a mediator, when used in a polymer-supported biosensor, as compared to other mediators. It appears the strength of the mediator binding to the enzyme is indicative of the mediator's ability to shuttle electrons in a biosensor setting, as evidenced by the change in performance.

4.4 Experimental –

*Synthesis of (2-chloroethoxy)ethoxymethylferrocene (**1**)*

In a 50 mL round bottom flask, 250 mg of (ferrocenylmethyl)trimethylammonium iodide (MM = 384.90 g/mol) was dissolved in 20 mL of acetonitrile. 0.78 mmol of 2-(2-chloroethoxy)ethanol (MM = 124.55 g/mol) were added to the flask with 20 mg of K_2CO_3. The solution was heated to solvent reflux with stirring and reacted for 12 hours. The solvent was removed via reduced pressure and the crude product was passed through an alumina column, eluted in 10:1 hexanes in ether. The yellow band that eluted afforded 190 mg of product in a 90% yield. NMR ($CDCl_3$): δ4.00-4.42 ppm (9H, m), δ3.48-3.82 ppm (10 H, m)

*Synthesis of (2-iodoethoxy)ethoxymethylferrocene **(2)***

This preparation is a modification of the procedure from Kanato et al. 15 mL of NaI in 2-butanone was prepared. The 190 mg of compound 1 were added dropwise and heated to solvent reflux overnight. After cooling the solution, water added to the mixture and extracted with hexanes. The hexanes were removed under reduced pressure and the crude product was passed through an alumina column in a 10:1 hexanes/ether mixture. The product was eluted in a yellow band, and the solvent was removed under reduced pressure to afford 228 mg of (2-iodoethoxy)ethoxymethlferrocene in 94% yield. NMR ($CDCl_3$): δ4.00-4.42 ppm (9H, m), δ3.48-3.82 ppm (10 H, m)

Synthesis of Fc-G2-LPEI

In a 50 mL round bottom flask, 100 mg of linear poly(ethylenimine) (MW=43.08 g/mol) was dissolved in 10 mL of acetonitrile and 1 mL of methanol. 190 mg of **2** was added with 50 mg of K_2CO_3. The solution was heated to reflux with stirring for 24 hours. The solvent was removed unreduced pressure. Diethylether was added to remove any unreacted ferrocene starting material, and then discarded. The remaining solid was dissolved in benzene and filtered to remove any salts. The benzene was removed under reduced pressure to afford 263 mg of polymer product in 91% yield. The resulting polymer was determined via NMR to be 15% substituted with ferrocene. NMR: δ3.90-4.54 (Fc-H 9H, m), δ3.16-3.90 (O-CH2-CH2-O 7.8 H, m), δ2.19-3.10 (CH2-N-CH2 26.82 H) δ1.90-2.10 (Fc-CH2-O, 2.4 H, s)

Fabrication of Fc-G2-LPEI electrodes

In a 1 mL vessel, 28 µL of a 10 mg/mL solution of Fc-G2-LPEI was mixed with 12 µL of a 10 mg/mL Glucose oxidase (GOX) solution and stirred in a vortexer. 1.5 µL of a variable weight ethylene glycol diglycidyl ether (EGDGE) solution was added to the mixture and stirred in a

vortexer. The new solution (3 μL) was pipetted onto a 3 mm glassy carbon electrode and allowed to cure for 24 hours.

Electrochemical Characterization of films

All electrochemical measurements were carried out on a CH Instruments Model 832 bipotentiostat in phosphate buffered saline (pH=7.42). Unless otherwise indicated, all data collected using the potentiostat used a three-electrode configuration, using a glassy carbon working electrode, a Pt wire auxiliary electrode, and a saturated calomel electrode (SCE) as a reference. Constant temperature of 25 ° C was maintained using a water jacket connected to a circulating water bath. Cyclic voltammetric measurements were carried out at a scan rate of 50 mV/sec. Constant potential measurements were conducted at 0.05 V greater than the E_{pa} of the material.

Chapter 5 – Steps Toward an Electrocatalytic Deoxydehydration Reaction Using N,N',N"-Trimethyl-1,4,7-triazacyclononanetrioxorhenium (VII) Hexafluorophosphate

5.1 – Introduction

Dexoydehydration reactions convert vicinal diols into alkenes. This type of transformation has drawn the attention of many groups since carbohydrates contain a large number of these vicinal diol functional groups. This transformation could, theoretically, allow carbohydrates to act as a renewable feedstock for fuels and chemicals. For example, looking at a four carbon carbohydrate - erythitol, it could be envisioned that a 1,3-diene could result, as shown in **Figure 5.01**. The substrate scope of this reaction includes carbohydrates, cyclic and acyclic alkanediols, and an assortment of functionalized diols with carboxylic acids and esters. Rhenium-based metal complexes comprise the majority of the active catalysts. However, it has also been demonstrated that vanadium and molybdenum-based complexes have successfully catalyzed DODH processes[84, 86, 88, 92, 144-145].

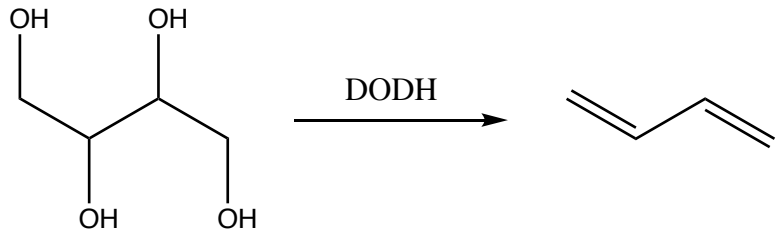

Figure 5.01 The DODH of erythritol into 1,3-butadiene. This been accomplished by Nicholas and Toste[84, 86, 144]

In considering the mechanism for the DODH reaction, it is believed that one of two paths can occur: Path A) Formation of a metalloglycolate metal complex, reduction, and then alkene extrusion; or Path B) Reduction of the metal complex, formation of the metalloglycolate, and then alkene extrusion. Figure **5.02** shows both paths through which

the catalytic DODH may proceed. Pathway A shows condensation of the glycol with a Re^{VII} trioxo species, reduction of this Re^{VII} glycolate, and then alkene extrusion. Pathway B shows reduction of the Re^{VII} complex to a Re^{V} complex, which condenses with the diol, and then proceeds through alkene extrusion. It has been demonstrated, however, that the path through which the reaction occurs varies, depending on the nature of the reductant and the catalyst. Some instances of this particular observation will be discussed in more detail to provide insight into creating an electrochemical pathway.

In alcohol-driven DODH reactions, kinetic studies of the catalytic conversion of hydrobenzoin in excess 3-octanol at 140 ° C have been conducted by Abu-Omar shown in Figure 5.02[146]. In these studies, 3-octanol acted as the solvent and the reductant[146]. These kinetic experiments showed an initial induction period, a zero-order dependence on the glycol, and a half-order dependence on methyltrioxorhenium (MTO).

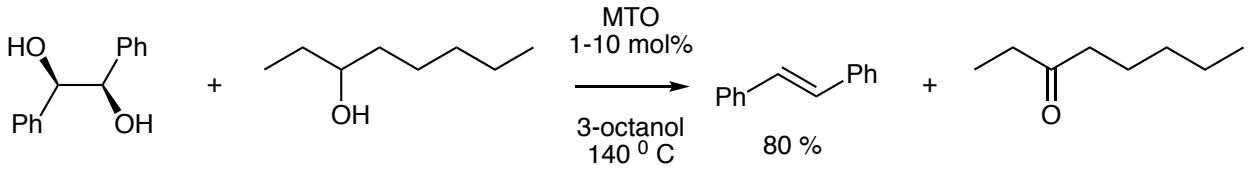

Figure 5.02 – The DODH of trans-stillbene using methyltrioxorhenium (MTO) and 3-octanol conducted by Abu-Omar[146].

The half-order dependence on the MTO indicates that there is a competing side reaction of the metal complex in solution. Formation of a Re dimer from a Re(VO dioxo species has been observed spectroscopically[147]. Formation of this dimer deactivates the MTO towards DODH. In addition, the mechanism in this study proposed a second reduction to a Re^{III} intermediate that acts as the catalytic complex. This mechanism proposed by Abu-Omar is unique in that it has not been considered in computational work relating to a metal-catalyzed DODH mechanism. Most computational studies have focused on the

proposed pathway shown in Figure **5.03** where a Re^{VII} complex is reduced and condensed with a glycol to produce a Re^{V} glycolate, which acts as the precursor to the alkene**.** The computational analysis by Wang et al determined that the rate-determining step in the mechanism of an MTO-catalyzed, alcohol driven DODH reaction was the initial reduction of the MTO to form $MeReO(OH)_2$. Further experimental work supported this conclusion[148]. Dethelfsen followed the reaction via spectroscopy, determined the order of reaction experimentally, and observed the Kinetic Isotope Effect (KIE) by deuterium labeling of the alcohol[149]. From these studies, it was concluded from this KIE of 2.1 for a C-D vs a C-H bond on the alchol and further spectroscopic tracking of the reaction by NMR that: 1) the rate-limiting step of the reaction was the reduction of MTO caused by the alcohol reductant; 2) the rhenium complex is reduced prior to glycol complexation with the reduced complex; and 3) the Re^{vii}-glycolate species is formed reversibly with MTO, but cannot undergo reduction. This rate dependence on the reduction of the metal complex suggests that an electrochemical adaptation of this DODH reaction could be beneficial in reducing the reaction time and temperature needed for this conversion.

Contrary to these findings is a computational study carried out by Wu et al. Investigating the DODH of 1,4-butenediol, two pathways were considered. The first path considered the rearrangement of the 1,4-diol to the allyl alcohol and then undergoing DODH. The second path considered a direct DODH of the 1,4-butendiol. Kinetic studies carried out suggested that a direct DODH was occurring on the 1,4-butenediol. Experimental work also supported that the first step of the DODH pathway involved reduction of the rhenium (VII) complex. The rate-determining step, however, was not the

reduction of the complex but rather the fragmentation of the rhenium (V) glycolate complex[150].

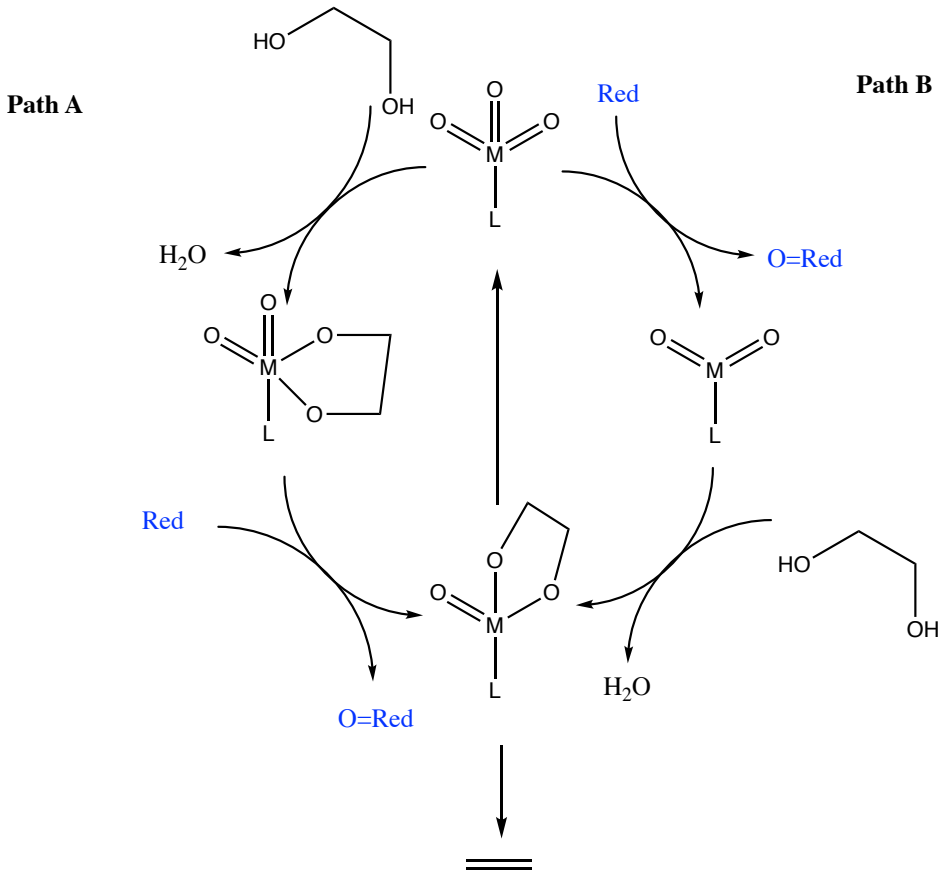

Figure 5.03. Two possible pathways for a DODH reaction. Pathway A shows condensation of the glycol with the metal complex, reduction of the metalloglycolate complex, and fragmentation of the alkene and regeneration of the metal complex. Pathway B shows reduction of the Metal complex followed by complexation of the glycol to form the metalloglycolate complex that fragments into the alkene and original metal complex.

5.1.1 - Project Goals and Experimental Design

In considering the possibility of an electrochemical reaction versus a thermal reaction, there are a few inherent benefits that have attracted organic chemists to electrochemical synthetic methods over the past two decades. An electrochemical adaptation of a DODH reaction could be beneficial in a few ways: 1) A chemical reductant may be replaced with an appropriate proton source, such as an acid. This could be a very cost-effective, as phosphines, common chemical reductants for DODH, can be expensive and are hard to recycle. 2) Electrochemical reactions often have very high reaction rates, comparatively, to those of their thermal chemical analogues. 3) The lack of a chemical reductant can allow for a simplified post-reaction work-up.

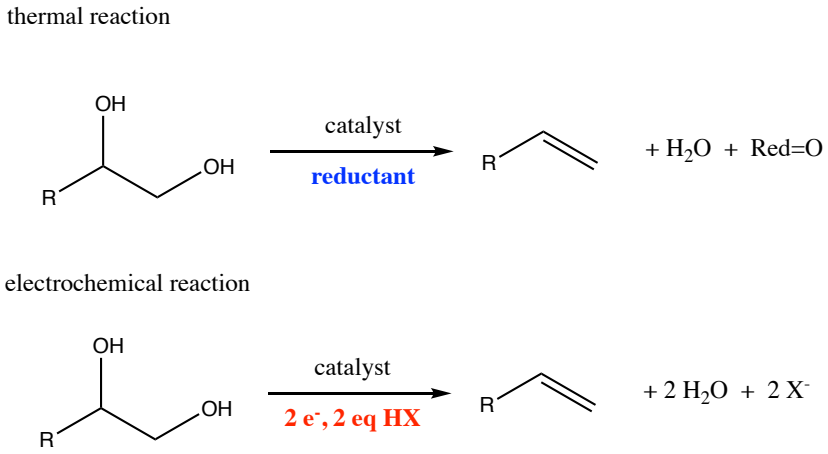

Figure 5.04 The envisioned differences between a thermal DODH reaction and an electrochemical DODH reaction

As previously discussed, mechanistic studies suggest that there are instances in which the rate-determining step is the reduction of the metal complex prior to glycol condensation. By converting this chemical reduction to an electrochemical reduction, it could be predicted that the rate of reaction would increase, as electrochemical redox

processes have rates that are significantly higher than their analogous chemical reductions[98].

In choosing a metal complex that could effectively act as an electrocatalyst, two main criteria were considered: 1) the compound should have previously demonstrated success as a thermal DODH catalyst, or a precedent for being a successful catalyst. 2) The compound should have previously studied electrochemical properties demonstrated in the literature. When solely considering the electrochemistry, it appeared that one metal complex could be appropriate for our needs. (N,N',N"-trimethyl-1,4,7-trimethyltriazacyclononane)trioxorhenium (VII) perrhenate (**2**) has been demonstrated to exhibit reversible electrochemistry in aqueous media[151]. Its electrochemistry is described herein. In addition, its cationic rhenium center seems to be attractive to an electrochemical DODH reaction, as it could be envisioned that the positive charge could attract electrons for reduction from an electrode's surface. The cationic rhenium center may favor the formation of a metalloglycolate species by acting as a Lewis acid. In addition, the analogous acyclic complex (N,N,N',N",N"-pentamethyldiethylenetriamine)trioxorhenium (VII) perrhenate (**1**) was believed to be equally attractive for a similar reason. It could also be envisioned that the acyclic ligand could "slip" to encourage complexation of the glycol to the metal center. In addition, the acyclic triamine ligand is much cheaper than the commercially available cyclic ligand. Both complexes were synthesized according to literature procedures[94]. Figure **5.05** shows the structures of (Me_5DETN)ReO_3ReO_4, complex **1,** and (Me_3TACN)ReO_3ReO_4, complex **2,** (Me_3TACN)ReO_3PF_6, complex **3**.

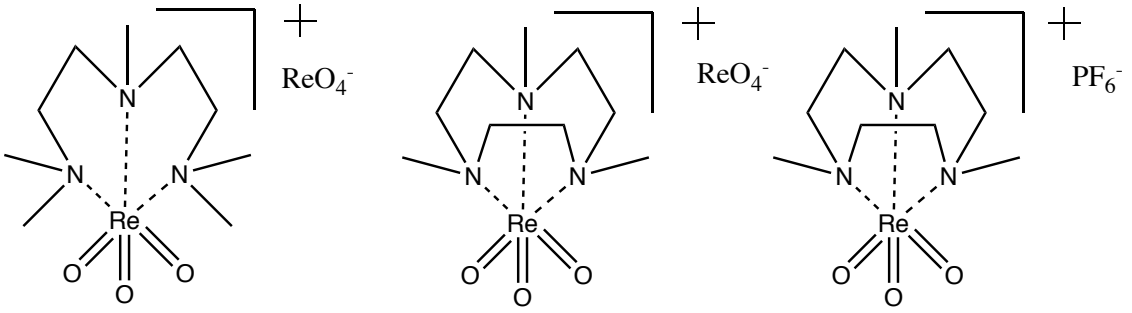

Figure 5.05 the structures of complexes 1, 2, and 3 used as candidates for potential DODH catalysts.

There have been examples of electrochemically active organorhenium compounds, such as methyltrioxorhenium (MTO), and (η-5-pentamethylcyclopentadienyl)trioxorhenium(VII)[152] (Cp^*ReO_3) analyzed in acetonitrile. Cp^*ReO_3 exhibits irreversible electrochemical behavior, as evidenced by only the presence of a one-electron reduction wave at -1.72 V vs Ag/AgCl[94, 152]. When MTO was analyzed via cyclic voltammetry, an irreversible one-electron reduction wave was observed in the voltammogram at -0.69 V vs Ag/AgCl[23, 69]. This suggested that both complexes degrade very quickly once reduced. One interesting feature of both of these complexes is that they can both be reduced via organophosphines in a formal two electron process with removal of an oxo group and are stable enough to be characterized by NMR, suggesting that an oxo-transfer mechanism, instead of an electron transfer mechanism is the preferred path of reduction[152].

When considering the possible catalytic cycle through which an electrocatalytic DODH might occur, it is reasonable to speculate that the pathway could be similar to the mechanism of the thermal DODH reaction. There are two main components of the

mechanism to consider: 1) formation of the Re(V) glycolate through either Path C or Path D; or 2) alkene extrusion from the Re(V) glycolate. To accomplish the electrochemical synthesis of the Re(V) glycolate, it would be necessary to investigate the electrochemistry of the metal complex in the absence and presence of proton sources before electrochemically synthesizing the Re(V)glycolate complex. A large portion of this work will focus on accomplishing this goal.

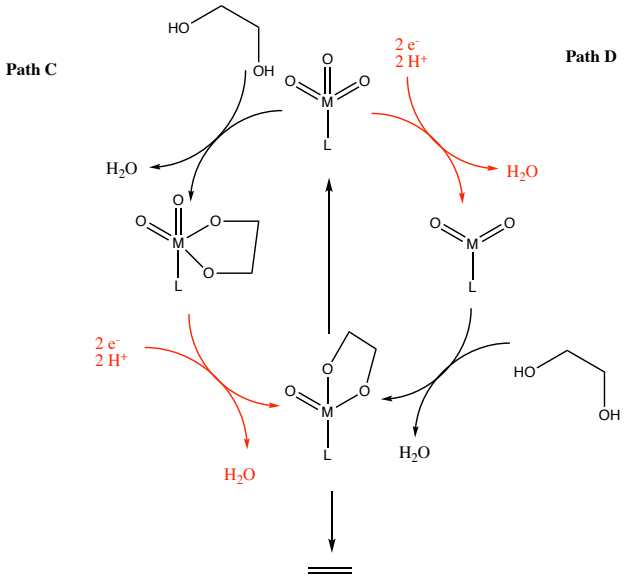

Figure 5.06 – The proposed mechanism through which an electrocatalytic DODH could occur. Path C shows condensation of the glycol with the Re(VII) complex occurs before reduction and alkene extrusion. Path D shows reduction of the Re(VII) complex to form the Rhenium (V) dioxo species which then condenses with the diol to form the Re(V) glycolate that then undergoes alkene extrusion. Steps with a red arrow indicate steps that are different than the pathways of the thermal reaction.

5.2 – Results and Discussion

5.2.1 - Thermal Reactivity

Complexes 1 and 2 were screened for thermal reactivity by using 1,2-decanediol as a model substrate. At 150 ° C in toluene using 2 molar equivalents of benzyl alcohol as a reductant

after 24 hours, it was noted that both complexes successfully catalyzed a thermal DODH. The acyclic triamine rhenium complex **1** yielded >95% 1-decene (entry 5.1), as determined by quantitative gas chromatographic methods established by McClain et al[82]. The cyclic triamine rhenium complex **2** was not as reactive under these conditions, as only 30% 1-decene was produced (entry 5.2). Based on the yields of 1-decene, complex **1** appeared most promising in terms of thermal reactivity. While both complexes appeared successful in catalyzing DODH, it was important to investigate the range of substrates that could be transformed by both catalysts. Two additional model compounds were used to determine the scope of reactivity: diethyl tartrate (DET) and 1-phenyl-1,2-ethanediol (PED), as these compounds are both structurally "activated" diols, since their corresponding Re(V) glycolates more readily undergo retrocyclization to form the alkene and the Re(VII) catalyst. Based on this inclination toward retrocyclization, it is reasonable to speculate both DET and PED have enhanced reactivity. Similar results have been reported by the Nicholas group and others[82, 84, 87-88, 145]. When complex **1** reacted with 1-phenyl-1,2-ethanediol, there was a slight increase in alkene yield to 39% (entry 5.3). However, there was evidence of other higher retention time products in the resulting chromatogram. These higher molecular weight materials have been previously observed by the Nicholas group when working with the DODH of 1-phenyl-1,2-ethanediol. One of these products was the condensed, unsaturated dimer of the diol, where GC-MS and NMR data indicated the product was α,β-unsaturated-1,4-diketone structure, shown in figure **5.07**[147]. Using the same chromatographic method, a peak with the same retention time was observed in this reaction at 15.5 minutes. Diethyl tartrate showed a dramatic increase in alkene production to form diethyl furmarate (DEF) yielding 76% (entry 5.4) when using benzyl alcohol as a

reductant. This increased alkene yield indicated that this molecule is more reactive with our metal complex catalyst. Thus, complex **2** was reacted with DET to investigate this idea (entry 5.5) under similar reaction conditions. DEF was produced in greater than 95% yield. This was surprising, as the initial thermal reactions with 1,2-decanediol suggested that catalyst **1** was more active in DODH than complex **2**.

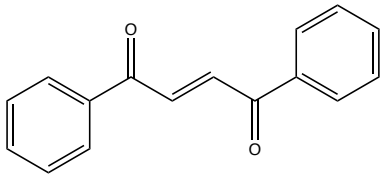

Figure 5.07 One of the products formed during the DODH of 1-phenyl-1,2-ethanediol determined by McClain[147].

Since the Nicholas group previously had experience with using perrhenate salts as DODH catalysts[91], it was reasonable to suspect that the perrhenate ion (ReO_4^-) could be acting as the catalytic portion of the molecule either in part, or in whole. In order to investigate the ability of the cationic rhenium species to act as a catalyst without the active perrhenate, it was necessary to perform an ion metathesis. By dissolving complex **2** in water and adding an aqueous solution of sodium hexafluorophosphate, a white precipitate of N,N',N"-trimethyl-1,4,7-triazacyclononanetrioxorhenium (VII) hexafluorophosphate (**3**) was produced. When a similar reaction was carried out on complex **1**, no precipitate formed. It was previously noted in the literature that **1** was much more sensitive to hydrolysis than complex **2**[152]. The hexafluorophosphate salt seemed an attractive anion, as it is non-coordinating and a common electrolyte used in electrochemical analysis[153]. Since complex **1** could not undergo metathesis, the focus moving forward will be solely on complexes **2** and **3**.

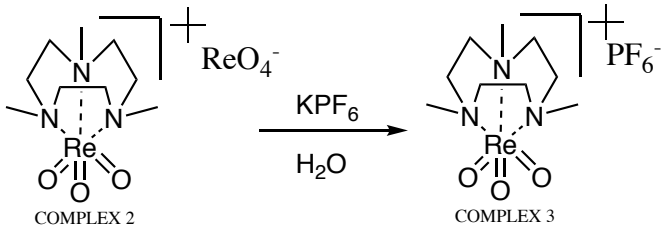

Figure 5.08 – The metathesis of perrhenate Complex 2 to form hexafluorophosphate Complex 3.

Entry	Substrate	Catalyst	Reductant	Alkene Yield
5.1	1,2-decandiol	$Me_5DETNReO_3ReO_4$	Benzyl alcohol	90%
5.2	1,2-decandiol	$Me_3TACNReO_3ReO_4$	Benzyl alcohol	32%
5.3	1-phenyl-1,2-ethanediol	$Me_5DETNReO_3ReO_4$	Benzyl alcohol	39%
5.4	DET	$Me_5DETNReO_3ReO_4$	Benzyl alcohol	76%
5.5	DET	$Me_3TACNReO_3ReO_4$	Benzyl alcohol	>95%
5.6	DET	$Me_3TACNReO_3PF_6$	Benzyl alcohol	0%
5.7	1,2-Decanediol	$Me_3TACNReO_3PF_6$	Benzyl alcohol	0%
5.8	DET	$Me_3TACNReO_3PF_6$	Indoline	74%
5.9	DET	$Me_3TACNReO_3PF_6$	Zn (dirty)	46%
5.10	DET	$Me_3TACNReO_3PF_6$	Zn (polished)	54%
5.11	1,2-decandiol	$Me_3TACNReO_3PF_6$	Indoline	60%

Table 5.1. Alkene yields determined by gas chromatography from thermal DODH reactions in this study run at 150 ° C in toluene; 5% catalyst loading and 2 eq of reductants. Reaction times for 1,2-decanediol and DET were 24 hours, while 1-phenyl-1,2-ethanediol was run for 12 hours.

Initial investigations of complex **3**, using similar reductants and reaction temperatures as the perrhenate complex 2, showed no activity using benzyl alcohol as a reductant with both 1,2-decanediol and DET as substrates (Entries 5.6 and 5.7). This suggested that it was indeed the perrhenate anion, or an adduct of the cationic metal complex and the perrhenate ion, acting as the active catalyst. McClain and Boucher-Jacobs, however,

demonstrated that an array of reductants could successfully carry out DODH reactions[82, 84]. It was also observed that the rhenium (V) dimethoxide complex from **3** had been isolated and characterized when complex **3** was mixed in methanol with zinc powder for 24 hours[154]. When indoline was the reductant instead of benzyl alcohol with DET as a substrate, 74% DEF was produced (entry 5.8). Comparing this reactivity to a similar reaction with complex **3** and 1,2-decanediol, it is noted that 60% 1-decene was produced using indoline as a reductant (entry 5.11). When 2 equivalents of unpolished (dirty) zinc were used as a reductant with DET, DEF was produced in 46% yield (entry 5.9), while zinc polished with 1.0 M HCl prior to use in the reaction yielded 54% DEF from DET (entry 5.10). This suggests, while reactive secondary alcohols were sufficient reductants for the perrhenate salt, the cationic rhenium complex **3** could not be reduced by benzyl alcohol. In summary, both new complexes showed the ability to act as DODH catalysts. The yield decreased when the perrhenate ion was exchanged with the hexafluorophosphate ion, but the use of stronger reductants demonstrated that the cationic rhenium (VII) complex is still a good catalyst for DODH on PED and DET with a variety of reductants. In order to get a better grasp of the nature of the reduction of the complex, the electrochemistry of hexafluorophosphate complex 3 was investigated.

5.2.2 - Electrochemistry

In working toward the second goal of our project of demonstrating electrochemical activity, it is essential to investigate the electrochemistry of the hexafluorophaosphate complex **3.** The perrhenate complex **2** was initially characterized by Chi-Ming and coworkers in aqueous solvent using cyclic voltammetry[151]. It was observed that the $(Me_3TACN)ReO_3ReO_4$ complex **2** underwent two separate single electron transfer

processes, as shown in the voltammograms in **Figure 5.08**. The first was a single electron and a single proton transfer to putatively generate $[Re^{VI}O_2OH(Me_3TACN)]^+$. The second electron transfer process, however, was determined to be pH dependent. Between pH values of 0.9 and 4.1, 2 H^+ were transferred. The rhenium (VI) intermediate was speculated to be either the oxodihydroxoRe(V) analogue, or a hydrated dioxoRe(V) species. At pH values greater than 4.1, a Pourbaix diagram determined that only one H^+ was transferred to generate either the hydrated dioxo rhenium (V) species, or the dihydroxo monooxo rhenium (V) species.[151]

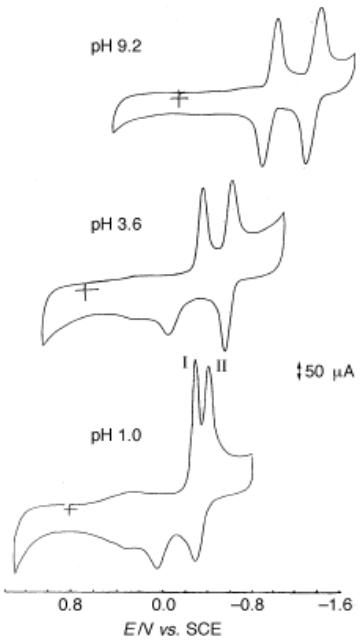

Couple I

$[Re^{VII}O_3(Me_3tacn)]^+ + H^+ + e^- \rightleftharpoons [Re^{VI}O_2(OH)(Me_3tacn)]^+$

Couple II

$0.9 < pH < 4.1$

$[Re^{VI}O_2(OH)(Me_3tacn)]^+ + 2H^+ + e^- \rightleftharpoons [Re^{V}O(OH_2)(OH)(Me_3tacn)]^{2+}$

or $[Re^{VI}O_2(OH)(Me_3tacn)]^+ + 2H^+ + e^- \rightleftharpoons [Re^{V}(OH)_3(Me_3tacn)]^{2+}$

$pH > 4.1$

$[Re^{VI}O_2(OH)(Me_3tacn)]^+ + H^+ + e^- \rightleftharpoons [Re^{V}O_2(OH_2)(Me_3tacn)]^+$

or $[Re^{VI}O_2(OH)(Me_3tacn)]^+ + H^+ + e^- \rightleftharpoons [Re^{V}O(OH)_2(Me_3tacn)]^+$

Figure 5.08. Cyclic voltammograms of 2 as a function of pH and the corresponding mechanisms for reduction. Figures reproduced from Reference 21.

It should be noted that a control solution of sodium perrhenate was analyzed by CV to confirm that it was indeed the $Me_3TACNReO_3$ species reacting at the electrode's surface. Due to the high solubility in water of complex **2**, but insufficient solubility in polar organic solvents, such as methanol, ethanol, n-propanol, acetonitrile, and dichloromethane, it is

very difficult to analyze the electrochemistry of both complex **2** and **3** in the same solvent for a direct comparison. As a result, complex **3** was analyzed using cyclic voltammetry in acetonitrile using 0.1 M N-tetrabutylammonium hexafluorophosphate as a supporting electrolyte. **Figure 5.09** shows the resulting voltammogram in acetonitrile in the absence of acids.

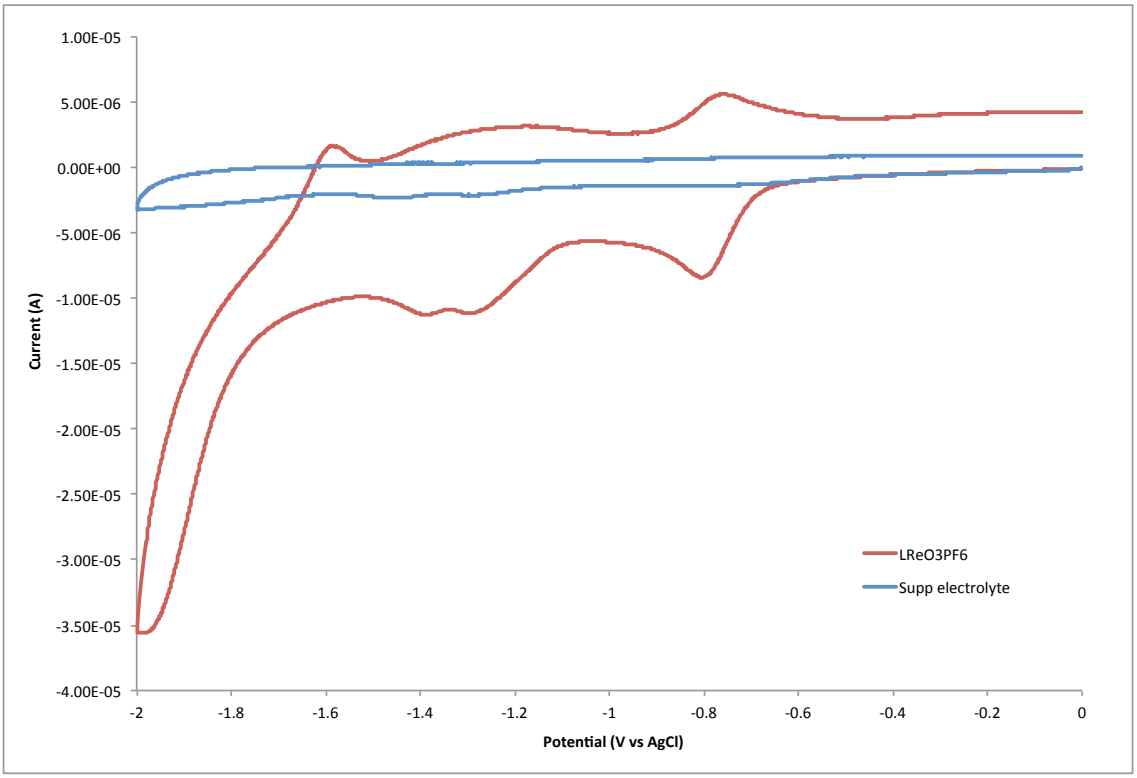

Figure 5.09. The voltammogram of Me3TACNReO3PF6 in acetonitrile using tetrabutylammonium hexafluorophosphate (0.1M) as a supporting electrolyte. Scan rate = 150 mV/sec

The resulting voltammogram of $(Me_3TACN)ReO_3PF_6$ shows three reductive peaks and two oxidative peaks peaks. The reductive peaks were observed at -0.806 V vs AgCl, -1.29 V vs AgCl, and -1.39 V vs AgCl. The lowest potential reduction peak at -1.39 V cs AgCl lines up with a small impurity detected in the supporting electrolyte voltammogram near -

1.45 V vs SCE. This impurity aligns with trace amount of oxygen reduction occurring from the presence of the supporting electrolyte. This suggests that the small detection was due to the impurity in the electrolyte. The amperometric response of the peak at -0.81 V vs AgCl is 6.7 μA and the amperometric response of the peak at -1.29 V vs AgCl is 5.3 μA. The similarity in size of each amperometric response suggests that the same number of electrons are transferred in each electrochemical reduction. This would likely correspond to a reduction where the rhenium goes from Re (VII) to Re(VI) at -0.806 V vs AgCl and from Re(VI) to Re(V) at -1.29 V. This electrochemical behavior, however, is quite different than other rhenium (VII) trioxo complexes[152]. Rhenium(VII) trioxo complexes containing a pentamethylcyclopentadienyl ligand (Cp*) and a tris-perazolylborate ligand (Tpz) demonstrate single wave, two electron reductions in DMF. The electrochemistry of the hexafluorophosphate complex 3 aligns more closely with its corresponding aqueous electrochemical behavior[151]. One significant difference, however, is that the hexafluorophosphate complex **3** does not demonstrate the same reversibility of each reduction as the aqueous perrhenate complex **2**.

The large reduction peak occurring at -2.0 V vs AgCl could be reduction of the supporting electrolyte, as it has been demonstrated that PF_6^- reduction occurs around -2.0 V vs SCE[155]. The oxidative peaks at -1.58 V vs AgCl and -0.757 V vs AgCl demonstrate amperometric responses of 1.8 μA and 3 μA, respectively. Since the oxidative peak at -1.58 V vs AgCl is more negative than the reduction of the Re(VI) to Re(V), it is unlikely that this oxidation is pertinent to the rhenium chemistry we are interested in. The oxidation at -0.75 V, however, is only 49 mV mV higher than the reduction peak at -0.81 V. This suggests

that there is a paired, one-electron transfer event that is quasi reversible, with a ratio of i_{pa}/i_{pc} = 0.45.

Based on the observed electrochemistry and the observations of the aqueous perrhenate system, a proposed structure of the reduced Re(V) species is shown in Figure 5.10.

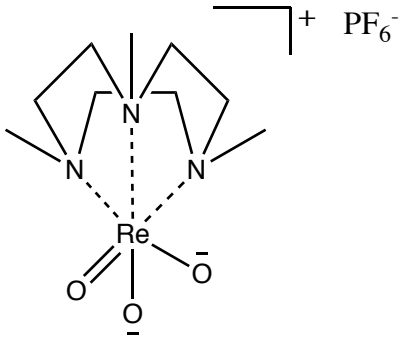

Figure 5.10 The proposed Rhenium (V) complex produced during the electrochemical reduction in the absence of added acid.

When previously studied in aqueous media, it was noted that the final reduction product was speculated to be either $[Re^{V}(OH)_3(Me_3tacn)]^{+2}$, or $Re^{V}O(OH)_2(Me_3tacn)]^{+}$, depending on the pH[151]. While in acetonitrile, it is reasonable to speculate that protons are not available to make the appropriate species. In our sample, it is reasonable to speculate that two electrons are transferred to the rhenium center of the complex. However, in the context of a DODH reaction, it is necessary to have protons present during the reduction. A series of acids was used to investigate the effect of protons on the reduction in acetonitrile.

5.2.3 – Electrochemistry of Hexafluorophosphate Complex 3 in the Presence of Proton Sources

In moving toward our goal of an electrocatalyic DODH, it is necessary to investigate the electrochemistry of the hexafluorophosphate complex **3** in the presence of a proton source.

In considering potential proton sources, water was the first candidate, as it is abundant and affordable. However, the hexafluorophosphate complex **3** was insoluble in water/acetonitrile mixtures that contained water concentrations as low as 3%. As a result, carboxylic acids, ammonium ions, phenol, and sulfonic acids were considered due to their solubility in acetonitrile and varying degree of acidity. Specifically, *p*-toluenesulfonic acid was selected as a strong acid source in water and has a pKa of 8.5 in acetonitrile[156]. As a slightly weaker acid, pentafluorobenzoic acid ($F_5BnCOOH$) was used, as it is an acid that is not likely to coordinate with a pK_a of approximately 2 in water, and 19 in acetonitrile.[156] Finally, the lower limits of the effects of protons were investigated by ammonium tetrafluoroborate (NH_4BF_4) and phenol, as they are both weak acids of differing functional groups with pK_a values of approximately 22 and 23 in acetonitrile, respectively[156].

All cyclic voltammograms were recorded at 150 mV/sec scan rate in 0.1 M NBu_4PF_6 in acetonitrile with two equivalents of each proton source relative to the concentration of complex **3**. Upon addition of ammonium tetrafluoroborate and phenol, the overall shape and $E_{1/2}$ remained unchanged, as shown in figures 5.10 and 5.11. However, upon addition of 2 equivalents of p-toluenesulfonic acid, there were two noticeable differences in the electrochemistry of the complex, as shown in Figure 5.12. The first reduction peak shifted positively from -0.806 V vs AgCl to -0.690 V vs AgCl. The amperometric response at -0.690 V vs AgCl was 13 μA. In addition, a more pronounced reduction peak is observed at -1.455 V vs AgCl with a "shoulder" at -1.29 V vs AgCl. The approximate amperometric response at -1.455 V vs AgCl was 15 μA. There is not an observable oxidation peak in the spectrum. The lack of oxidation peak suggests that a chemical reaction could be occurring after reduction of the metal complex, potentially with the solvent.

Based on the previously observed electrochemistry of complex **3** in the absence of the p-toluenesulfonic acid, it is likely that the reduction occurring at -0.690 V vs AgCl corresponds to the reduction of Re(VII) to Re(VI). In considering the magnitude in the shift in the reduction potential of the Re(VII) to Re(VI) step, it is likely that the addition of the acid facilitates reduction of the metal complex, as it could generate the monohydroxo/oxo anion instead of the anionic dioxo form of the Re(VI) complex. This phenomenon has been observed in the aqueous electrochemistry of the perrhenate complex[151]. When considering the second observed reduction, however, the reduction potential is largely unaltered. The E_{pc} of the second reductive wave of the hexafluorophosphate complex **3** is not significantly different in the presence of p-toluenesulfonic acid. The Epc of the "shoulder" observed matches directly with the E_{pc} of the metal complex. This suggests that the addition of the acid may not affect the electrochemical reduction of the Re(VI) to the Re(V) complex. The large second reductive peak, however, has a E_{pc} of -1.45 V vs AgCl. If this corresponds to the reduction of the Re(VI) to Re(V) complex, then it may be that addition of acid hinders the reduction instead of facilitating it. In order to investigate this further, acids weaker than p-toluenesulfonic acid were used.

The voltammogram of the hexafluorophosphate complex **3** in the presence of two equivalents pentafluorobenzoic acid demonstrates three reductive waves are observed in the voltammogram; there are not any oxidative waves observed, as shown in figure 5.12. The Epc of each wave are -0.746 V, -1.072 V, and -1.513 V vs AgCl. The first wave at -0.746 V vs AgCl has an i_{pc} of 10.6 μA, the second wave at -1.072 V vs AgCl has an ipc of 2.7 μA, and the final wave at -1.513 has an i_{pc} of 9.6 μA. Based on the proximity of the third wave's Epc to that of the pure acid suggests that this last peak corresponds to the reduction of protons.

The first peak, which likely corresponds to the Re(VII) to Re(VI) oxidation, is shifted positively by approximately 60 mV. This is a smaller shift than that observed from TsOH. This is reasonable, as pentafluorobenzoic acid is a weaker acid that has a pK_a = 2.1 in water, while TsOH has a pK_a = -2.3 in water. This is in good agreement with the behavior of the electrochemistry of the aqueous perrhenate system. In solutions of pH between 7 and 4, the change in the E_{pc} of the first reduction step was less noticeable. One notable feature that is observed in the presence of pentafluorobenzoic acid but not in the presence of p-toluenesulfonic acid is the second reduction wave at -1.07 V. While the i_{pc} is only about 1/5 of the wave at -0.746 V, it could be that this wave corresponds to the Re(VI) reduction to the Re(V) reduction. This would suggest the F_5-BzCOOH is a more appropriate acid to facilitate the reduction of the hexafluorophosphate complex **3** to the dihydroxo rhenium (V) reduced species, as shown in Figure 5.15.

Each acid altered the $E_{1/2}$ of both reductive waves, and the potentials of the reduction waves of the Re(VII)-Re(VI) and the Re(VI0-Re(V) couple are altered more drastically by acids with lower pKa values. This is consistent with the electrochemical behavior observed in aqueous solution. One interesting observation, however, is that the Re(VI) – Re(V) couple shows a lower potential in the presence of p-TsOH than pentafluorobenzoic acid. Since both reductions are essential for the formation of a Re(V)-glycolate, the more appropriate acid to be used in a preparative electrolysis is the pentafluorobenzoic acid.

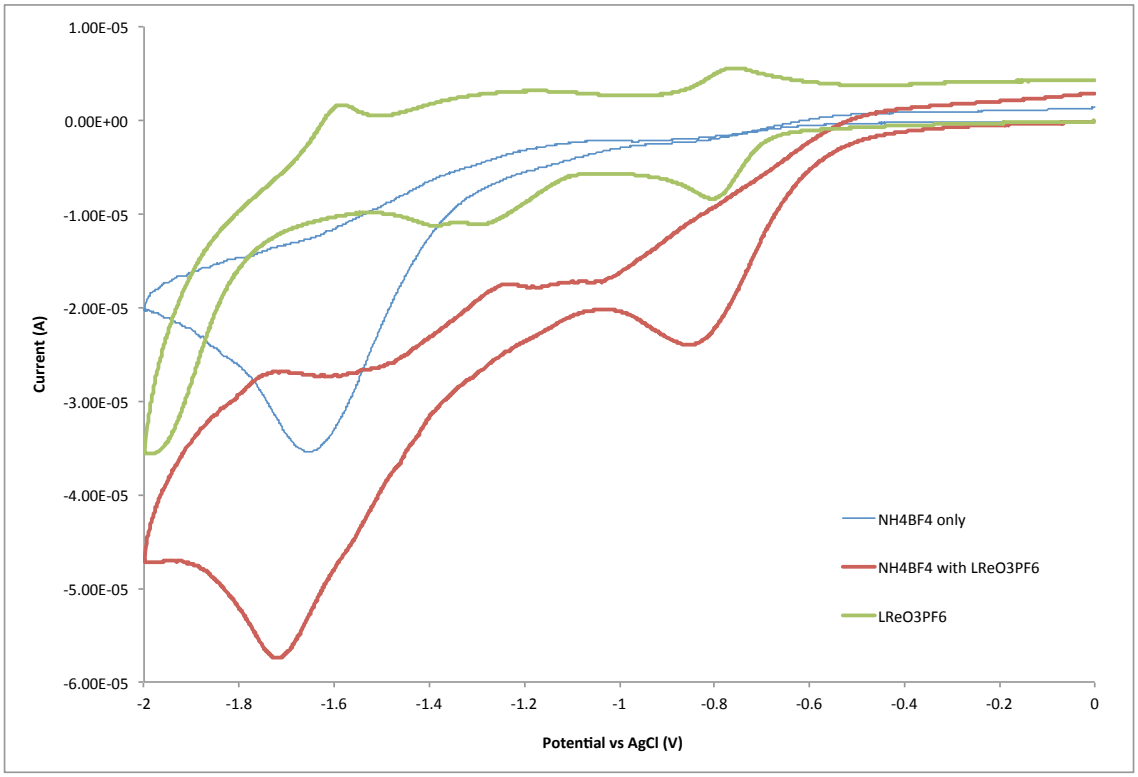

Figure 5.11. the voltammograms ammonium tetrafluoroborate (blue) of $Me_3TACNReO_3PF_6$ in the absence (green) and the presence (red) of ammonium tetrafluoroborate in acetonitrile using tetrabutylammonium heafluorophosphate (0.1M) as a supporting electrolyte. Scan rate = 150 mV/sec

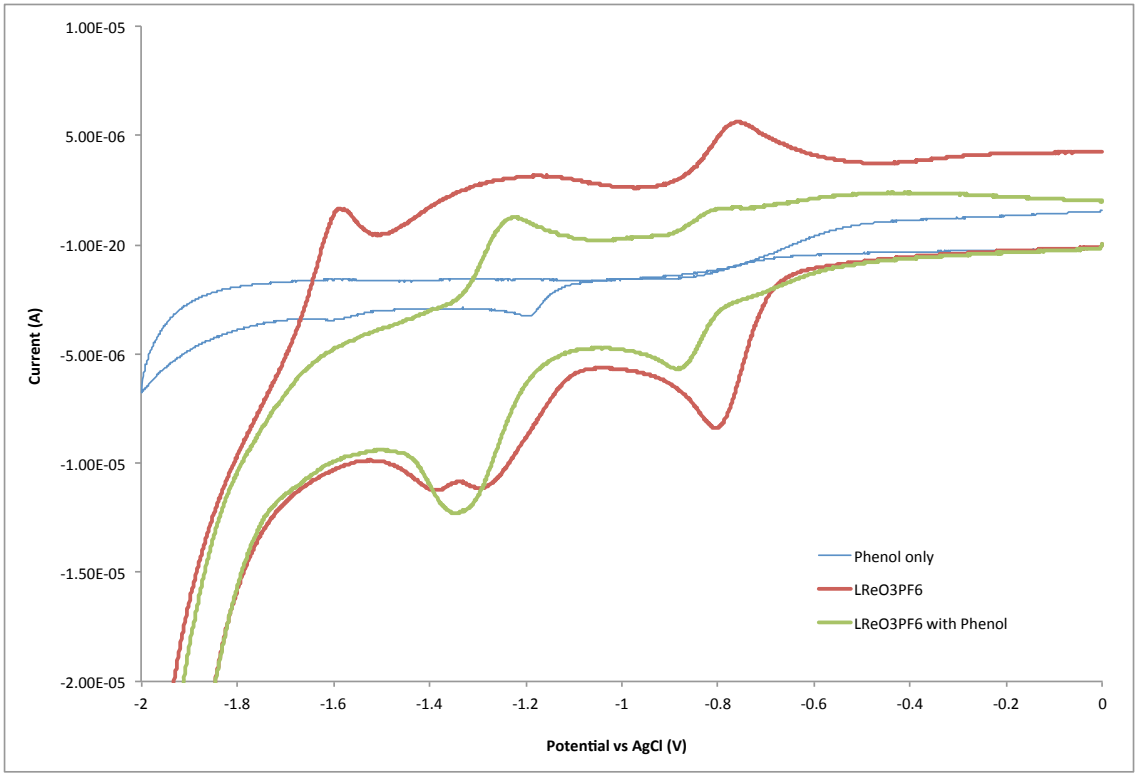

Figure 5.12. The voltammograms of phenol (blue) and $Me_3TACNReO_3PF_6$ in the presence (green) and the absence (red) of phenol in acetonitrile using tetrabutylammonium heafluorophosphate (0.1M) as a supporting electrolyte. Scan rate = 150 mV/sec

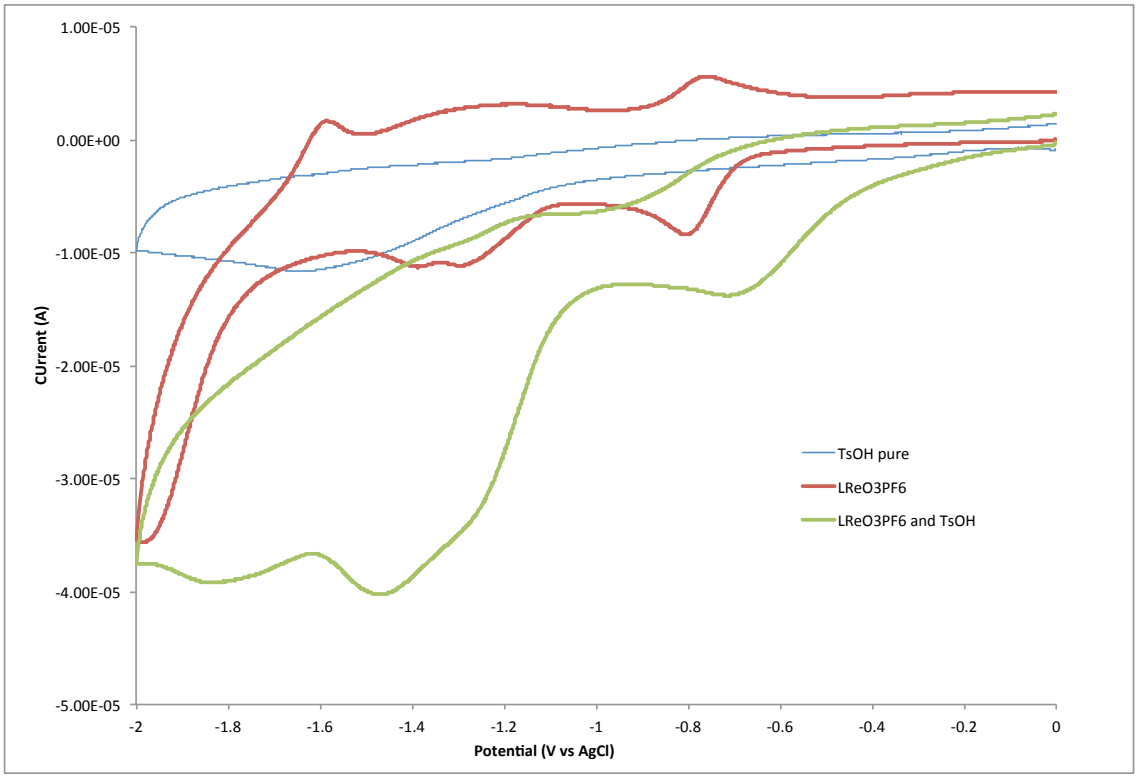

Figure 5.13. The voltammograms of p-toluenesulfonic acid (blue) and $Me_3TACNReO_3PF_6$ in the absence (red) and presence (green) of p-toluenesulfonic acid in acetonitrile using tetrabutylammonium heafluorophosphate (0.1M) as a supporting electrolyte. Scan rate = 150 mV/sec

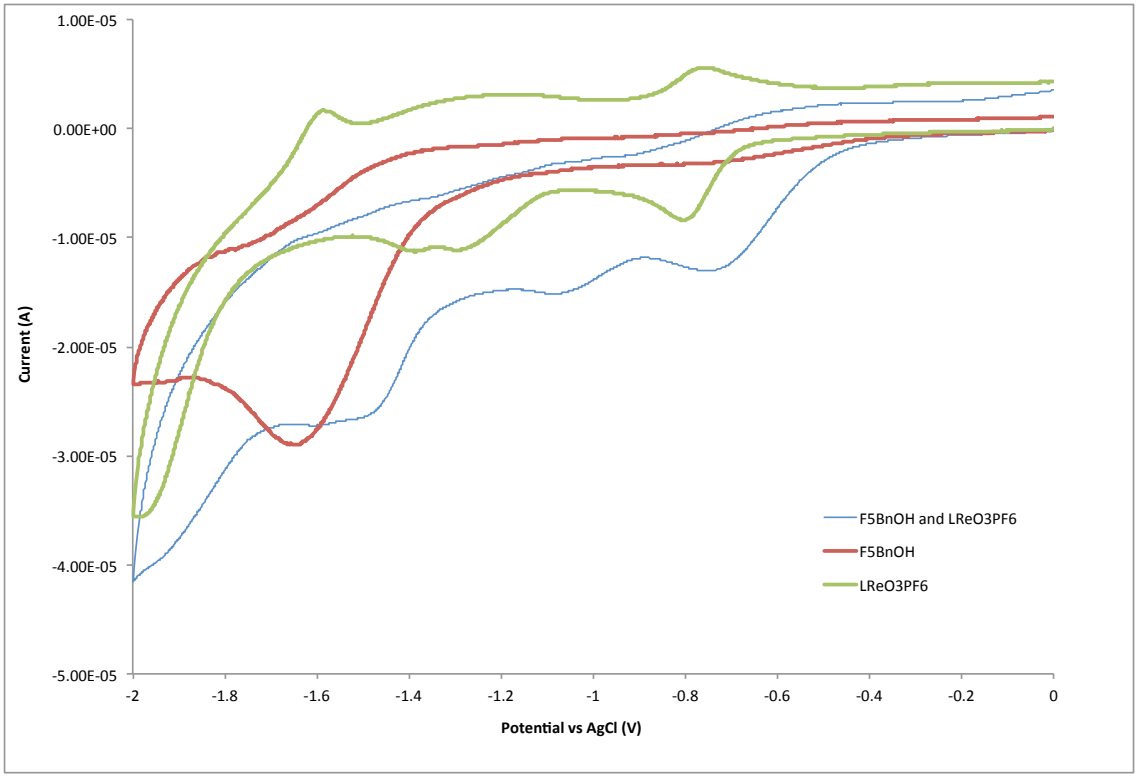

Figure 5.14. The voltammograms of pentafuorobenzoic acid (red) and $Me_3TACNReO_3PF_6$ in the absence (green) and presence (blue) of pentafuorobenzoic acid in acetonitrile using tetrabutylammonium heafluorophosphate (0.1M) as a supporting electrolyte. Scan rate = 150 mV/sec

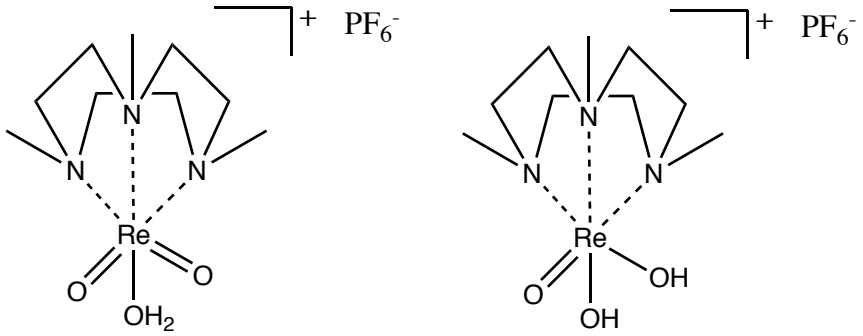

Figure 5.15 The structure of two possible tautomers of the 1,4,7-Trimethyltriazacyclononanerhenium (V) dihydroxo monooxo hexafluorophosphate complex that results from hexafluorophosphate complex 3 is reduced electrochemically in the presence of pentafluorobenzoic acid.

5.2.4 – Formation of the Rhenium (V) Glycolate Complex Via Bulk Electrolysis

With the reduced Re(V) dihydroxocomplex prepared electrochemically, the next logical step in moving to an electrocatalytic DODH reaction was forming the Re(V) glycolate species electrochemically. The Nicholas group has previously synthesized Re(VII) glycolates using methyltrioxo rhenium and styrene glycol, or through methyltrioxorhenium and styrene oxide. However, attempts to form the Rhenium (VII) glycolate using hexafluorophosphate complex **3** were unsuccessful when replicated using this methodology as outlined in Figure 5.15.[77, 157-158]. The most significant difference between the two systems is that MTO has a coordination number of 4 and can increase the coordination number to five. The hexafluorophosphate complex **3**, however, has a coordination number of 6. This suggests that the seven coordinate complex formed between styrene glycol and complex 3 would be very sterically hindered. In addition, it is noted that there is not a literature precedent for a rhenium (VII) glycolate complex formed using hexafluorophosphate complex **3** or perrhenate complex **2** and a glycol. Re (V) glycolates have been produced using a methodology that starts with a $ReOCl_3(PPh_3)_2$ complex[77, 159]. By reacting the complex in the presence of the glycol and the ligand, the desired Re(V) glycolate can be achieved. This suggests that the Rhenium (V) complex is necessary to form the metal glycolate. Preparation of the rhenium (V) glycolate from styrene glycol was carried out in deuterated dichloromethane to afford a red solution. Analysis of the mixture via NMR shown in Figure 5.17 indicates formation the styrene glycol rhenium (V) complex, as evidenced by new proton peaks occurring between δ 5.0 and 6.0 ppm. These signals align with metalloglycolates formed by the Nicholas group and others[92, 152].

a)

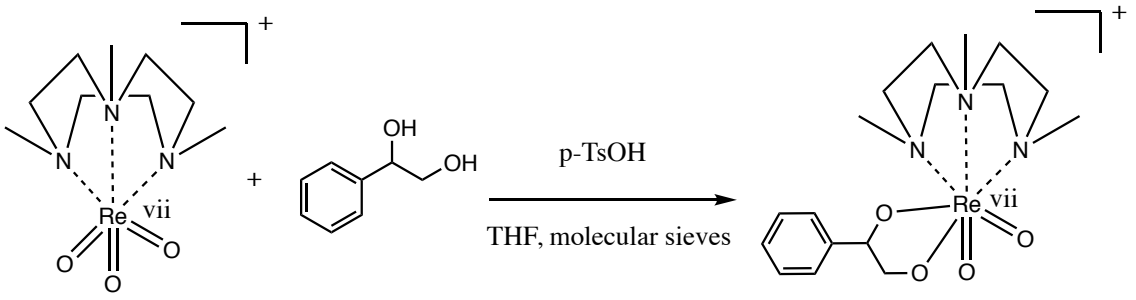

b)

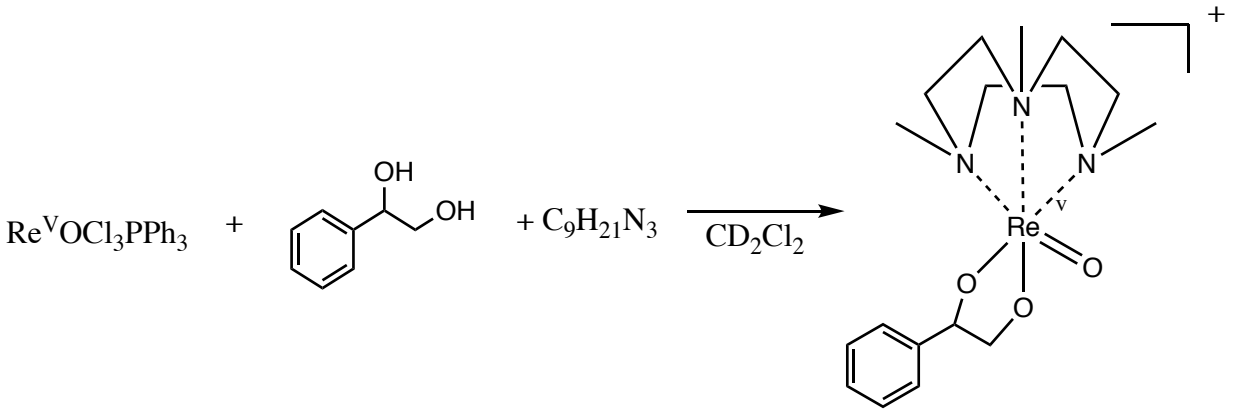

Figure 5.16 a) The reaction methodology used by Abu-Omar to form the rhenium (VII) glycolate complex using styrene glycol. b) Synthesis of a rhenium (V) glycolate complex using Trichloromonooxorhenium (V) bistriphenylphosphine, styrene glycol, and 1,4,7-trimethyltriazacyclononane ($C_9H_{21}N_3$), modified from a procedure modified by Boehm [77, 159].

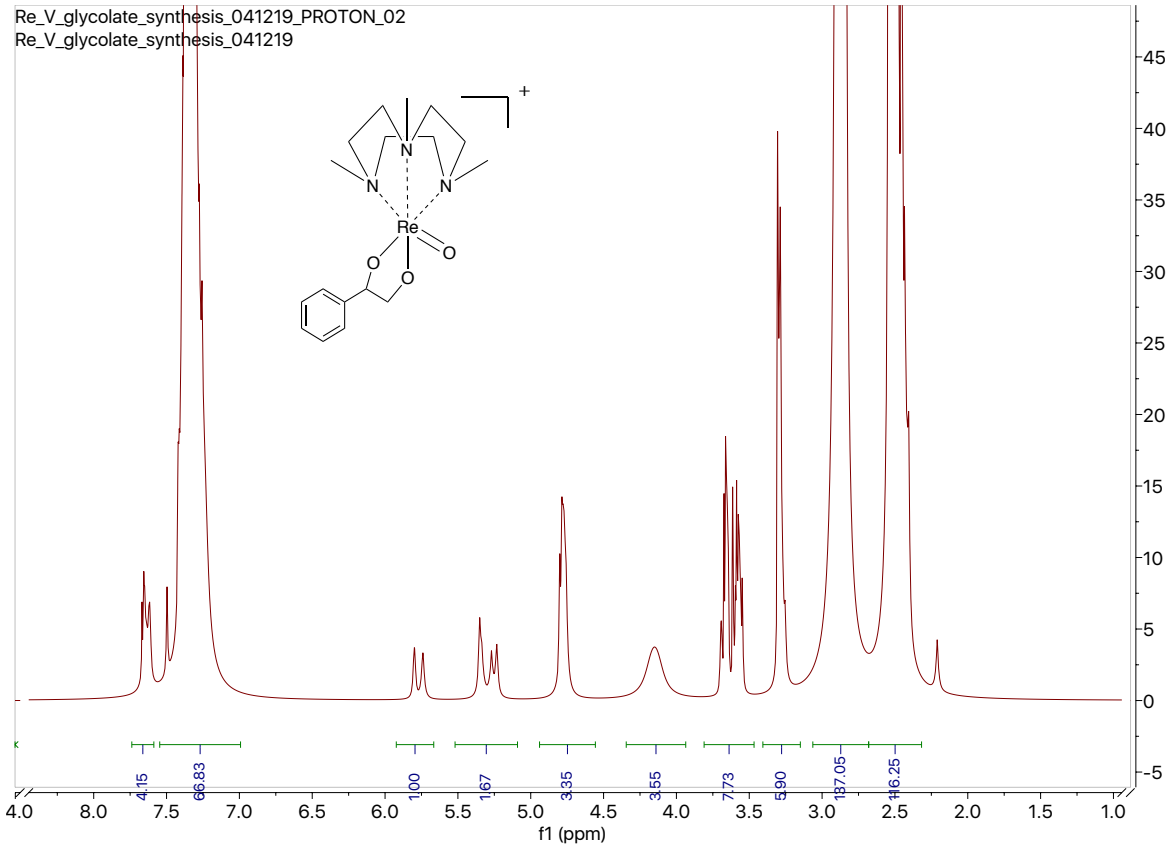

Figure 5.17: The ^{1}H nuclear magnetic resonance spectrum of the reaction mixture containing styrene glycol, $ReOCl_3(PPh_3)_2$, and 1,4,7-Trimethyltriazacyclononane.

The multiplet pattern at δ7.6 ppm corresponds to the protons attached to the benzene ring of the styrene glycol, while the doublet at δ5.8 ppm corresponds to the benzylic hydrogen, and the signals between δ5.2 and δ5.4 ppm correspond to the two terminal hydrogens from the glycol. The singlet near δ3.25 ppm and the multiplet near 3.6 ppm correspond to the hydrogen atoms on the methyl group and methylene groups on the ligand, respectively. This aligns with previously synthesized rhenium (V) glycolates made in the Nicholas group using methyltrioxorhenium as a starting catalyst, as well as other rhenium (V) glycolates using a TACN ligand[92]. One significant difference in the results from the synthesis reported in the literature is that our metalloglycolate is soluble in both THF and methylene chloride.

This difference could be due to the chloride ion still being coordinated to the inner sphere of the coordination complex, instead of becoming an outer sphere ion, as shown in Figure 5.18. This could be confirmed further by using a solution of silver hexafluorophosphate to precipitate the chloride, however, the (TACN)ReO_3 complex is not soluble in methylene chloride, and precipitation of both complexes may occur. Attempts to form the rhenium (V) glycolate were not successful in acetonitrile. With the Re(V) glycolate synthesized chemically, a logical progression is to try and prepare the Re(V) glycolate complex via electrochemical methods.

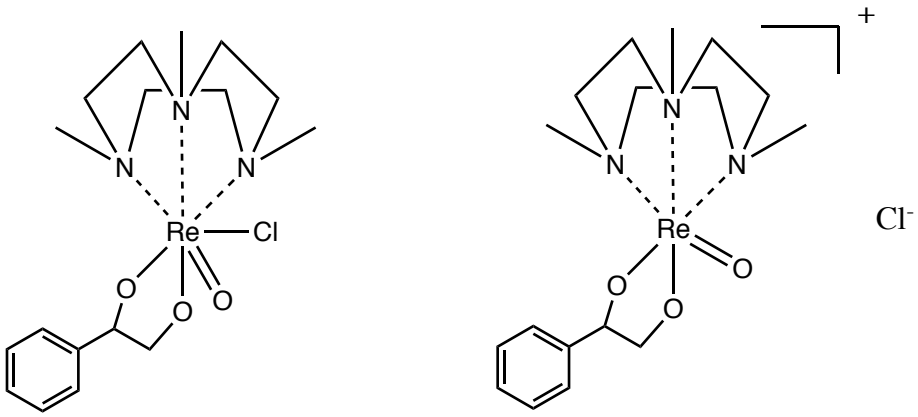

Figure 5.18 – The two forms of the Re(V)glycolate complex where chloride is included in the inner sphere of coordination (left) and where chloride is dissociated as an outer sphere ligand (right).

By using bulk electrolysis and coulometry, it is reasonable that the reduction of the rhenium (VII) complex **3** to the rhenium (V) complex shown in Figure 5.15 could be obtained[98, 155]. In considering the method of the electrolysis, a constant potential electrolysis is more appealing than a constant current electrolysis. The constant potential electrolysis could be more selective to the reduction of the TACN-Re (VII) complex **3** to the corresponding TACN-Re(V) complex. However, it was essential to investigate the effect of

styrene glycol on the reduction of the hexafluorophosphate complex **3** to determine if the glycol affected the electrochemical behavior.

Cyclic voltammograms of the TACN-Re(VII) complex **3** were recorded using a glassy working electrode and a Pt wire counter electrode in 0.1M tetrabutylammonium hexafluorophosphate, 0.010 M styrene glycol, and 0.010 M pentafluorobenzoic acid, as shown in Figure 5.19. Addition of styrene glycol to the system of complex **3** did not appear to alter the voltammogram, as there are still three reductive waves at the same potential. Bulk electrolysis was conducted on the mixture using a carbon felt working electrode and a Pt wire counter electrode at -1.6 V vs AgCl under a stream of nitrogen. After electrolysis, the system was analyzed via Electrospray Ionization – Mass Spectrometry, as the tetrabutylammonium ion in the supporting electrolyte is NMR-active. It is expected that that the Re(VII) complex should appear in the mass spectrum at m/z=406.11, as the complex is already cationic. Formation of the corresponding rhenium (V) glycolate should afford a new peak at m/z=510.18. Due to the rhenium in the complex, a unique isotopic distribution pattern should be observed that allows for a facile detection of the rhenium complex. Predictions of the mass spectrum patterns are shown in Figure 5.18 for TACN-Re(VII) complex 3 and its corresponding rhenium (V) glycolate.

An aliquot of the reaction mixture was analyzed via mass spectrometry. The resulting mass spectrum showed major peaks at m/z = 242, m/z = 629, and m/z = 519. These observed peaks do not exhibit the necessary isotopic distribution. The large overwhelming signal at m/z = 242 corresponds to the background tetrabutylammonium cation. Attempts to reduce the concentration of the supporting electrolyte did not drastically change the mass spectrum of the complex. As a result, the supporting electrolyte

was switched from tetrabutylammonium hexafluorophosphate to potassium hexafluorophosphate. The electrochemical behavior of the system did not change upon switching supporting electrolytes. Figure 5.18 shows the voltammograms of the reaction mixture before and after the electrolysis.

After the electrolysis, there is a change in the voltammogram of the reaction products, as seen in figure 5.20. The current of the peaks is no longer measureable at -0.75 V vs AgCl and -1.42 V vs AgCl. This suggests that the rhenium (VII) complex is disappearing. However, the color of the solution does not change, suggesting the Re(V) glycolate was not formed. Analysis of the mixture by mass spectrometry resulted in a complex mixture that appears to be complexes of the potassium and hexafluorophosphate ions. Figure 5.18 shows the mass spectrum of the electrolysis mixture containing potassium hexafluorophosphate.

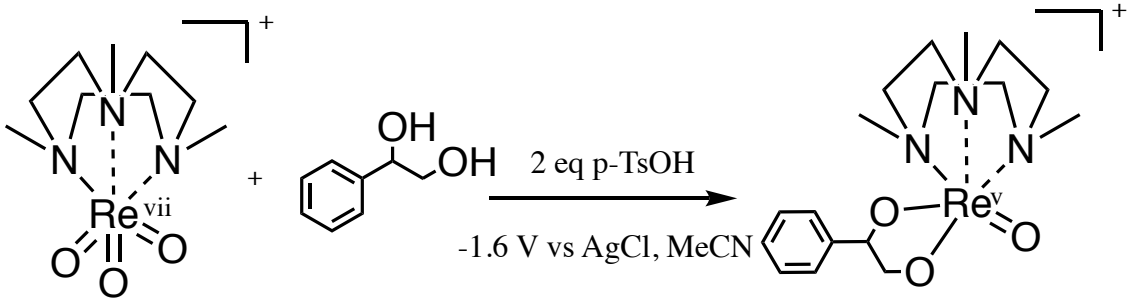

Figure 5.19 The proposed electrochemical synthesis of the rhenium (V) glycolate conducted by bulk electrolysis.

a)

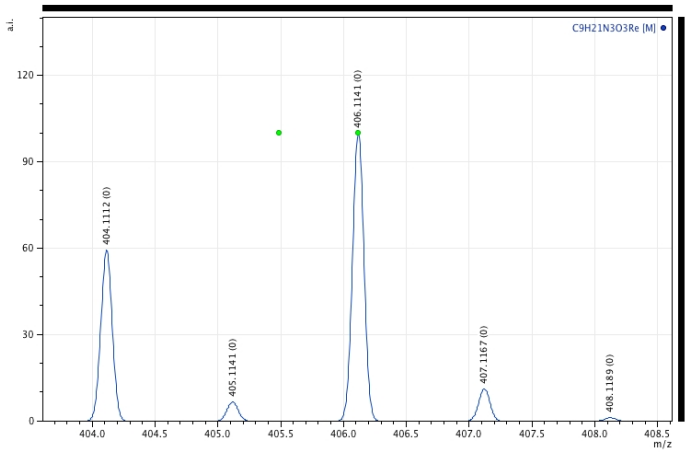

b)

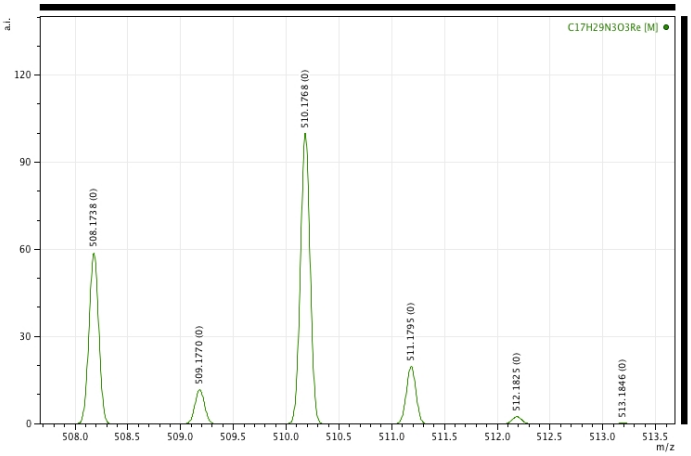

Figure 5.20 Predictions of a) Re(VII) complex 3 $[C_9H_{21}N_3ReO_3]^+$ and b) Re(V) glycolate $[C_{17}H_{21}N_3ReO_3]^+$. Simulations were developed using the program mMass.

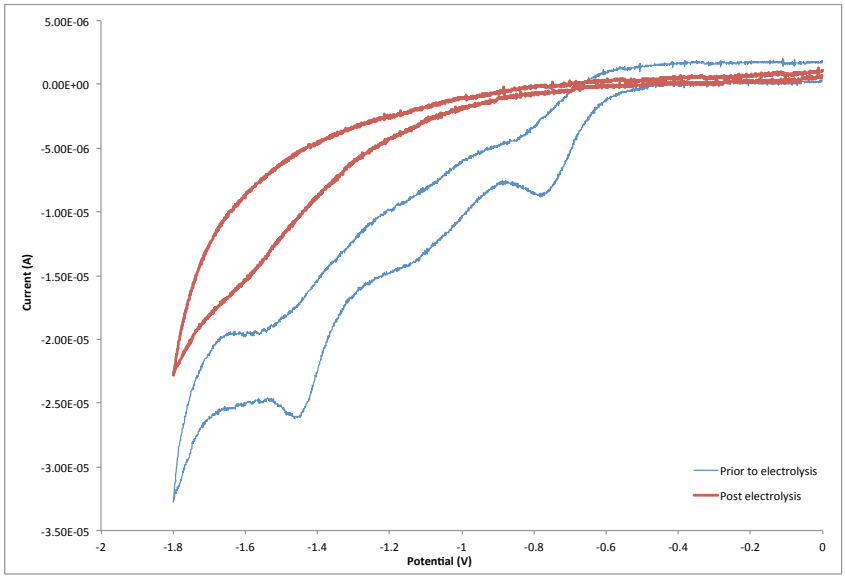

Figure 5.21 – The cyclic voltammograms of the rhenium hexafluorophosphate complex 2, styrene glycol, and pentafluorobenzoic acid in 0.1M potassium hexafluorophosphate before (blue line) and after (red line) electrolysis.

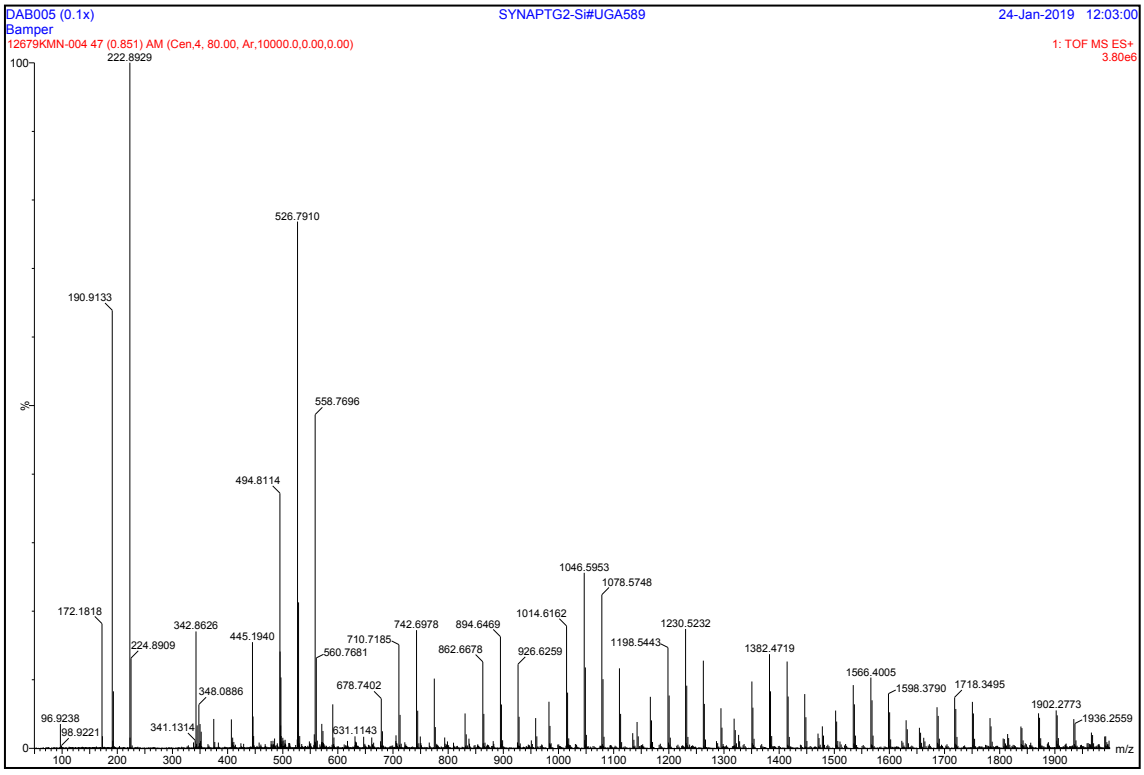

Figure 5.22 The mass spectrum of the electrolysis product mixture made from rhenium (VII) PF_6 complex 3, styrene glycol, and pentafluorobenzoic acid.

Within the mass spectrum, there is not a detectable rhenium isotopic distribution, suggesting that the background matrix is overwhelming the rhenium signal. All peaks observed correspond to a variety of potassium and hexafluorophosphate ion clusters. However, with the replacement of the tetrabutylammonium ion by the potassium ion, NMR can be used to analyze the reaction mixture for the presence of the metalloglycolate. The NMR spectrum did not indicate the presence of the metalloglycolate, as there are not any peaks between the region of δ5.00 and δ6.00 ppm.

In considering potential reasons why the metalloglycolate was not detected under the electrolytic conditions, it is important to consider the different components of the mixture. The first consideration is the choice of acid used in the system, pentafluorobenzoic acid. It could be envisioned that the five fluorine groups on the benzene ring could inductively stabilize a radical anion. This radical could potentially react even further with the generated TACN-Re(V) species. It is possible that the loss of oxidation peaks in the cyclic voltammogram could indicate a chemical reaction that occurs after generation of the TACNRe(V) glycolate. A second potential problem from the acid is that it is not strong enough to sufficiently protonate the reduced TACN-Re(V) species to generate the TACNRe(V) glycolate. The pK_a of pentafluorobenzoic acid is approximately 19 in acetonitrile, suggesting, that while the acid is sufficiently strong to alter the redox potential, it may not be strong enough to generate the metalloglycolate[156]. To address these potential issues, the acid was changed in the reaction mixture. Methanesulfonic acid has a pKa near 10 in acetonitrile[156]. In addition, the methyl group on the acid acts as a poor electron stabilizer due to a lack of inductive stabilization, which should eliminate the possibility of undesired electrochemical processes involving the acid[160]. Analysis of a reaction mixture

containing 0.010 M rhenium complex 2, 0.010 M styrene glycol, 0.020 M methanesulfonic acid, and 0.1 M KPF_6 shows three reductive peaks at -1.05 V vs AgCl, -1.27 V vs AgCl, and -1.50 V vs AgCl. The voltammogram is shown Figure 5.21. One new feature that had not been detected before are two oxidative shoulders at -1.10 V vs AgCl and -0.80 V. These reductive peaks are lower in potential than the mixture with pentafluorobenzoic acid very similar in potential to the electrolysis mixture prepared with p-toluenesulfonic acid. This observation is not consistent with aqueous experiments conducted on the TACN-Re(VII) perrhenate complex 2.

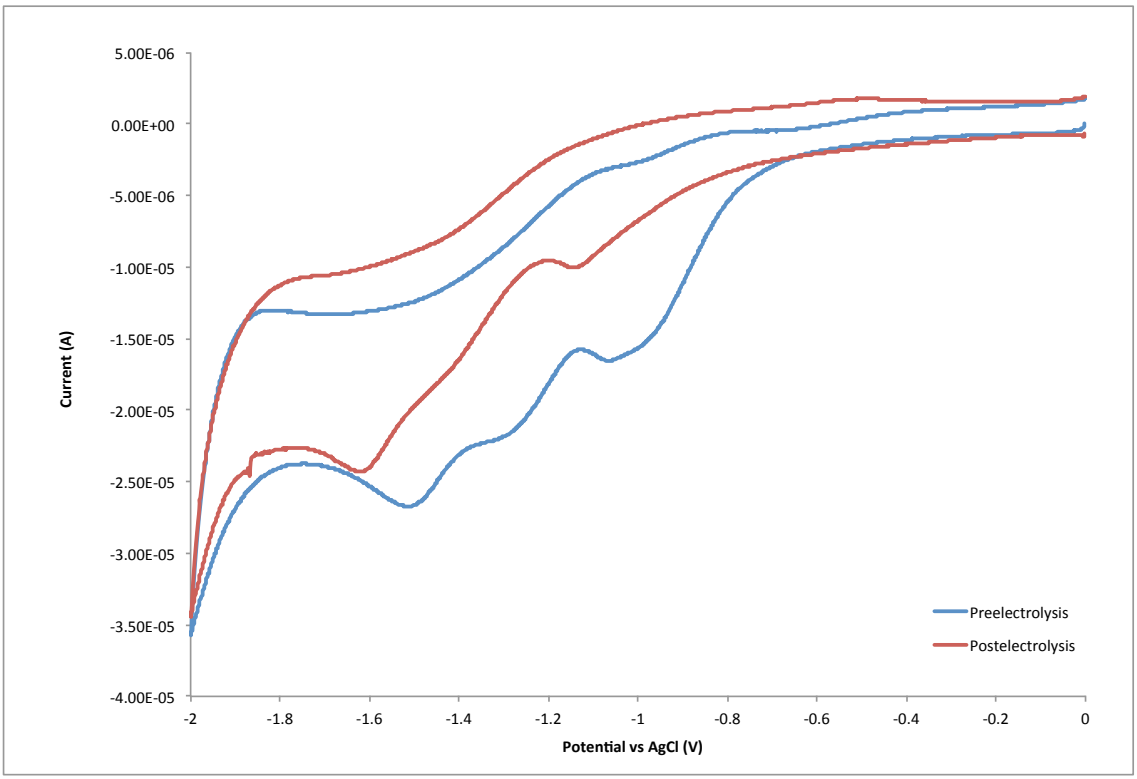

Figure 5.23 The cyclic voltammograms of the mixture containing 0.010 M Re complex 2, 0.010 M styrene glycol, 0.020 M $MeSO_3H$, and 0.1 M KPF_6 in acetonitrile. Cyclic voltammograms were obtained at a scan rate of 150 mV/sec using a glassy carbon working electrode, a Pt wire auxiliary electrode, and a AgCl reference electrode.

After electrolysis at -1.6 V vs AgCl, the amperometric response of each peak was decreased. The reductive peaks shifted from -1.05 V vs AgCl, -1.28 V vs AgCl, and -1.5 V vs AgCl to -1.13 V, a shoulder is seen near 1.41 V vs AgCl, and -1.61 V, respectively. The decrease in the amperometric response could be due to the Re (VII) complex **3** being reduced to a Re (V) complex. One interesting observation in Figure 5.21 is that the potential of the reduction peaks shifted farther negative after electrolysis. It is reasonable to speculate that the change in the potential of the reduction peaks is due to a lower concentration of acid. It is likely that the concentration of available protons decreased during electrolysis, meaning the effective pH of the solution increased, as the reduction peak was shown to be pH dependent, and it could it be similarly encountered in the aprotic system. As the concentration of protons decreased, the amount of catalyst that is protonated decreases. This means that the potential of the electroactive species shifted back to the potential of the metal complex, which was more negative than the protonated complex.

The analytical methods previously used to detect the metalloglycolate, however, do not enable for a simple analysis of the electrolysis mixture, as the matrix provides an obscured mass spectrum. Thus our approach changed to an indirect detection method of the metalloglycolate. If the metalloglycolate is produced, even in small quantities, then thermolysis of the reaction mixture could lead to the production of styrene. The heated mixture could then be analyzed by GC in a similar fashion to the thermal catalytic reaction. After electrolysis, the mixture containing TACN-Re complex 3, styrene glycol, methansulfonic acid, and KPF_6 was concentrated by passing nitrogen over the reaction mixture. A 1 mL aliquot of the concentrate was mixed with 1 mL of toluene, and then

transferred into a high-pressure reactor vessel. The mixture was reacted at 125 ° C for 3 hours in a toluene-acetonitrile mixture. The reaction was analyzed via GC for any evidence of styrene, implying that the reduced metal complex and the glycol would form the metalloglycolate and then fragment at the higher temperatures, effectively creating one cycle of the DODH reaction. Analysis of the mixture using gas chromatography, however, did not indicate the presence of styrene. There was a decrease observed in the concentration of styrene glycol in the reaction mixture, however, this was most likely due to precipitation of the styrene glycol upon the addition of toluene.

In considering other reasons why the rhenium (V) glycolate may not have formed, a likely reason could be poor degassing methods of passing nitrogen over the solution for 15 minutes prior to electrolysis. While this method eliminated the signal from oxygen in the voltammogram, there may still be sufficient oxygen to immediately oxidize any TACN-Re (V) complex formed. To ensure that oxygen was removed from the system prior to electrolysis, the electrochemical set-up was moved inside of a nitrogen glove bag, and the reaction solution was degassed using a freeze-pump-thaw method. Even in these oxygen-free conditions, however, the metalloglycolate was not detected. This could be due to a follow-up chemical reaction is occurring after the reduction of the rhenium (VII) species, possibly the acetonitrile. It could be imagined that the acetonitrile could be nucleophilically attacking the electrophilic $(TACN)Re^{v}O(OH)_2$ or the coordination results in a deactivated $TACNRe^{V}O(OH)_2$.

Further experimentation in different solvents may work to solve this issue. Acetonitrile was initially used, as it is sufficiently polar to dissolve the hexafluorophosphate complex **3**, and has been demonstrated to be electrochemically stable over a large

electrochemical window. We previously described the formation of the TACN-Re(V) glycolate using a $ReOCl_3(PPh_3)_2$ starting material in methylene chloride, and we noted that attempts to form the TACN- Re(V) glycolate were unsuccessful using the same methodology in acetonitrile. This suggests that acetonitrile is not a suitable solvent for formation of the metalloglycolate. This could be caused by the nitrile portion of the solvent molecules interacting or coordinating with the rhenium (V) complex. It could be envisioned that using other non-polar non-coordinating solvents may serve to provide additional opportunities to afford the desired metalloglycolate.

Additionally, elemental zinc has been demonstrated to chemically cause a reduction of the TACN-Re (VII) hexafluorophosphate complex in methanol and form the corresponding TACN-Re(V)$O(OMe)_2$ complex. We also demonstrated that elemental zinc was a successful reductant for the thermal catalytic DODH. This suggests that zinc may be a suitable working electrode. It could also be imagined that the presence of zinc hexafluorophosphate as a supporting electrolyte could be beneficial in the reduction, however, the reduction of Zn^{+2} occurs at -0.96 V vs AgCl. While this may negate the benefit of using electrochemical methods to eliminate the need for a chemical reductant, it could provide the appropriate means to electrochemically produce the metalloglycolate. In addition, it is reasonable to speculate that the zinc electrode would not be sacrificial, as an abundance of electrons are available at the working electrode under reducing conditions. Further analysis using a zinc working electrode may provide beneficial insight into electrochemically synthesizing the metalloglycolate. A potential issue in this approach could be the reducing properties of zinc toward protons from the acid, but this could be

overcome with the use of a potentially a weaker acid and an abundance of electrons from the electrode under reducing potentials.

In considering another component of the reaction mixture as a potential reason that the Re(V) glycolate was not detected, the glycol could be an additional factor. The phenyl ring on styrene glycol is a mild electron-withdrawing group. The benefit of incorporating an electron-withdrawing group on the glycol is that the fragmentation process becomes easier. However, it could be imagined that this makes the alcohol less nucleophilic. By incorporating an electron-donating group into the glycol, it is possible that the Re(V) glycolate may form more easily.

5.3 – Conclusions

In conclusion, two new metal complexes were demonstrated to be effective catalysts for deoxydehydration processes, giving between 39% and >95% yields of alkenes using a variety of reductants, including aromatic and elemental reductants. Converting the perrhenate complex **2** to hexafluorophosphate complex **3**, there was a change in the yield of the product in a thermal catalytic system. In addition to the necessity of a stronger reducing agent, this suggests that the perrhenate ion and the cationic complex worked in conjunction to provide effectively two catalysts to the system, as evidenced by a drastic decrease in yield, or even 0% yield in some cases, when the perrhenate ion was exchanged for the hexafluorophosphate ion. When a stronger reducing agent was used in the thermal process, yields greatly increased, suggesting that electrons from a surface can be used to reduce the complex **3** to make the corresponding rhenium (V) complex.

The cyclic voltammogram of $(Me_3TACN)ReO_3PF_6$ in acetonitrile showed two reduction peaks, corresponding to the Re (VII) to Re (VI) and Re (VI) to Re(V). The addition of various acids altered the potential at which the rhenium complex was reduced, with weaker acids demonstrating a smaller change in the reduction and stronger acids causing a larger change in the reduction potential. This effect parallels the $(Me_3TACN)ReO_3ReO_4$ response to changes in pH in aqueous solution. This suggests that the hexafluorophosphate complex 3 electrochemically behaves similarly to the perrhenate complex 2. The main difference between the behavior of the aqueous perrhenate complex and the hexafluorophosphate complex is that the electrochemical reduction of hexafluorophosphate complex 3 is not reversible, as there is only a reduction peak. This suggests that there could be a chemical reaction after the reduction occurs. The nature of this reaction is unknown. It could be imagined that acetonitrile could coordinate with the newly formed Re(V) complex. Attempts to reduce the metal complex using bulk electrolysis did not yield the metalloglycolate potentially due to a competing reaction that is not characterized. Attempts to alleviate this issue and electrochemically synthesize the metalloglycolate by direct and indirect methods were not successful. Components including the acid, solvent, and working electrode were discussed as potential sources of the problem and could be addressed in future experiments. Future experiments could include a survey of solvents in which the electrochemical measurements are performed to try and eliminate any post-reduction reactions with acetonitrile. In addition, it may be beneficial to conduct experiments using a zinc electrode, as we have demonstrated that elemental zinc is capable of reducing the $Me_3TACNReO_3PF_6$ complex 3. Looking forward to an electrocatalytic DODH process, it is important to consider the fragmentation of the Re(V) glycolate into the

corresponding alkene and Re(VII) complex. High temperatures are often required to observe this fragmentation. As such, a high-pressure/high-temperature electrochemical apparatus will be required.

5.4 - Experimental

Reagents

All reagents listed were purchased from commercial sources and used without further purification, unless otherwise described.

NMR Measurements

All NMR measurements were recorded on a Varian 300 MHz NMR spectrometer. Data was processed using varian software.

Electrochemical Measurements

All electrochemical measurements were taken on a Chemical Instruments 832 Bipotentiostat using a 3-electrode set-up: a 3 mm glassy carbon working electrode, a AgCl wire treated with 3 M HCl for 12 hours as a reference electrode, and a Pt wire auxiliary electrode. Measurements were taken in acetonitrile using 0.1 M tetrabutylammonium hexafluorophosphate or 0.1 M potassium hexfluorophosphate as a supporting electrolyte. Tetrabutylammonium hexafluorophosphate was recrystallized from methanol to remove any impurities, and potassium hexafluorophosphate was used without further purification.

Synthesis of Complex 1 ($Me_5DETN)ReO_3ReO_4$[94]

In a nitrogen atmosphere, a solution containing 75 mg (0.47 mmol) N,N,N',N",N"-pentamethyldiethylenetriamine in 10 mL of THF was prepared. To this clear, colorless solution, 10 mL of THF containing 192 mg (0.397 mmol) of Re_2O_7 was added dropwise to

form a blue-white precipitate. The solution was stirred for two hours and the resulting white precipitate was collected via filtration to yield 186 mg (72% yield). NMR: δ3.42 ppm (15 H, singlet); δ2.62-2.82 ppm (8 H, multiplet)

Synthesis of Complex 2 ($Me_3TACN)ReO_3ReO_4$[94]

In a nitrogen atmosphere, a solution containing 75 mg (0.47 mmol) 1,4,7-N,N',N"-trimethyltriazacyclononane in 10 mL of THF was prepared. To this clear, colorless solution, 10 mL of THF containing 192 mg (0.397 mmol) of Re_2O_7 was added dropwise to form a blue-white precipitate. The solution was stirred for two hours and the resulting white precipitate was collected via filtration to yield 200mg (77% yield). NMR (D_2O): δ3.31 ppm (9 H, s); δ3.22 ppm (6 H, m); δ3.41 ppm (6 H, m)

Metathesis of Complex 2 to form Complex 3 ($Me_3TACN)ReO_3PF_6$[94]

100 mg (0.145 mmol) of Complex 2 was dissolved in 10 mL of deionized water. 10 mL of 1.0 M sodium hexafluorophosphate was added to afford a white precipitate. The white precipitate was stirred for twenty minutes and recovered via filtration and dried for an hour in a 70 ° C oven. The mass of the resulting precipitate was 70 mg (>95% yield). The air stable complex was stored in a desiccator until use. NMR (CD_3CN): δ3.31 ppm (9 H, s); δ3.22 ppm (6 H, m); δ3.41 ppm (6 H, m)

General Procedure for Deoxydehydration Reactions using Complexes 1 and 2

0.20 mmol of diol (either PDE, DET, or 1,2-decanediol) was added to an Ace reactor thick-walled reactor tube. 5 mg (0.010 mmol) of Complex 1 or Complex 2 were added with 0.4

mmol of reductant. 2.00 mL of toluene were added to the tube as a solvent. Upon sealing the reactor vessel, the atmosphere inside the tube was purged and then filled with nitrogen three times. The reactor vessel was submerged in a 150 ° C oil bath for either 24 hours (for DET and 1,2-decanediol) or 12 hours (for PED). The resulting solutions were analyzed via quantitative GC.

Characterization by Gas Chromatography

Reactions were analyzed using a Shimadzu gas chromatograph with a flame Ionization detector. All samples were run on a Shimadzu 2014-GC, equipped with a 3% SE-54 packed column, FID and thermal program 40 °C for 5 min; 20 deg/min to 250 °C; then 7 min at 250 °C or in decanediol reactions using heptadecane as standard 40 °C for 3min; 6 deg/min to 65 °C; 2 min at 65 °C; 20 deg/min to 100 °C; 2 min at 100 °C; 15 deg/min to 250 °C; 3 min at 250 °C. Calibrations of

Analysis Date & Time : 4/14/2015 4:09:32 PM
User Name : Admin
Vial# : 3
Sample Name : DAB108 B DD
Sample ID : DAB 108b DD
Sample Type : Unknown
Injection Volume : 1.00
ISTD Amount :

Data Name : C:\GCsolution\Data\Dan Bamper\DAB 108 B DD.gcd
Method Name : C:\GCsolution\Mike method1.gcm

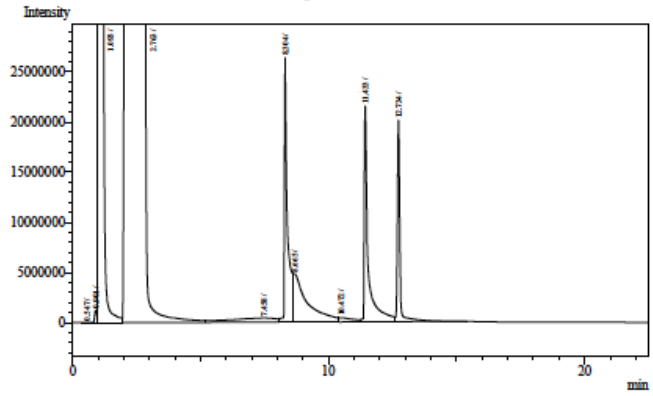

Peak#	Ret.Time	Area	Height	Conc.	Unit	Mark	ID#	Cmpd Name
1	0.547	148416	22900	0.001				
2	0.901	6557849	1206064	0.026		V		
3	1.093	5189287014	618945466	20.281		V		
4	2.763	19561569689	629032748	76.452		V		
5	7.458	49771311	3990057	0.195		V		
6	8.304	228859179	26322998	0.894		V		
7	8.665	179647025	4820141	0.702		V		
8	10.472	15023797	423240	0.059		V		
9	11.433	222633514	21458947	0.870		V		
10	12.734	1333395235	200530888	0.521		V		
Total		25586893029	3226846491					

styrene, styrene glycol, biethyltartrate, and diethylfumarate were prepared using heptadecane as an internal standard were prepared using three points for each calibration. Calibration plots of the ratio of GC response of the analyte to internal standard vs the ratio of the concentration of the analyte to the concentration internal standard were prepared and used to determine the yield of each thermal catalytic reaction. A sample chromatogram is shown above.

Electrolysis of Rhenium Complex 3 in the presence of Glycol and Acid

5.0 mg of (Me_3TACN)ReO_3PF6 complex 3 was dissolved in 15 mL of a 0.1 M potassium hexafluorophosphate or a 0.1 M solution of tetrabutylammonium hexafluorophosphate solution in acetonitrile with 2.2 equivalents of acid. 1.5 equivalents of the corresponding glycol was dissolved in the catalyst-acid mixture. The mixture was degassed under nitrogen for 15 minutes and a nitrogen environment was maintained during electrolysis. Electrolysis was carried out at the indicated voltage using a three electrode system: a carbon felt working electrode, a Pt wire auxiliary electrode, and a AgCl reference electrode. The voltage of electrolysis was 100 mV more negative than the lowest reduction peak of the cyclic voltammogram that corresponded to the second reduction of the rhenium complex. The time of rhenium electrolysis was calculated once the resulting current was observed, according to the following calculation.

$$t = \frac{m_R}{MM_R} \cdot \frac{2\ mol\ e^-}{1\ mol\ Re} \cdot \frac{96485\ C}{1\ mol} \cdot \frac{1}{i_{obs}}$$

where m_R is the mass of rhenium used to prepare the solution, MM_R is the molar mass of the rhenium complex, t is the time in seconds, and i_{obs} is the observed current once the electrolysis starts.

Synthesis of (Me$_3$TACN)ReO(O$_2$C$_8$H$_8$)

This synthesis is adapted from a procedure reported by Bohn and Weighardt[159]. In 5 mL of deoxygenated deuterated dichloromethane, 40 mg of $ReOCl_3(PPh_3)_2$ was added to 76 mg of 1,4,7-trimethyltriazacyclononane and 40 mg of 1-phenyl-1,2-ethandiol. The resulting red solution was stirred for two hours under nitrogen, and the resulting mixture was analyzed via NMR, the spectrum of which was provided in Section 5.4.2. Glycolate: Phenyl rings - δ 7.60 (4.15 H), ethylene protons – δ 5.75 (1.00 H), 5.25 (1.67 H)

Mass Spectrometry Measurements

Electrospray Ionization Mass Spectrometry measurements were taken on an Agilent time of flight mass spectrometer. Summaries of a typical mass spectrum from a reaction mixture are tabulated below (reaction mixture typically contains 0.1 M KPF_6, 0.005 M Re complex, 0.010 M glycol, 0.010 M acid in MeCN).

m/z	Probable formula
222.89	$K_2PF_6^+$
342.86	$K_2PF_6(MeCN)^+$
494.81	$K_2(PF_6)_2(MeCN)^+$
531.89	$K_3(PF_6)_2(MeCN)_3$
558.77	$K_3(PF6)_3$

Chapter 6 – Conclusions and Future Work

6.1 Conclusions

The majority of this work focused on the development of a new method for and the application of a Langmuir binding isotherm between ferrocene derivatives and Glucose Oxidase (GOx). A binding isotherm between (ferrocenylmethyl)trimethylammonium chloride (FcTAMCl) and GOx was developed. The binding constant, K_a, for this interaction was 2.49×10^7. The stoichiometry of this interaction was investigated by simulated equilibrium conditions. A strong agreement was observed between the prediction of a 2:1 ferrocene to GOx ratio and the amperometric response of the system at saturating conditions. It was also shown the iodide was able to act as a mediator for GOx in catalytic conditions.

This isotherm was applied to additional ferrocene derivatives, such as ((methoxy)ethoxy)ethoxymethylferrocene (FcG2OMe), ferrocene carboxylic acid (FcCOOH), and bis(trimethylaminomethyl)ferrocenyl chloride ($Fc(TAMCl)_2$). Each derivative was found to bind to the GOx. The K_a values were determined to be 1.56×10^6, 4.33×10^7, and 4.08×10^6 for FcCOOH, FcG2OMe, and $Fc(TAMCl)_2$, respectively. In attempting to draw a connection between the determined K_a and the effectiveness of a molecule to act as an electron transport mediator (ETM) for GOx, the ratio of the amperometric response in the presence (i_{cat}) and absence (i_{pa}) of glucose was compared. Values for i_{cat}/i_{pa} were determined to be 15.5, 5.5, 3.5, and 6 for FcTAMCl, FcCOOH, FcG2OMe, and $Fc(TAMCl)_2$, respectively. It should be noted that the compound highest binding coefficient did not demonstrate the largest i_{cat}/i_{pa}. This suggested that a large binding coefficient may not be beneficial to a second generation bioelectrode. However, where there was not a correlation in solution state measurements, it could be imagined that a high K_a could allow for a stronger interaction between GOx and ferrocene in a polymer-supported state.

A new linear poly(ethylenimine) material was made using the largest K_a as a guide. A ferrocenyl glycol-modified linear poly(ethylenimine) (FcG2LPEI) (15% ferrocene substitution) was

fabricated into an electrode material using ethylene glycol diglycidyl ether (EGDGE) as a cross-linking agent. The new FcG2LPEI material was compared against a ferrocenylmethyl-functionalized linear poly(ethylenimine) (FcC1LPEI) for amperometric performance. Initially, the FcG2LPEI cross-linked with a solution of 30% (v/v) EGDGE did not perform as well as the FcC1LPEI with a similarly substituted ferrocene material (14%) as J_{max} values of 232 μA/cm^2 and 320 μA/cm^2, respectively. However, after varying the concentration of EGDGE, a material cross-linked with 15% (v/v) EGDGE exhibited a J_{max} of 698 μA/cm^2. This suggests that a large K_a is beneficial in mediator selection, and to identify potential component selection for polymer-supported bioelectrode preparation.

The remainder of the work summarized in this document was targeted toward the development of an electrocatalytic deoxydehydration (DODH) reaction. Two new triamine rhenium (VII) trioxo complexes, (pentamethyldiethylenetriamine)trioxorhenium (VII) perrhenate [(Me_5DETN)ReO_3ReO_4] and (1,4,7-trimethyltriazacyclononane)trioxorhenium (VII) perrhenate [(Me_3TACN)ReO_3ReO_4], were demonstrated to successfully catalyze a deoxydehydration reaction on multiple compounds containing vicinal diols using a variety of reductants. When the perrhenate ion in (Me_3TACN)ReO_3ReO_4 was exchanged for a hexafluorophosphate, a corresponding metal complex, (Me_3TACN)ReO_3PF_6, was prepared. Stronger reducing agents were needed in order for the new hexafluorophsophate complex to successfully act as a catalyst for DODH. This suggests that use of the perrheenate ion in conjunction with a cationic rhenium complex could enhance the catalytic capabilities through cooperation. Electrochemical experiments were conducted on (Me_3TACN)ReO_3PF_6 in acetonitrile in the presence and absence of an assortment of acids with various pKa values. Two peaks were always observed for the hexafluorophosphate complex with a similar amperometric response, suggesting that the observed reductive waves are Re(VII) -> Re (VI) and a Re(VI) to Re(V). The reduction potential of each peak shifted depending on the identity of the acid used in the electrochemical mixture.

Bulk electrolysis was used in attempting to form electrochemically a Re (V) metalloglycolate from $(Me_3TACN)ReO_3PF_6$ and styrene glycol in the presence of various acids. However, the corresponding Re(V) glycolate was not detected. This could be due to interference from acetonitrile, as the $(Me_3TACN)ReO(CH_2OCHOC_6H_5)PF_6$ complex formed in methylene chloride, but did not form in acetonitrile. To achieve the electrochemical formation of the metalloglycolate, additional experiments need to be carried out. In considering factors that could influence the formation of the Re (V) glycolate include the strength of the acid in acetonitrile, and the type of electrode used. In considering the nature of the electrocatalytic reaction, the fragmentation of the Re(V) glycolate is often the rate determining step[161]. This suggests that any possibility of developing an electrocatalytic DODH would require a high temperature, high pressure electrochemical apparatus that is sealed to exclude oxygen.

6.2 Future Work

In developing a new tool for use in the development of bioelectrode materials, additional experiments are required to investigate the full utility of our new binding method. There is a logical progression, however, in which these experiments should be conducted. A larger array of ferrocene derivatives with more diverse functional groups, including methyl groups on the ferrocene should be investigated with GOx for potential binding interactions. This could provide insight into the impact the functional group has on the strength of the cinding constant, K_a. In addition, this screening process could provide insight into the ideal functional groups for mediators to appropriately bind to the amino acid residues in the active site, potentially leading to a new generation of biofuel cell materials. Other enzyme-mediator systems should be screened for this interaction to determine if this tool is applicable to multiple enzyme-mediator systems, or if this tool is limited to GOx and ferrocene.

Additional experiments should be targeted toward the fabrication of materials, beginning with the FcG2LPEI material. Material components aside from the mediator have been demonstrated

to affect the maximum current density, J_{max}, of the material. For example, the percent substitution of ferrocene on the LPEI material has been demonstrated to alter the J_{max} of the material, and the Nicholas group has demonstrated that there is an ideal substitution of ferrocene for each material. By varying the percent substitution of ferrocene on the FcG2LPEI material, the maximum percent substitution could be investigated to determine if there is any correlation between K_a and the amount of mediator used in material fabrication. Other material properties, such as the length of the spacer between the mediator and the polymer support, have demonstrated an effect. It could be imagined that varying the length of the glycol ether chain could impact K_a, as we have demonstrated that the length of the spacer can alter J_{max}[64, 141].

In developing an electrocatalytic deoxydehydration (DODH), it will first be necessary to electrochemically synthesize a Re(V) glycolate, as this intermediate is key in the DODH mechanism. A variety of solvents and counter ions attached to the $(Me_3TACN)ReO_3$ cation could affect the formation and electrochemical behavior of the Re(VII) complex and the corresponding metalloglycolate. One important factor to consider in this preparation and analysis is the method through which the reaction will be analyzed. It could be imagined that the deep red metalloglycolate could be monitored using UV-Vis spectroscopy. In addition, the use of a zinc working electrode paired with a zinc-based supporting electrolyte could be helpful in achieving the Re(V) glycolate, as Zn has been used to generate other TACNRe(V) glycolates and is an effective reductant in the thermal catalytic DODH[159]. This could provide crucial insight into the formation of the desired glycolate. The nature of the glycol used in the DODH reaction could also assist in formation of themetalloglycolate. The phenyl ring of styrene glycol is a weak electron withdrawing group, which assists in the fragmentation of the Re(V) glycolate into the corresponding alkene and Re(VII) complex. In considering the ultimate goal of an electrocatalytic reaction, a high pressure/high-temperature reaction vessel will be required as the fragmentation of the metalloglycolate is often the rate-determining step in the catalytic process.

References

1. Petroleum, B., Statistical Review of World Energy. **2015**.
2. Energy Explained - Renewable Energy. April 2017 ed.; Administration, U. E. I., Ed. 2018.
3. Perlack, R. D. S., B. J., Review in Energy Usage. Energy, U. D. O., Ed. Oak Ridge National Labs, Oakridge, TN, 2011.
4. Burdge, J., *Chemistry*. 2nd ed.; McGraw Hill: 2011.
5. Linden, D., *Handbook of Batteries*. 3rd ed.; McGraw-Hill: 2002.
6. Rej, S. E., Dominique, Chronic Kidney Disease in Lithium-Treated Older Adults. *Drugs Aging* **2014,** *32*, 31-42.
7. Nacy, A. M., X; Nikolla E, Nanostructured Nickelate Oxides as Efficient and Stable Electrocatalysts for Li-O2 Batteries. *Top Catalysis* **2015,** *58*, 513-521.
8. Zou, C.; Zhang, L.; Hu, X.; Wang, Z.; Wik, T.; Pecht, M., A review of fractional-order techniques applied to lithium-ion batteries, lead-acid batteries, and supercapacitors. *J. Power Sources* **2018,** *390*, 286-296.
9. Zheng, F.; Kotobuki, M.; Song, S.; Lai, M. O.; Lu, L., Review on solid electrolytes for all-solid-state lithium-ion batteries. *J. Power Sources* **2018,** *389*, 198-213.
10. Potter, M. C., The Action of Bacillus lactis aerogenes on Glucose and Mannitol. II. The Investigation of the 2,3-Butanediol and the Acetylmethylcarbinol Formed; the Effect of Free Oxygen on their Production; the Action of B. lactis aerogenes on Fructose. *Proceedings of the Royal Society of London. Series B, Containing Papers of a Biological Character* **1911,** *84*, 260-276.
11. Yahiro, A. T. L., S. M.;Kimble, D. O., *Biochimica et Biophysica Acta - Specialized Section on Biophysical Subjects* **1964,** *88*, 375-383.
12. Wingard Jr, L. B. S., C. H.; Castner, J.F., *Enzyme and Microbial Technology* **1982,** *88*, 375-383.
13. Rao, A.; Sathiavelu, A.; Mythili, S., Mini review on nanoimmobilization of lipase and cellulase for biofuel production. *Biofuels* **2017**, Ahead of Print.
14. Le, T. X. H.; Bechelany, M.; Cretin, M., Carbon felt based-electrodes for energy and environmental applications: A review. *Carbon* **2017,** *122*, 564-591.
15. Grattieri, M.; Minteer, S. D., Self-Powered Biosensors. *ACS Sens.* **2018,** *3* (1), 44-53.
16. Ghassemi, Z.; Slaughter, G., Biological fuel cells and membranes. *Membranes (Basel, Switz.)* **2017,** *7* (1), 3/1-3/12.
17. Gamella, M.; Koushanpour, A.; Katz, E., Biofuel cells - Activation of micro- and macro-electronic devices. *Bioelectrochemistry* **2018,** *119*, 33-42.
18. El Ichi-Ribault, S.; Alcaraz, J.-P.; Boucher, F.; Boutaud, B.; Dalmolin, R.; Boutonnat, J.; Cinquin, P.; Zebda, A.; Martin, D. K., Remote wireless control of an enzymatic biofuel cell implanted in a rabbit for 2 months. *Electrochim. Acta* **2018,** *269*, 360-366.
19. Degani, Y. H., A., Direct electrical communication between chemically modified enzymes and metal electrodes. I. Electron transfer from glucose oxidase to metal electrodes via electron relays, bound covalently to the enzyme. *The Journal of Physical Chemistry* **1987,** *91* (6), 1285-1289.
20. Ricci, F. P., G. , Sensor and biosensor preparation, optimisation and applications of Prussian Blue modified electrodes. *Biosensors and Bioelectronics* **2005,** *21* (3), 389-407.
21. Schofield, C. J. R., P. J., Oxygen sensing by HIF hydroxylases. *Nat Rev Mol Cell Bio* **2004,** *5* (5), 343-354.
22. Wohlfahrt, G. W., S.; Hendle, J.; Schomburg, D.; Kalisz, H.; Hecht, H.-J., 1.8 and 1.9 A resolution structures of the Penicillium amagasaskiense and Aspergillus niger glucose oxidase as a basis for modeling substrate complexes. *Acta Crystallogr., Sect. D* **1999,** *D55*, 969-977.
23. Chen, J.; Bamper, D.; Glatzhofer, D. T.; Schmidtke, D. W., Development of Fructose Dehydrogenase-Ferrocene Redox Polymer Films for Biofuel Cell Anodes. *J. Electrochem. Soc.* **2015,** *162* (3), F258-F264.
24. Marcus, R. A., The theory of oxidation-reduction reactions involving electron transfer. I. *The Journal of Chemical Physics* **1956,** *24* (5), 966-978.

25. Heller, A., Electrical wiring of redox enzymes. *Acc. Chem. Res.* **1990,** *23* (5), 128-34.
26. Cracknell, J. A. V., K. A.; Armstrong, F. A., Enzymes as Working or Inspirational Electrocatalysts for Fuel Cells and Electrolysis. *Chemical Reviews* **2008,** *108* (7), 2439-2461.
27. Meredith, M. T. M., M.; Hickey, D. P.; Artyushkova, K.; Glatzhofer, D. T.; Minteer, S. D., Anthracene-Modified Multi-Walled Carbon Nanotubes as Direct Electron Transfer Scaffolds for Enzymatic Oxygen Reduction. *ACS Catalysis* **2011,** *1* (12), 1683-1690.
28. Barton, S. C. K., H. H.; Binyamin, G.; Zhang, Y; Heller, A., Electroreduction of O2 to Water on the "Wired" Laccase Cathode. *The Journal of Physical Chemistry B* **2001,** *105* (47), 11917-11921.
29. Szamocki, R. F., V.; Levin, L.; Forchiasin, F.; Calvo, E. J., *Electrochimica Acta* **2009,** *54* (7), 1970-1977.
30. Kleppe, K., The effect of hydrogen peroxide on glucose oxidase from Aspergillus niger. *Biochemistry* **1966,** *5* (1), 139-143.
31. Greenfield, P. F. K., J. R.; Laurence, R. L, Inactivation of immobilized glucose oxidase by hydrogen peroxide. *Analytical Biochemistry* **1975,** *65* (1), 109-124.
32. Kirstein, D. K., W.; Mohr, P., Preparation and properties of immobilized glucose oxidase. *Acta Biotechnol. et Medica Germanica* **1980,** *39* (11), 1121-1128.
33. Bourdillon, C. H., C.; Thomas, D., Increase in operational stability of immobilized glucose oxidase by the use of an artificial cosubstrate. *Biotech. Bioeng.* **1985,** *27* (11), 1619-1622.
34. Kamin, R. A. W., G. S., Rotating ring-disk enzyme electrode for biocatalysis kinetic studies and characterization of the immobilized enzyme layer. *Anal. Chem.* **1980,** *52* (8), 1198-1205.
35. Bourdillon, C. B., J. P,; Thomas, D., Covalent linkage of glucose oxidase on modified glassy carbon electrodes. Kinetic phenomena. *J. Am. Chem. Soc.* **1980,** *102*, 4231.
36. Cass, A. E. G. D., G.; Francis, G. D.; Hill, H. A. O.; Aston, W. J.; Higgins, I. J.; Plotkin, E. V.; et. al., Ferrocene-mediated enzyme electrode for amperometric determination of glucose. *Anal Chem* **1984,** *56*, 667.
37. Green, M. J. H., H. A. O.;, Amperometric enzyme electrodes. *J. Chem. Soc., Faraday Trans. 1* **1986,** *82* (4), 1237.
38. Liaudet, E. B., F.; Calvo, E. J., Electrochemical study of sulfonated ferrocenes as redox mediators in enzyme electrodes. *J. Electroanal. Chem.* **1990,** *23* (1), 252.
39. Rusling, J. F. I., K., Voltammetric determination of electron-transfer rate between an enzyme and a mediator. *Anal. Chim. Acta* **1991,** *252*, 23-27.
40. Gregg, B. A.; Heller, A., Cross-linked redox gels containing glucose oxidase for amperometric biosensor applications. *Anal. Chem.* **1990,** *62* (3), 258-63.
41. Mizutani, F. A., M., Ferrocene-attached bovine serum albumin as a mediator between glucose oxidase and an electrode. *Denki Kagaku* **1988,** *56*, 1100.
42. Schuhmann, W.; Ohara, T. J.; Schmidt, H. L.; Heller, A., Electron transfer between glucose oxidase and electrodes via redox mediators bound with flexible chains to the enzyme surface. *J. Am. Chem. Soc.* **1991,** *113* (4), 1394-7.
43. Ye, L.; Haemmerle, M.; Olsthoorn, A. J. J.; Schuhmann, W.; Schmidt, H. L.; Duine, J. A.; Heller, A., High current density "wired" quinoprotein glucose dehydrogenase electrode. *Anal. Chem.* **1993,** *65* (3), 238-41.
44. Forrow, N. J.; Sanghera, G. S.; Walters, S. J., The influence of structure in the reaction of electrochemically generated ferrocenium derivatives with reduced glucose oxidase. *J. Chem. Soc., Dalton Trans.* **2002,** (16), 3187-3194.
45. Forrow, N. J. W., S. J., Transition Metal Half-Sandwich Complexes as Redox Mediators to Glucose Oxidase. *Biosens. Bioelectron.* **2004,** *19*, 763-770.
46. Monteiro, T. A., M. G., Electrochemical Enzyme Biosensors Revisited: Old Solutions for New Problems. *Critical Review in Analytical Chemistry* **2018,** *49* (1), 44-66.

47. Abreu, C.; Nedellec, Y.; Ondel, O.; Buret, F.; Cosnier, S.; Le Goff, A.; Holzinger, M., Glucose oxidase bioanodes for glucose conversion and H2O2 production for horseradish peroxidase biocathodes in a flow through glucose biofuel cell design. *J. Power Sources* **2018,** *392*, 176-180.
48. Meredith, M. T.; Hickey, D. P.; Redemann, J. P.; Schmidtke, D. W.; Glatzhofer, D. T., Effects of ferrocene methylation on ferrocene-modified linear poly(ethylenimine) bioanodes. *Electrochim. Acta* **2013,** *92*, 226-235.
49. Andrieux, C. P.; Haas, O.; Saveant, J. M., Catalysis of electrochemical reactions at redox-polymer-coated electrodes. Mediation of the iron(III)/iron(II) oxido-reduction by a polyvinylpyridine polymer containing coordinatively attached bisbipyridine chlororuthenium redox centers. *J. Am. Chem. Soc.* **1986,** *108* (26), 8175-82.
50. Calvo, E. J.; Etchenique, R.; Danilowicz, C.; Diaz, L., Electrical Communication between Electrodes and Enzymes Mediated by Redox Hydrogels. *Anal. Chem.* **1996,** *68* (23), 4186-4193.
51. Chatani, Y.; Tadokoro, H.; Saegusa, T.; Ikeda, H., Structural studies of poly(ethylenimine). 1. Structures of two hydrates of poly(ethylenimine): sesquihydrate and dihydrate. *Macromolecules* **1981,** *14* (2), 315-21.
52. Ju, H.; Leech, D., [Os(bpy)2(PVI)10Cl]Cl polymer-modified carbon fiber electrodes for the electrocatalytic oxidation of NADH. *Anal. Chim. Acta* **1997,** *345* (1-3), 51-58.
53. Koide, S.; Yokoyama, K., Electrochemical characterization of an enzyme electrode based on a ferrocene-containing redox polymer. *J. Electroanal. Chem.* **1999,** *468* (2), 193-201.
54. Mikeladze, E.; Schulte, A.; Mosbach, M.; Blochl, A.; Csoregi, E.; Solomonia, R.; Schuhmann, W., Redox hydrogel-based bienzyme microelectrodes for amperometric monitoring of L-glutamate. *Electroanalysis* **2002,** *14* (6), 393-399.
55. Ohara, T. J.; Rajagopalan, R.; Heller, A., Glucose electrodes based on cross-linked [Os(bpy)2Cl]+/2+ complexed poly(1-vinylimidazole) films. *Anal Chem* **1993,** *65* (23), 3512-7.
56. Ohara, T. J.; Rajagopalan, R.; Heller, A., Glucose electrodes based on cross-linked bis(2,2'-bipyridine)chloroosmium(+/2+) complexed poly(1-vinylimidazole) films. *Anal. Chem.* **1993,** *65* (23), 3512-17.
57. Merchant, S. A.; Glatzhofer, D. T.; Schmidtke, D. W., Effects of Electrolyte and pH on the Behavior of Cross-Linked Films of Ferrocene-Modified Poly(ethylenimine). *Langmuir* **2007,** *23* (22), 11295-11302.
58. Palmore, G. T. R. K., H. H, Electro-enzymic reduction of dioxygen to water in the cathode compartment of a biofuel cell. *Journal of Electroanalytical Chemistry* **1999,** *464* (1), 110-117.
59. Meredith, M. T.; Kao, D.-Y.; Hickey, D.; Schmidtke, D. W.; Glatzhofer, D. T., High Current Density Ferrocene-Modified Linear Poly(ethylenimine) Bioanodes and Their Use in Biofuel Cells. *J. Electrochem. Soc.* **2011,** *158* (2), B166-B174.
60. Soukahrev, V. M., N.; Heller A., Oxygen sensing by HIF hydroxylases. *J. Am. Chem. Soc.* **2004,** *126*, 8368.
61. Fei, M. M., N.; Heller, A, Long tethers binding redox centers to polymer backbones enhance electron transport in enzyme "Wiring" hydrogels. *J. Am. Chem. Soc.* **2003,** *123* (16), 4951-4957.
62. Perevalova, E. G. R., M. D.; Grandberg, K. I., *Methods of Elementoorganic Chemistry*. Nauka: Moscow, 1983.
63. Hickey, D. P.; Giroud, F.; Schmidtke, D. W.; Glatzhofer, D. T.; Minteer, S. D., Enzyme cascade for catalyzing sucrose oxidation in a biofuel cell. *ACS Catal.* **2013,** *3* (12), 2729-2737.
64. Hickey, D. P.; Halmes, A. J.; Schmidtke, D. W.; Glatzhofer, D. T., Electrochemical Characterization of Glucose Bioanodes Based on Tetramethylferrocene-Modified Linear Poly(ethylenimine). *Electrochim. Acta* **2014,** *149*, 252-257.
65. Hickey, D. P. FERROCENE-MODIFIED LINEAR POLY(ETHYLENIMINE) BIOELECTRODE MATERIALS FOR USE IN GLUCOSE/O2 BIOFUEL CELLS. University of Oklahoma, 2014.
66. Giroud, F.; Hickey, D. P.; Schmidtke, D. W.; Glatzhofer, D. T.; Minteer, S. D., A Monosaccharide-Based Coin-Cell Biobattery. *ChemElectroChem* **2014,** *1* (11), 1880-1885.

67. Kano, K. I., T., Fundamentals and practices of mediated bioelectrocatalysis. *Anal. Sci.* **2000,** *16* (10), 1013-1021.
68. delle Noci, S. F., M.; Favero, G.; Tosi, M. ; Ferri, T.; Mazzei, F., Electrochemical Kinetic Characterization of Redox Mediated Glucose Oxidase Reaction: A simplified Approach. *Electroanalysis* **2007,** *20* (2), 163-169.
69. Chen, J.; Munje, R.; Godman, N. P.; Prasad, S.; Glatzhofer, D. T.; Schmidtke, D. W., Improved Performance of Glucose Bioanodes Using Composites of (7,6) Single-Walled Carbon Nanotubes and a Ferrocene-LPEI Redox Polymer. *Langmuir* **2017,** *33* (31), 7591-7599.
70. Zebda, A.; Gondran, C.; Le Goff, A.; Holzinger, M.; Cinquin, P.; Cosnier, S., Mediatorless high-power glucose biofuel cells based on compressed carbon nanotube-enzyme electrodes. *Nat. Commun.* **2011,** *2* (June), 1365/1-1365/6, S1365/1-S1365/3.
71. Miyake, T.; Yoshino, S.; Yamada, T.; Hata, K.; Nishizawa, M., Self-regulating enzyme-nanotube ensemble films and their application as flexible electrodes for biofuel cells. *J. Am. Chem. Soc.* **2011,** *133* (13), 5129-5134.
72. Bartlett, P. N.; Al-Lolage, F. A., There is no evidence to support literature claims of direct electron transfer (DET) for native glucose oxidase (GOx) at carbon nanotubes or graphene. *Journal of Electroanalytical Chemistry* **2018,** *819*, 26-37.
73. Zhu, Z.; Kin, T. T.; Sun, F.; You, C.; Percival, Z. Y. H., A high-energy-density sugar biobattery based on a synthetic enzymatic pathway. *Nat Commun* **2014,** *5*, 3026.
74. Monteiro, T.; Almeida, M. G., Electrochemical Enzyme Biosensors Revisited: Old Solutions for New Problems. *Crit. Rev. Anal. Chem.* **2018**, Ahead of Print.
75. Merchant, S. A.; Meredith, M. T.; Tran, T. O.; Brunski, D. B.; Johnson, M. B.; Glatzhofer, D. T.; Schmidtke, D. W., Effect of Mediator Spacing on Electrochemical and Enzymatic Response of Ferrocene Redox Polymers. *J. Phys. Chem. C* **2010,** *114* (26), 11627-11634.
76. Cook, G. K. A., M. A., Toward Nonoxidative Routes to Oxygenated Organics: Stereospecific Deoxydehydration of Diols and Polyols to Alkenes and Allylic Alcohols Catalyzed by the Metal Oxo Complex (C5Me5)ReO3. *J. Am. Chem. Soc.* **1996,** *118* (2), 9448-9449.
77. Abu-Omar, M. M.; Appelman, E. H.; Espenson, J. H., Oxygen-Transfer Reactions of Methylrhenium Oxides. *Inorg. Chem.* **1996,** *35* (Copyright (C) 2012 American Chemical Society (ACS). All Rights Reserved.), 7751-7757.
78. Gable, K. P. J., J. J. J, Extrusion of Alkenes from Rhenium(V) Diolates: The Effect of Substitution and Conformation. *J. Am. Chem. Soc.* **1995,** *117* (3), 955-962.
79. Gable, C. B.; Tierce, J. C.; Simison, D.; Ward, D.; Motte, K., Costs of HIV+/AIDS at CD4+ counts disease stages based on treatment protocols. *J Acquir Immune Defic Syndr Hum Retrovirol* **1996,** *12* (4), 413-20.
80. Gable, K. P. Z., F. A., Kinetic Isotope Effects in Cycloreversion of Rhenium (V) Diolates. *J. Am. Chem. Soc.* **2002,** *124* (15), 3970-3979.
81. Raju, S. J., J. T. B. H.; Lutz, M.; Klein Gebbink, R. J. M., Catalytic Deoxydehydration of Diols to Olefins by using a Bulky Cyclopentadiene-based Trioxorhenium Catalyst. *ChemSusChem* **2013,** *6* (9), 1673-1680.
82. McClain, J. M., III; Nicholas, K. M., Elemental Reductants for the Deoxydehydration of Glycols. *ACS Catal.* **2014,** *4* (7), 2109-2112.
83. Liu, P.; Nicholas, K. M., Mechanism of sulfite-driven, MeReO3-catalyzed deoxydehydration of glycols. *Organometallics* **2013,** *32* (6), 1821-1831.
84. Boucher-Jacobs, C.; Nicholas, K. M., Oxo-rhenium-catalyzed deoxydehydration of polyols with hydroaromatic reductants. *Organometallics* **2015,** *34* (10), 1985-1990.
85. Ziegler, J. E. A., M. J.; Evans, A. J.; Abu-Omar, M. M, *Inorg. Chem.* **2009,** *48* (21), 9998-10000.
86. Shiramizu, M. T., F. D, Deoxygenation of biomass-derived feedstocks: oxorhenium-catalyzed deoxydehdration of sugars and sugar alcohols. *Angew. Chem., Int. Ed. Engl.* **2012,** *51* (32), 8082-8086.

87. Boucher-Jacobs, C.; Nicholas, K. M., Catalytic Deoxydehydration of Glycols with Alcohol Reductants. *ChemSusChem* **2013,** *6* (4), 597-599.
88. Chapman, G., Jr.; Nicholas, K. M., Vanadium-catalyzed deoxydehydration of glycols. *Chem Commun (Camb)* **2013,** *49* (74), 8199-201.
89. Sharkey, B. E.; Denning, A. L.; Jentoft, F. C.; Gangadhara, R.; Gopaladasu, T. V.; Nicholas, K. M., New solid oxo-rhenium and oxo-molybdenum catalysts for the deoxydehydration of glycols to olefins. *Catal. Today* **2018,** *310*, 86-93.
90. Gopaladasu, T. V.; Nicholas, K. M., Carbon Monoxide (CO)- and Hydrogen-Driven, Vanadium-Catalyzed Deoxydehydration of Glycols. *ACS Catal.* **2016,** *6* (3), 1901-1904.
91. Boucher-Jacobs, C. N., K., *Deoxydehydration of Polyols*. Springer Berlin Heidelberg: 2014; p 1-22.
92. Ahmad, I.; Chapman, G.; Nicholas, K. M., Sulfite-Driven, Oxorhenium-Catalyzed Deoxydehydration of Glycols. *Organometallics* **2011,** *30* (10), 2810-2818.
93. Arceo, E. E., J. A.; Bergman, R. G., Rhenium-Catalyzed Didehydroxylation of Vicinal Diols to Alkenes Using a Simple Alcohol as a Reducing Agent. *J. Am. Chem. Soc.* **2010,** *132* (33), 11408-11409.
94. Herrmann, W. A. R., P. W.; kuhn, F. E.; Elison, M.; Artus, G.; Scherer, W.; Romao, C. C.; lopes, A.l Basset, J.-M., Multiple Bonds between main-group elements and trainsition metals 145 Coordination chemistry of dirhenium heptoxide: covalent adducts and "ionic perrhenyl perrhenates". *Inorg. Chem.* **1995,** *34* (19), 4701-4707.
95. You, B.; Han, G.; Sun, Y., Electrocatalytic and photocatalytic hydrogen evolution integrated with organic oxidation. *Chem Commun (Camb)* **2018,** *54* (47), 5943-5955.
96. Sauer, G. S.; Lin, S., An Electrocatalytic Approach to the Radical Difunctionalization of Alkenes. *ACS Catal.* **2018,** *8* (6), 5175-5187.
97. Perathoner, S.; Centi, G., Catalysis for solar-driven chemistry: The role of electrocatalysis. *Catal. Today* **2018**, Ahead of Print.
98. Lund, H. H., O, *Organic Electrochemistry*. 4th edition ed.; Marcel Dekker: 2001.
99. Amiri, M.; Bezaatpour, A.; Jafari, H.; Boukherroub, R.; Szunerits, S., Electrochemical Methodologies for the Detection of Pathogens. *ACS Sens.* **2018**, Ahead of Print.
100. Freitas, M.; Nouws, H. P. A.; Delerue-Matos, C., Electrochemical Biosensing in Cancer Diagnostics and Follow-up. *Electroanalysis* **2018**, Ahead of Print.
101. Lee, N. Y., A review on microscale polymerase chain reaction based methods in molecular diagnosis, and future prospects for the fabrication of fully integrated portable biomedical devices. *Microchim. Acta* **2018,** *185* (6), 1-22.
102. Ma, X.-m.; Sun, M.; Lin, Y.; Liu, Y.-j.; Luo, F.; Guo, L.-h.; Qiu, B.; Lin, Z.-y.; Chen, G.-n., Progress of visual biosensor based on gold nanoparticles. *Fenxi Huaxue* **2018,** *46* (1), 1-10.
103. Gao, Y.; Choi, S., Stepping Toward Self-Powered Papertronics: Integrating Biobatteries into a Single Sheet of Paper. *Adv. Mater. Technol. (Weinheim, Ger.)* **2017,** *2* (1), n/a.
104. Liu, B.; Yan, C.; Si, W.; Sun, X.; Lu, X.; Ansorge-Schumacher, M.; Schmidt, O. G., Biobatteries: Ultralong-Discharge-Time Biobattery Based on Immobilized Enzymes in Bilayer Rolled-Up Enzymatic Nanomembranes (Small 13/2018). *Small* **2018,** *14* (13), n/a.
105. Cass, A. E. G.; Davis, G.; Green, M. J.; Hill, H. A. O., Ferricinium ion as an electron acceptor for oxido-reductases. *J. Electroanal. Chem. Interfacial Electrochem.* **1985,** *190* (Copyright (C) 2013 American Chemical Society (ACS). All Rights Reserved.), 117-27.
106. Chen, L.-Q.; Zhang, X.-E.; Xie, W.-H.; Zhou, Y.-F.; Zhang, Z.-P.; Cass, A. E. G., Genetic modification of glucose oxidase for improving performance of an amperometric glucose biosensor. *Biosens. Bioelectron.* **2002,** *17* (10), 851-857.
107. Kuwabata, S.; Okamoto, T.; Kajiya, Y.; Yoneyama, H., Preparation and Amperometric Glucose Sensitivity of Covalently Bound Glucose Oxidase to (2-Aminoethyl)ferrocene on an Au Electrode. *Anal. Chem.* **1995,** *67* (10), 1684-90.

108. Ryabov, A. D., Interactions and reactions of organometallic compounds with enzymes and proteins. *Angew. Chem.* **1991,** *103* (Copyright (C) 2013 American Chemical Society (ACS). All Rights Reserved.), 945-55 (See also Angew. Chem., Int. Ed. Engl., 1991, 30(8), 931-41).
109. Hodak, J. E., R.; Calvo, E. J.; Singhal, K.; Bartlett, P. N, Layer-by-Layer Self-Assembly of Glucose Oxidase with a Poly(allylamine)ferrocene Redox Mediator. *Langmuir* **1997,** *13* (10), 2708-2716.
110. Weibel, M. K. B., H. J. J., *J. Biol. Chem.* **1971,** *246*, 2734.
111. Ikeda, T. M., K.; Senda, M., Theory of catalytic current at the biocatalyst electrode with entrapped mediator. *Anal. Sci.* **1988,** *4* (2), 133-138.
112. Habermuller, K. M., M.; Schuhmann, W., Electron-transfer mechanisms in amperometric biosensors. *Fresenius J Anal Chem* **2000,** *366* (6-7), 560-568.
113. Merchant, S. A.; Tran, T. O.; Meredith, M. T.; Cline, T. C.; Glatzhofer, D. T.; Schmidtke, D. W., High-Sensitivity Amperometric Biosensors Based on Ferrocene-Modified Linear Poly(ethylenimine). *Langmuir* **2009,** *25* (13), 7736-7742.
114. Cass, A. E. G.; Davis, G.; Green, M. J.; Hill, H. A. O., Ferricinium ion as an electron acceptor for oxido-reductases. *J. Electroanal. Chem. Interfacial Electrochem.* **1985,** *190* (1-2), 117-27.
115. Bently, C. L. B., A. M.; Hollenkamp, A. F.; Mahon, P. J.; Zhang, J., Electrochemistry of Iodide, Iodine, and Iodine Monochloride in Chloride-Containing Nonhaloaluminate ionic liquids. *Anal Chem* **2016,** *83* (3), 1915-1921.
116. Chang, H. C.; Bumpus, J. A., Iodide oxidation and iodine reduction mediated by horseradish peroxidase in the presence of ethylenediaminetetraacetic acid (EDTA): the superoxide effect. *Proceedings of the National Science Council, Republic of China, Part B: Life Sciences* **2001,** *25* (2), 82-89.
117. Brown, R. S.; Luong, J. H. T., Bioelectrocatalysis and diffusion kinetics of the glucose oxidase:glucose reaction using a water-soluble 1,1'-dimethylferrocene-2-hydroxypropyl-β-cyclodextrin complex. *Electroanalysis (N. Y.)* **1994,** *6* (5-6), 391-6.
118. Creanga, C.; El Murr, N., Kinetic study for implementation of a disposable "redox-flexible" glucose biosensor. *Electrochim. Acta* **2010,** *55* (27), 7818-7823.
119. Atlaf, F. Q., R.; Ahmed, S.; Khan, A. Y.; Naseer, A., Electrochemical Adsorption Studies of Urea on Copper Surface in Alkaline Medium. *Journal of Electroanalytical Chemistry* **2010,** (642), 98-101.
120. Subramanian, R. L., V., Effect of Adsorption of Some Azoles on Copper Passivation in Alkaline Medium. *Corrosion Science* **2002,** *44*, 535-554.
121. Lipkowski, J. R., P.N., *Adsorption of Molecules at Metal Electrodes*. VCH: New York, 1992.
122. Damaskin, B. B. P., O.A.; Batrakov, V.V., *Adsorption of Organic Compounds on Electrodes*. Plenum Press: New York, 1971.
123. Cui, L. G., S.; Kaifer, A., Electrochemistry of the Inclusion Complexes Formed Between the Cucurbituril[7] Host and Several Cationic and Neutral Ferrocene Derivatives. *Langmuir* **2009,** *25* (24), 13763-13769.
124. A., E., Über die von der molekularkinetischen Theorie der Wärme geforderte Bewegung von in ruhenden Flüssigkeiten suspendierten Teilchen. *Annalen der Physik* **1905,** *322* (8), 549-560.
125. Dunitz, J. D.; Orgel, L. E.; Rich, A., The crystal structure of ferrocene. *Acta Crystallographica* **1956,** *9* (4), 373-375.
126. Lednicer, D. H., C., N,N-demethylaminomethylferrocene methiodide. *Organic Synthesis, Coll. Vol 5* **1973,** *40*, 31.
127. Sassolas, A. B., L.J.; Leca-Bouvier, B. D.;, Immobilization strategies to develop enzymatic biosensors. *Biotechnology Advances* **2012,** *30* (3), 489-511.
128. WIllner, I. Y., Y. M.; Willner, B.; Tel-Vered, R., Integrated enzyme-based biofuel cells-A review. *Fuel Cells* **2009,** *9* (1), 7-24.
129. Cosnier, S. L. G., A.; Hlzinger, M., Towards glucose biofuel cells implanted in human body for powering artificial organs: Review. *Electrochemistry Communications* **2014,** *38* (0), 19-23.

130. Mao, F. M., N. Heller, A., Long tethers binding redox centers to polymer backbones enhance electron transport in enzyme "wiring" hydrogels. *Journal of the American Chemical Society* **2003,** *125* (16), 4951-4957.
131. Heller, A., Electron-conducting redox hydrogels: design, characteristics and synthesis. *Current Opinion in Chemical Biology* **2006,** *10* (6), 664-672.
132. Ryabov, A. D. S., V. S.; Alexandrova, L.; le Lagadoc, L.; Pfeffer, M., New Synthesis and New Bio-Application of Cyclometalated Ruthenium(II) Complexes for Fast Mediated Electron Transfer with Peroxidase and Glucose Oxidase. *Inorganic Chemistry* **2001,** *40*, 6529.
133. Bartlett, P. N. T., P; Whitaker, R. G., Kinetic aspects of the use of modified electrodes and mediators in bioelectrochemistry. *Prog. React. Kinet.* **1991,** *16*, 55.
134. Frederick, K. R. T., J.; Emerick, S. R.; Masiarz, F. R; *et al*, Glucose oxidase from Aspergillus niger. Cloning, gene sequence, secretion from Saccharomyces cerevisiae and kinetic analysis of a yeast-derived enzyme. *Journal of Biological Chemistry* **1990,** *265* (7), 3793.
135. Swoboda, B. E. P.; Massey, V., Purification and Properties of the Glucose Oxidase from Aspergillus niger. *Journal of Biological Chemistry* **1965,** *240* (5), 2209-2215.
136. Ryabov, A. D.; Goral, V. N., Steady-state kinetics, micellar effects, and the mechanism of peroxidase-catalyzed oxidation of n-alkylferrocenes by hydrogen peroxide. *JBIC, J. Biol. Inorg. Chem.* **1997,** *2* (Copyright (C) 2013 American Chemical Society (ACS). All Rights Reserved.), 182-190.
137. Toone, E. J., *Advances in Enzymology and Related Areas of Molecular Biology, Protein Evolution*. Wiley: 2006; Vol. 75.
138. Mano, N., Using Smart Source Parsing. *J. Biotechnol* **2011**.
139. Milburn, C. C. L., H. J.; Theodossis, A.; Bull, S.D.; Hough, D.W., Danson, M.J.; Taylor, G. L, The structural basis of substrate promiscuity in glucose dehydrogenase from the hyperthermophilic archaeon Sulfolobus solfataricus. *Journal of Biological Chemistry* **2006,** *281*, 14796-14804.
140. Mao, F.; Mano, N.; Heller, A., Long Tethers Binding Redox Centers to Polymer Backbones Enhance Electron Transport in Enzyme “Wiring” Hydrogels. *Journal of the American Chemical Society* **2003,** *125* (16), 4951-4957.
141. Merchant, S. A.; Meredith, M. T.; Tran, T. O.; Brunski, D. B.; Johnson, M. B.; Glatzhofer, D. T.; Schmidtke, D. W., Effect of Mediator Spacing on Electrochemical and Enzymatic Response of Ferrocene Redox Polymers. *J. Phys. Chem. C* **2010,** *114* (Copyright (C) 2013 American Chemical Society (ACS). All Rights Reserved.), 11627-11634.
142. Merchant, S. A.; Tran, T. O.; Meredith, M. T.; Cline, T. C.; Glatzhofer, D. T.; Schmidtke, D. W., High-Sensitivity Amperometric Biosensors Based on Ferrocene-Modified Linear Poly(ethylenimine). *Langmuir* **2009,** *25* (Copyright (C) 2013 American Chemical Society (ACS). All Rights Reserved.), 7736-7742.
143. Meredith, M. T.; Kao, D.-Y.; Hickey, D.; Schmidtke, D. W.; Glatzhofer, D. T., High Current Density Ferrocene-Modified Linear Poly(ethylenimine) Bioanodes and Their Use in Biofuel Cells. *J. Electrochem. Soc.* **2011,** *158* (Copyright (C) 2013 American Chemical Society (ACS). All Rights Reserved.), B166-B174.
144. Boucher-Jacobs, C.; Nicholas, K. M., Deoxydehydration of polyols. *Top. Curr. Chem.* **2014,** *353* (Selective Catalysis for Renewable Feedstocks and Chemicals), 163-184.
145. Vkuturi, S.; Chapman, G.; Ahmad, I.; Nicholas, K. M., Rhenium-catalyzed deoxydehydration of glycols by sulfite. *Inorg Chem* **2010,** *49* (11), 4744-6.
146. Liu, S. S., A.l Smeltx, J.; Yang, L.; Wegenhart, B.; Yi, J.; Kenttamaa, H.; Ison, E.; Abu-Omar, M. M., Mechanism of MTO-catalyzed deoxydehydration of diols to alkenes using sacrificial alcohols. *Organometallics* **2013,** *32*, 3210-3219.
147. McClain, J. M., III. SURVEY OF CATALYST AND REDUCTANT EFFECTS ON OXORHENIUM CATALYZED DEOXYDEHYDRATION OF GLYCOLS. University of Oklahoma, 2015.
148. Qu, S. D., Y.; Wen, M.; Wang, Z.-X., Mechanism of the Methytrioxorhenium-catalyzed Deoxydehydration of Polyols: a new pathway realized. *Chem. - Eur. J.* **2013,** *19* (3827-3832).

149. Dethelfsen, J. R. F., P, nsitu Spectroscopic investigation of the rhenium-catalyzed deoxydehydration of vicinal diols. *ChemCatChem* **2015,** *7* (I), 1184-1196.
150. Wu, D. Z., Y.; Su, H., Mechanistic Study of Oxorhenium-catalyzed deoxydehydration and allylic alcohol isomerizations. *Chem. - Asian J.* **2016,** *11* (10), 1565-1571.
151. Chi-Ming, C. C., J. Y. K.; Cheung, K.-K.; Wong, W.-Y., Reversible proton-coupled ReVII-ReVI and ReVI-ReV couples and crystal structure of [ReVO2(H2O)Me3TACN)][BPh4]. *J. Chem. Soc., Dalton Trans.* **1997,** *13*, 2437-2350.
152. Hermann, W. A. K., P.l; Rypda, K.; Tremmel, J.; Blom, R.; Alberto, R.; Behm, J.; ALbach, R.; Bock, H.; Solouki, B.; Mink, J.; Lichtenberger, D.; Gruhn, N., Multiple Bonds between main-group elements and trainsition metals 86: Methyltrioxorhenium (VII) and trioxo (n5-pentamethylcyclopentadienyl)rhenium (VII): structures, spectroscopy, and electrochemistry. *J. Am. Chem. Soc.* **1991,** *113*, 6527-6537.
153. Elgrishi, N. R., K. J.; McCarthy, B. D.; Rountree, E. S.; Eisenhart, T. T.; Dempsey, J. L., A Practical Beginner's Guide to Cyclic Voltammetry. *J. Chem. Educ.* **2018,** *95*, 197-206.
154. Bohm, G. W., K.; Nuber, B.; Weiss, J., Coordination Chemistry of rhenium (V), -(IV), and -(III) with the macrocyclic ligands 1,4,7-trizazcyclononane and its N-methylated derivative. *Inorg. Chem.* **1991,** *30*, 3464-3476.
155. Bard, A., The Electrochemistry of Organic Compounds in Aprotic Solvents - Methods and Applications. 379-393.
156. Kütt, A.; Selberg, S.; Kaljurand, I.; Tshepelevitsh, S.; Heering, A.; Darnell, A.; Kaupmees, K.; Piirsalu, M.; Leito, I., pKa values in organic chemistry – Making maximum use of the available data. *Tetrahedron Letters* **2018,** *59* (42), 3738-3748.
157. Yi, J.; Liu, S.; Abu-Omar, M. M., Rhenium-Catalyzed Transfer Hydrogenation and Deoxygenation of Biomass-Derived Polyols to Small and Useful Organics. *ChemSusChem* **2012,** *5* (Copyright (C) 2013 American Chemical Society (ACS). All Rights Reserved.), 1401-1404, S1401/1-S1401/34.
158. Ziegler, J. E.; Zdilla, M. J.; Evans, A. J.; Abu-Omar, M. M., H2-Driven Deoxygenation of Epoxides and Diols to Alkenes Catalyzed by Methyltrioxorhenium. *Inorg. Chem.* **2009,** *48* (Copyright (C) 2013 American Chemical Society (ACS). All Rights Reserved.), 9998-10000.
159. Boehm, G.; Wieghardt, K.; Nuber, B.; Weiss, J., Coordination chemistry of rhenium(V), -(IV), and -(III) with the macrocyclic ligands 1,4,7-triazacyclononane (L) and its N-methylated derivative (L'). Crystal structures of [LReCl3]Cl, [L2Re2Cl2(μ-Cl)(μ-OH)]I2·2H2O, [L2Re2I2(μ-O)2]I2·2H2O, and [L'2Re2Cl4(μ-O)]ZnCl4. Effect of π-donors on the Re-Re bond distance. *Inorg. Chem.* **1991,** *30* (18), 3464-76.
160. Gernon, M. D. W., M.; Buszta, T.; Janney, P., Environmental Benefits of methanesulfonic acid: comparative properties and advantages. *Geen Chemistry* **1999,** *1* (1), 127-140.
161. Liu, P.; Nicholas, K. M., Mechanism of sulfite-driven, MeReO3-catalyzed deoxydehydration of glycols. *Organometallics* **2013,** *32* (Copyright (C) 2013 American Chemical Society (ACS). All Rights Reserved.), 1821-1831.